

Interaction processes in cold gases of alkali atoms

Citation for published version (APA):

Abeelen, van, F. A. (1999). *Interaction processes in cold gases of alkali atoms*. [Phd Thesis 1 (Research TU/e / Graduation TU/e), Applied Physics and Science Education]. Technische Universiteit Eindhoven.
<https://doi.org/10.6100/IR528499>

DOI:

[10.6100/IR528499](https://doi.org/10.6100/IR528499)

Document status and date:

Published: 01/01/1999

Document Version:

Publisher's PDF, also known as Version of Record (includes final page, issue and volume numbers)

Please check the document version of this publication:

- A submitted manuscript is the version of the article upon submission and before peer-review. There can be important differences between the submitted version and the official published version of record. People interested in the research are advised to contact the author for the final version of the publication, or visit the DOI to the publisher's website.
- The final author version and the galley proof are versions of the publication after peer review.
- The final published version features the final layout of the paper including the volume, issue and page numbers.

[Link to publication](#)

General rights

Copyright and moral rights for the publications made accessible in the public portal are retained by the authors and/or other copyright owners and it is a condition of accessing publications that users recognise and abide by the legal requirements associated with these rights.

- Users may download and print one copy of any publication from the public portal for the purpose of private study or research.
- You may not further distribute the material or use it for any profit-making activity or commercial gain
- You may freely distribute the URL identifying the publication in the public portal.

If the publication is distributed under the terms of Article 25fa of the Dutch Copyright Act, indicated by the "Taverne" license above, please follow below link for the End User Agreement:

www.tue.nl/taverne

Take down policy

If you believe that this document breaches copyright please contact us at:

openaccess@tue.nl

providing details and we will investigate your claim.

Interaction Processes in Cold Gases of Alkali Atoms

PROEFSCHRIFT

ter verkrijging van de graad van doctor aan de
Technische Universiteit Eindhoven, op gezag van de
Rector Magnificus, prof.dr. M. Rem, voor een
commissie aangewezen door het College voor
Promoties in het openbaar te verdedigen
op donderdag 16 december 1999 om 16.00 uur

door

Frank Anton van Abeelen

geboren te Son en Breugel

Dit proefschrift is goedgekeurd door de promotoren:

prof.dr. B.J. Verhaar

en

prof.dr. H.C.W. Beijerinck

Druk: Universiteitsdrukkerij Technische Universiteit Eindhoven

CIP-DATA LIBRARY TECHNISCHE UNIVERSITEIT EINDHOVEN

Abeelen, Frank Anton van

Interaction Processes in Cold Gases of Alkali Atoms / by Frank Anton van Abeelen. -
Eindhoven: Technische Universiteit Eindhoven, 1999. - Proefschrift. -

ISBN 90-386-0937-X

NUGI 812

Trefw: atoombotsingen / Bose-Einstein-condensatie / atomen; wisselwerkingen /
alkalimetalen / laserspectroscopie

Subject Headings: optical cooling of atoms; trapping / scattering of atoms, molecules,
and ions / phase coherent atomic ensembles; quantum condensation phenomena /
interatomic potentials and forces / laser-modified scattering and reactions

aan mijn ouders

Frank van Abeelen
Group for Theoretical and Experimental Atomic Physics and Quantum Electronics
Department of Physics
Eindhoven University of Technology
P.O. Box 513
5600 MB Eindhoven
The Netherlands

Cover Alkali atoms with electron cloud, nuclear spin, and electronic spin; the two atoms on the left are colliding and temporarily in different internal states than the noninteracting atoms on the right and at the back. Some formulas used in the description of cold collisions between alkali atoms are visible in the background.

Contents

1	Introduction	3
1.1	Atoms in Cold Dilute Gases	3
1.2	Cold-Atom Interaction Processes	4
1.3	This Thesis	6
2	Basic Concepts	9
2.1	The Effective Hamiltonian	9
2.2	Coupled Channels and Rate Coefficients	14
2.3	Scattering Properties in the Ultracold Limit	19
2.4	The Accumulated Phase Method	22
2.5	Feshbach Resonances	24
2.6	Photoassociation	28
3	Time-Dependent Feshbach Resonance Scattering and Anomalous Decay of a Na Bose-Einstein Condensate	33
3.1	Introduction	33
3.2	Anomalous Decay in Type 2 Runs	34
3.3	Two-State Model	36
3.4	Results	38
3.5	Two-Step Three-body Decay in Type 1 Runs	39
3.6	Conclusions	40
4	Photoassociation as a Probe of Feshbach Resonances in Cold-Atom Scattering	43
4.1	Introduction	43
4.2	Photoassociation as a Probe of Feshbach Resonances	44
4.3	Numerical Calculation of the Signal	45
4.4	An Analytical Model	47
4.5	Conclusions	50
5	Observation of a Feshbach Resonance in Cold-Atom Scattering	53
5.1	Introduction	53
5.2	Experimental Method	54
5.3	Observation of a Feshbach Resonance	56
5.4	Determination of ^{85}Rb Interaction Parameters	59

5.5	Conclusions	60
6	Sympathetic Cooling of ^6Li Atoms	63
6.1	Introduction	63
6.2	Reexamination of the Li + Li Accumulated Phases	64
6.3	^7Li - ^6Li Collisions	67
6.4	Collisions between Identical Isotopes	70
6.5	Conclusions	72
7	Determination of Collisional Properties of Cold Na Atoms from Analysis of Experimental Data	75
7.1	Introduction	75
7.2	Method	77
7.3	Bound-States Analysis	78
7.4	Photoassociation Data	83
7.5	Feshbach Resonances	85
7.6	Predictions and Conclusions	87
	Summary	91
	Samenvatting	93
	Dankwoord	96
	Curriculum Vitae	97

1

Introduction

1.1 Atoms in Cold Dilute Gases

One of the most fascinating new developments in atomic, molecular and optical physics is the realization of Bose-Einstein condensation (BEC) in dilute atomic gases. First in gases of the alkali atoms rubidium [1,2] sodium [3], and lithium [4], and later hydrogen [5]. BEC occurs when the de Broglie wavelength of the atoms in a bosonic gas becomes comparable to or larger than the mean interparticle separation. This calls for a very low temperature of the gas: typically below 500 nK at densities of around 10^{13} atoms per cubic centimeter. For hydrogen, the transition temperature turned out to be near 50 μ K for a density of 10^{14} atoms/cm³. A condensate is characterized by a macroscopic number of particles in the same quantum mechanical state described by a field function that depends on only one position vector. It is probably the most striking manifestation of the quantum nature of matter.

Quantum statistical effects that are essentially identical to BEC in gases have been observed and studied before in the superfluidity of liquid helium and the phenomenon of superconductivity. These effects are, however, difficult to study at a fundamental level because the particles are in a liquid or solid and strongly interacting. Observation of weakly interacting dilute gases relates much more to BEC in its ideal form (BEC in an ideal gas for which the concept was originally formulated by Einstein [6]) and allows a theoretical description from first principles. In analogy to lasers where large numbers of photons – massless bosons – are emitted in the same mode, Bose-Einstein condensates could be used as a source of coherent matter waves. The first steps toward this goal have been taken [7,8].

Besides BEC the interest in Fermi degeneracy in cold dilute alkali gases has rapidly grown [9–11]. Fermi degeneracy is the generic name for all quantum statistical effects that occur in a system of fermionic particles when their de Broglie wavelength becomes of the order of the interparticle distance. A gas of fermionic lithium atoms is predicted to become superfluid at temperatures and densities comparable to those at which the BEC experiments are performed [9,11].

Although all the above phenomena occur in dilute gases, atomic interactions play a crucial role in them. For example, they determine the shape and stability of Bose-Einstein condensates and set limits on the experimental possibilities. Due to the low

densities binary collisions nevertheless dominate, facilitating a detailed theoretical description. But interactions between cold atoms have become the subject of intensive study not only because of their importance to the above new areas of cold-atom physics, but also because it is possible to manipulate them with radiative or static magnetic fields and because cold-atom interaction processes have proved to be a powerful tool for measuring atomic and molecular parameters. This thesis contains theoretical contributions to the investigation of cold-atom interaction processes that address each of these three aspects.

1.2 Cold-Atom Interaction Processes

The low-temperature regime for atomic interaction processes is usually divided into the cold (roughly 1 mK to 1 μ K) and ultracold ($\lesssim 1 \mu$ K) regime. Light forces are used to cool gas samples to temperatures in the cold regime (laser cooling [12]). In this regime a few partial waves contribute to collisions. In the ultracold regime only s -waves contribute and elastic collisions between the atoms can be characterized by only one parameter: the scattering length a . The sign of the scattering length indicates whether the atomic interaction is effectively repulsive ($a > 0$) or attractive ($a < 0$). Bose-Einstein condensates in dilute gases are in the ultracold regime.

Below about 1 μ K, the mean translational kinetic energy of the atoms lies below the recoil energy from a photon scattering event and cooling with light forces is no longer possible. Instead, evaporative cooling in a magnetic trap is used. This kind of trap is based on the shift in the internal energy of the atoms under the influence of a magnetic field. Alkali atoms can exist in one of several hyperfine states that are associated with different orientations of their magnetic dipole moment. Depending on this orientation, there are states with increasing energy and with decreasing energy with increasing field strength. These are called low-field and high-field seeking, respectively. Thus, atoms polarized in a low-field seeking state can be confined in a static magnetic field with a local minimum in field strength. A magnetic field maximum cannot exist in free space, so that high-field seeking states cannot be trapped in this way.

The basic idea of evaporative cooling is a gradual lowering of the potential walls enclosing the atom (for technical details see [13]). This leads to the escape of atoms with the highest translational energies. The atoms with lower energies that cannot escape rethermalize through elastic collisions and the Maxwell-Boltzmann distribution is continuously changed to that for a much lower temperature. This cooling method is a good example of the important role that atomic interactions play in cold-atom physics: the rethermalization rate, and therefore the evaporative cooling rate, depends on the elastic scattering cross section proportional to a^2 .

A second example is formed by inelastic collisions: collisions that change the internal

state of the colliding atoms. If low-field seeking atoms are converted to high-field seeking in a magnetic trap, trap loss will result. The most important cause of trap loss, however, is exothermal collisions where one or both colliding atoms make a transition to a state with a lower internal energy; the excess internal energy is converted into translational energy. Energy differences between the internal states are often of the order of 1 K and thus much larger than the depth of traps for ultracold atoms. With knowledge of inelastic collision rates one can predict which (combinations of) internal states can be confined in which trap for how long.

Thirdly, the properties of a condensate strongly depend on the scattering length a . The behavior of an ultracold dilute atomic gas is conveniently described in a field-theory formalism where the actual interactions between the atoms have been replaced by a delta-function pseudopotential proportional to a . A condensate that has formed in the gas is described by a coherent field $\phi(\vec{x}, t)$. In the mean-field approximation the behavior of ϕ is governed by the Gross-Pitaevskii equation [14]

$$i\hbar\dot{\phi} = \left(-\frac{\hbar^2}{2m}\nabla^2 + V_{trap}(\vec{x}) + U|\phi|^2 \right) \phi \quad (1.1)$$

with

$$U = \frac{4\pi\hbar^2 a}{m}, \quad (1.2)$$

where m is the atomic mass and V_{trap} is the trap potential. The mean-field or self-energy term $U|\phi|^2$ results from a Hartree-Fock average of the above delta-function pseudopotential. It is an example of a ‘‘coherent’’ collisional effect proportional to a rather than to its square. Other examples are the refraction of matter waves [15] and atomic clock frequency shifts [16].

The sign of the scattering length plays a pivotal role in the stability of Bose-Einstein condensates. The repulsive interaction associated with positive a tends to stabilize a condensate. For negative a , Eq. (1.1) with $V_{trap} = 0$ does not have a stationary solution. In practice, this probably means that the repulsive interactions will bring all atoms close together, three- and many-body collisions will produce molecules and the gas may even condense to a solid. With a harmonic trap potential the Gross-Pitaevskii equation does have a stable solution, but only if the mean-field energy is less than the spacing of the trap levels [17]. This sets a maximum to the number of atoms in the condensate. When $a = 0$ the atoms effectively do not interact and the stationary solution of the Gross-Pitaevskii equation equals the single-atom ground-state wave function in the trap potential (except for normalization).

In order to more fully understand the effect of atomic interactions on condensates, it would clearly be desirable to be able to tune the scattering length to an arbitrary value. This would allow for studies of BEC in very strong or weak interaction limits,

and it might also be possible to study the dynamics of the collapse of a condensate induced by a sudden switch of the sign of a , all in a single experiment. One promising method to realize this, proposed by Tiesinga *et al.* [18], employs magnetically tunable Feshbach resonances. Feshbach resonances are scattering resonances that arise when the total energy (internal + translational) of a pair of colliding atoms matches the energy of a quasibound two-atom state, leading to the resonant formation of this state during the collision. Magnetic tuning is possible if the magnetic moments of the free and quasibound states are different, and this allows for the tuning of the scattering length. In collaboration with Heinzen and his group at the University of Texas, Austin, a part of the work reported in this thesis was devoted to observing and analyzing such a resonance for the first time in ^{85}Rb . Almost simultaneously, Ketterle's group at MIT observed a Feshbach resonance in a sodium condensate.

Finally, we return to the cold regime and mention photoassociation spectroscopy as a powerful tool to measure atomic interaction parameters and to gain insight in scattering processes. In fact, we demonstrated that photoassociation is a good probe for observing Feshbach resonances and our colleagues in Austin indeed used this method. In the photoassociation process a laser optically excites two colliding ground-state atoms into a bound electronically excited molecular state, which then decays back to free atoms with translational energy large enough to leave the trap. The resulting decrease in the number of trapped atoms is measured. The potential of this method lies in the fact that the transition rate to the molecular state is very sensitive to the shape of the ground-state radial wave function.

1.3 This Thesis

This thesis is based on five papers, published in the literature, that address different topics related to interactions between cold and ultracold alkali atoms. Before we proceed to these research contributions, however, we want to introduce the reader to some fundamental concepts of cold collision physics and methods of calculation that we use. This is done in chapter 2. It describes the different interaction terms that appear in the Schrödinger equation for interaction processes between alkali atoms and how we calculate collision rates and scattering lengths. Special attention is given to scattering properties in the ultracold limit and a useful parametrization of the interactions valid in the entire relevant energy range. At the end of this chapter, Feshbach resonances and photoassociation are treated in more detail.

Chapter 3, which contains the first published paper, deals with Feshbach resonances in a time-dependent magnetic field. We explain the extremely rapid decay that was observed in an experiment investigating these resonances in a Na Bose-Einstein condensate. Chapters 4 and 5 describe our work on the ^{85}Rb Feshbach resonance, leading

to a prediction for ^{85}Rb interaction parameters that are crucial for the actual application of this resonance to change the sign and strength of the atomic interactions in a ^{85}Rb condensate. In chapter 6 we redirect our attention to Fermi degeneracy. Its realization is complicated by the fact that evaporative cooling does not work for spin-polarized fermions at very low temperatures. We show, through analysis of photoassociation data and measured bound-state binding energies, and via calculation of scattering properties, that there are two possible solutions in the case of ^6Li : sympathetic cooling (cooling ^6Li with evaporatively cooled bosonic ^7Li atoms) or using ^6Li atoms in different internal states. The thesis is concluded with a chapter in which we present a thorough simultaneous analysis of three different experiments on Na that we have used to determine with high precision all parameters describing the interactions between cold Na atoms. This has enabled us to make accurate predictions for all Na cold-atom scattering properties. These predictions have been of great help to experimental groups, especially Ketterle's group at MIT. Moreover, our results have been used to confirm the reliability of *ab initio* calculations of van der Waals interactions.

References

- [1] M.H. Anderson, J.R. Ensher, M.R. Matthews, C.E. Wieman, and E.A. Cornell, *Science* **269**, 198 (1995).
- [2] C.J. Myatt, E.A. Burt, R.W. Ghrist, E.A. Cornell, and C.E. Wieman, *Phys. Rev. Lett.* **78**, 586 (1997).
- [3] K.B. Davis, M.-O. Mewes, M.R. Andrews, N.J. van Druten, D.S. Durfee, D.M. Kurn, and W. Ketterle, *Phys. Rev. Lett.* **75**, 3969 (1995); M.-O. Mewes, M.R. Andrews, N.J. van Druten, D.M. Kurn, D.S. Durfee, and W. Ketterle, *Phys. Rev. Lett.* **77**, 416 (1996).
- [4] C.C. Bradley, C.A. Sackett, J.J. Tollett, and R.G. Hulet, *Phys. Rev. Lett.* **75**, 1687 (1995); C.C. Bradley, C.A. Sackett, and R.G. Hulet, *Phys. Rev. Lett.* **78**, 985 (1997).
- [5] D.G. Fried, T.C. Killian, L. Willmann, D. Landhuis, S.C. Moss, D. Kleppner, and T.J. Greytak, *Phys. Rev. Lett.* **81**, 3811 (1998).
- [6] A. Einstein, *Sitzungsber. Kgl. Preuss. Akad. Wiss.* **1924**, 261 (1924); *ibid.* **1925**, 3 (1925).
- [7] M.-O. Mewes, M. R. Andrews, D. M. Kurn, D. S. Durfee, C. G. Townsend, and W. Ketterle, *Phys. Rev. Lett.* **78**, 582 (1997).
- [8] L. Deng, E.W. Hagley, J. Wen, M. Trippenbach, Y. Band, P.S. Julienne, J.E. Simsarian, K. Helmerson, S.L. Rolston, and W.D. Phillips, *Nature* **398**, 218 (1999).
- [9] H.T.C. Stoof, M. Houbiers, C.A. Sackett, and R.G. Hulet, *Phys. Rev. Lett* **76**, 10 (1996); M. Houbiers, R. Ferwerda, H.T.C. Stoof, W.I. McAlexander, C.A. Sackett, and R.G. Hulet, *Phys. Rev. A* **56**, 4864 (1997).
- [10] B. DeMarco, D.S. Jin, *Phys. Rev. A* **58**, R4267 (1998).
- [11] J.M.V.A. Koelman, Ph. D. thesis, Eindhoven University, The Netherlands, 1988 (unpublished), p. 41.

- [12] *Laser Cooling and Trapping of Atoms*, J. Opt. Soc. Am. B **6**, special issue (1989).
- [13] W. Ketterle and N.J. van Druten, in *Advances in Atomic, Molecular, and Optical Physics* **36**, edited by B. Bederson and H. Walther (Academic Press, London, 1996).
- [14] F. Dalfovo, S. Giorgini, L.P. Pitaevskii, and S. Stringari, Rev. Mod. Phys. **71**, 463 (1999)
- [15] J. Vigué, Phys. Rev. A **52**, 3973 (1995).
- [16] B.J. Verhaar, in *Atomic Physics* **14**, edited by C.E. Wieman, D.J. Wineland, and S.J. Smith (AIP, New York, 1995), p. 351–368.
- [17] Yu. Kagan, E.L. Surkov, and G.V. Shlyapnikov, Phys. Rev. Lett. **79**, 2604 (1997).
- [18] E. Tiesinga, A.J. Moerdijk, B.J. Verhaar, and H.T.C. Stoof, Phys. Rev. A **46**, R1167 (1992); E. Tiesinga, B.J. Verhaar, and H.T.C. Stoof, *ibid.* **47**, 4114 (1993).

2

Basic Concepts

2.1 The Effective Hamiltonian

In a quantum mechanical description of interaction processes between alkali atoms (without external forces), one should in principle take into account the electric and magnetic forces between all electrons and nuclei involved in the process. A large part of a collision between cold alkali atoms, however, takes place at large interatomic separations ($r \gtrsim 15$ Bohr radii), where a picture of separated atoms is a good starting point. At smaller separations the interaction between the atoms is completely dominated by Coulomb forces that can relatively easily be fully taken into account. These observations suggest that a simplified description is possible. This is confirmed by previous experience, gathered to a large extent in our group. It shows that the problem can be reformulated in terms of an effective Hamiltonian [1,2] that depends only on the inter-nuclear separation(s) and the total nuclear and electron spins of the individual atoms. It is essentially based on the well-known Born-Oppenheimer approximation and the Shizgal [3] approximation, which assumes that all spins are located at the position of their respective nucleus.

For collisions of two ground-state alkali atoms we have used the Hamiltonian

$$H = \frac{\vec{p}^2}{2\mu} + \sum_{j=1}^2 \left(V_j^{hf} + V_j^Z \right) + V^c, \quad (2.1)$$

comprising the relative kinetic energy operator with reduced mass μ , a single-atom hyperfine and Zeeman term for each atom, and a central two-atom interaction term V^c . The hyperfine terms V_j^{hf} are given by

$$V_j^{hf} = \frac{a_j^{hf}}{\hbar^2} \vec{s}_j \cdot \vec{v}_j, \quad (2.2)$$

where \vec{s}_j and \vec{v}_j are the electron and nuclear spin operators of atom j and a_j^{hf} a constant related to the hyperfine splitting. We will use lower case letters for single-atom spin operators and quantum numbers and reserve capital letters for two-atom spins. Since alkali atoms have only one valence electron, $s_1 = s_2 = \frac{1}{2}$. In ground-state atoms the hyperfine splitting originates from the Fermi-contact term. The Zeeman interaction terms are included to account for the magnetic field present in many cold-atom scattering experiments. Choosing the z -axis of the laboratory frame along the

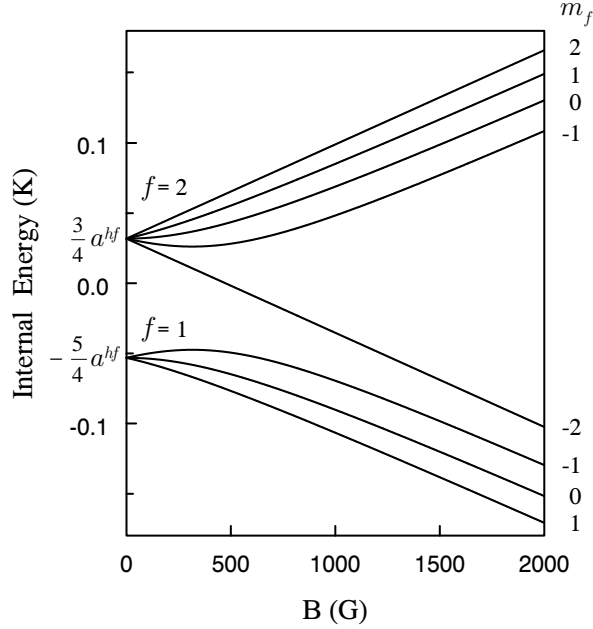


Figure 2.1 Hyperfine diagram for ground-state Na atoms ($a^{hf} = 42.51$ mK). The hyperfine diagrams for ground-state atoms of other alkali species with nuclear spin quantum number $i = \frac{3}{2}$ can be obtained by scaling to the appropriate value of a^{hf} . For ${}^7\text{Li}$, $a^{hf} = 19.28$ mK.

magnetic field $\vec{B} = B \hat{z}$, they have the familiar form

$$V_j^Z = (\gamma_e s_{zj} - \gamma_N i_{zj}) B. \quad (2.3)$$

We assume that variations in the magnetic field are negligible over distances of the order of the interaction range (~ 50 nm).

Asymptotically, where the two-atom interaction V^c can be neglected, the system is described by separate atoms, each in an eigenstate of its own hyperfine and Zeeman operators. These are the magnetic-field dependent hyperfine states $|f, m_f\rangle$, where $\vec{f} = \vec{s} + \vec{i}$ and the quantization axis is parallel to \vec{B} . For larger magnetic fields f is not a good quantum number, but it is still used to label the one-atom eigenstates. Figure 2.1 shows the hyperfine diagram for ${}^{23}\text{Na}$ with $i = \frac{3}{2}$. The states with $f = i + \frac{1}{2}$ and $m_f = \pm f$ are called the doubly polarized states. Here, the electron and nuclear spins are fully stretched in the same direction parallel or antiparallel to the magnetic field. Consequently, their spin structure does not depend on the magnetic field strength, contrary to that of the other hyperfine states. The differences in field dependence between the hyperfine states are responsible for Feshbach resonances. Tensor products of the one-atom hyperfine states will form the basis for the description of ground-state collisions.

The central interaction V^c represents all Coulomb interactions between the electrons and the nuclei of both atoms. It depends only on the quantum number S associated with the magnitude of the total electron spin $\vec{S} = \vec{s}_1 + \vec{s}_2$, which can be 0 or 1 for alkali atoms, and the internuclear distance r :

$$V^c = V_S(r) P_S + V_T(r) P_T, \quad (2.4)$$

with P_S and P_T the projection operators on the singlet ($S = 0$) and triplet ($S = 1$) subspaces. The potentials V_S and V_T are the two Born-Oppenheimer molecular potential curves connected to the ${}^2S_{1/2} + {}^2S_{1/2}$ separated-atom limit; in spectroscopic notation the corresponding molecular electronic states are $X\,{}^1\Sigma_g^+$ and $a\,{}^3\Sigma_u^+$. If, for the sake of simplicity, we temporarily limit ourselves to the valence electrons with coordinates \vec{r}_1 and \vec{r}_2 , these states $\Psi_{S,T}$ have the asymptotic behavior

$$\Psi_{S,T}(r; \vec{r}_1, \vec{r}_2) \underset{r \rightarrow \infty}{=} \frac{1}{\sqrt{2}} [\varphi_A(\vec{r}_1) \varphi_B(\vec{r}_2) \pm \varphi_A(\vec{r}_2) \varphi_B(\vec{r}_1)], \quad (2.5)$$

where φ_A and φ_B are the atomic ${}^2S_{1/2}$ states centered at nucleus A or B . Referring to the subspaces in which they work V_S and V_T are called singlet and triplet potential. Note that in the effective Hamiltonian (2.1) the atomic reduced mass is used instead of the nuclear mass which one would expect from the standard Born-Oppenheimer procedure. This effectively accounts [4] for the adiabatic correction terms (proportional to $\langle \Psi_{S,T}(r; \vec{r}_1, \vec{r}_2) | d^2/dr^2 | \Psi_{S,T}(r; \vec{r}_1, \vec{r}_2) \rangle$).

The singlet and triplet potentials are quite different. The singlet potential is the most attractive one of the two. Due to the Pauli principle the triplet curve is much shallower and the internuclear separation where the potentials become strongly repulsive is several Bohr radii a_0 larger for V_T than for V_S . A comparison of the number of bound states supported by the potentials is also illustrative: for sodium the singlet potentials has 66 zero angular momentum bound states, while the triplet potential has only 16. Figure 2.2 shows the curves for sodium.

At large separations ($r > 16 a_0$ to $19 a_0$, depending on the atom species), the central potentials may be written as

$$V_{S,T}(r) = -\frac{C_6}{r^6} - \frac{C_8}{r^8} - \frac{C_{10}}{r^{10}} \mp V_E(r). \quad (2.6)$$

The first term represents the van der Waals interaction. It is followed by the next two terms in an electric multipole expansion of the Coulomb interactions between the charge distributions of the two colliding atoms: the dipole-quadrupole and quadrupole-quadrupole interactions. The different permutation symmetries of the molecular electronic wave functions Ψ_S and Ψ_T are responsible for the exchange energy $V_E(r)$. The dispersion coefficients C_6 , C_8 and C_{10} can be calculated with a model containing parameters that are fitted to measured quantities such as the atomic static electric dipole

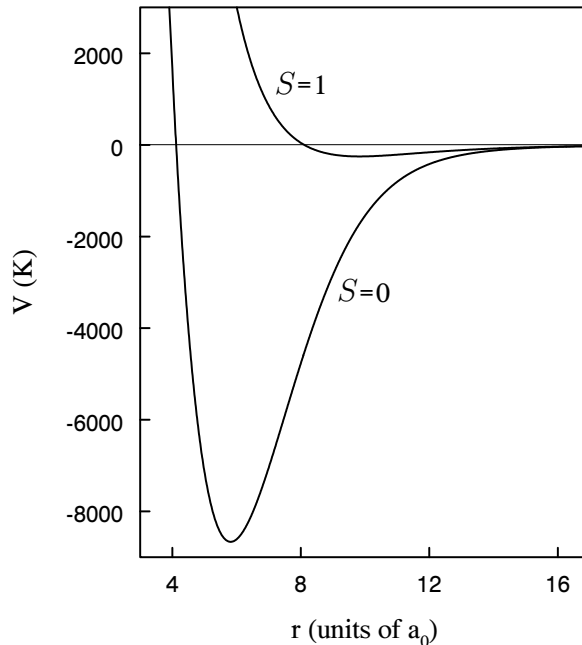


Figure 2.2 Na_2 singlet ($S = 0$) and triplet ($S = 1$) ground-state potentials.

polarizabilities, or even completely *ab initio*. For several years, the coefficients calculated by Marinescu *et al.* [5] for all pairs of identical alkali atoms up to cesium have been the most widely used. They have an estimated accuracy of about 5 %. In the meantime even more accurate values have been calculated for all Li coefficients [6] and for the van der Waals coefficients C_6 [7] for the other alkalis. It should be emphasized that all electrons of the atom pair, including the core electrons of both atoms, are taken into account in these calculations.

Smirnov and Chibisov have derived a general analytic formula for the long-range exchange interaction energy. It has the form [8]

$$V_E(r) = A r^{7/2\alpha-1} e^{-2\alpha r}, \quad (2.7)$$

where $-\alpha^2/2$ is the atomic valence electron binding energy and A is equal to an integral depending on α and a normalization parameter for the atomic long-range valence electron wave function. The α and A parameters following from present standard atomic data have been summarized recently for all pair of identical alkali atoms up to Cs [9]. In a small r -range near the beginning of the long-range region ($r \approx 20 a_0$), the exchange interaction V_E is of the same order of magnitude as the hyperfine-Zeeman energies. This is a crucial region because transitions between hyperfine states take place here. Trap loss caused by these transitions is called exchange decay. Accurate

knowledge of the long-range potential is very important in the theory of interaction processes between cold atoms because the potential is effective up to large r for small collision energies.

Several methods are used to determine the inner part of V_S and V_T , either based on analyzing experimental data or on *ab initio* calculations. By means of the Rydberg-Klein-Rees (RKR) procedure [10] it is possible to construct a potential curve from the energy spacings of bound states, which can be measured with spectroscopic techniques. The part of the curve that can be obtained with this procedure is limited by the inner and outer turning points of the measured bound states. If the RKR curve does not overlap the long-range tail (2.6), it is often connected to it by means of a cubic spline. The strongly repulsive inner wall is usually extrapolated to smaller r as far as necessary. A hybrid potential constructed in this way will certainly contain errors and will not perfectly reproduce the measured energy spacings. To correct this one often turns to Inverse Perturbation Analysis (IPA) [11, 12]. The required r -dependent correction to the potential is written as a sum of basis functions with unknown coefficients which are optimized with a least-squares method that minimizes χ^2 for the bound-state energy spacings. This procedure is repeated for the resulting potential until convergence is reached.

Good results [12] have been achieved with IPA potentials, but high-precision calculations of collisional properties for small collision energies based on these potentials have still been limited by the quality of some bound-state energy measurements or the absence of data on the highest bound states that control the low collision energy behavior. Recently, however, several high-precision measurements of the binding energies of these states [13–15] have become available. On top of that the experimental determination of Feshbach resonance fields [16, 17] and measurement of the low-energy continuum wave function itself via photoassociation [18–21] have provided important data on the atomic interactions. In this thesis we have used this new information to improve our knowledge of the Li, Na, and Rb interactions. For describing atomic interaction processes in the low-temperature limit, one does not need complete potential curves. Instead a few interaction parameters suffice. We have used this fact in our calculations. Details will be given in section 2.4.

The *ab initio* approach [22, 23] to the inner part of the potential curves so far has not led to potentials that are accurate enough for doing reliable cold collision calculations. To our knowledge, only one curve [24] – for the Na triplet potential – published after the appearance of our paper on sodium interactions (chapter 7 of this thesis), may be able to compete with interaction parameters found from high-precision measurements.

An interaction that is often included in the effective Hamiltonian (2.1), but has been omitted here, is the magnetic dipole-dipole interaction. It has one electron-electron and two electron-nuclear contributions (the nuclear-nuclear contribution can always be

neglected) that can each be written in the form

$$V^d = \mu_0 \frac{\vec{\mu}_1 \cdot \vec{\mu}_2 - 3(\hat{r} \cdot \vec{\mu}_1)(\hat{r} \cdot \vec{\mu}_2)}{4\pi r^3}, \quad (2.8)$$

where $\vec{\mu}_1$ is the spin magnetic dipole moment of the electrons or the nucleus of one atom and $\vec{\mu}_2$ that of the electrons or nucleus of the other atom. This weak interaction can cause inelastic collisions that lead to loss of atoms from a trap. But this decay process has a time constant (typically 1 min or longer) that is several orders of magnitude larger than that for the inelastic processes (exchange decay, photoassociation) studied in this thesis. Also, it has a negligible effect on elastic processes. Therefore we have left it out of our calculations. Finally, we mention the second-order spin-orbit interaction which couples the molecular ground state to molecular states with one or two excited atoms. This interaction is important in interactions between the heaviest alkali atoms cesium and francium, but relatively unimportant or negligible in case of the lighter ones.

2.2 Coupled Channels and Rate Coefficients

In the framework of the effective Hamiltonian the hyperfine states $|f, m_f\rangle$ form a complete basis for the internal state of an atom. If two distinguishable atoms (with different numbers of protons or neutrons) interact, the collision can be conveniently described using two-body internal-state vectors of the form

$$|\alpha\beta\rangle \equiv |\alpha\rangle_1 |\beta\rangle_2, \quad (2.9)$$

where the subscripts indicate atom 1 or 2 and α and β label the one-atom hyperfine states in shortened form. In collisions between atoms of the same species, the atoms behave as indistinguishable compound bosons (f is an integer) or fermions (f is half-odd-integral) and their total state vector (internal + orbital motion) is required to be (anti)symmetric under exchange of atoms. It is then useful to introduce the (anti)symmetrized two-body hyperfine states

$$\left| \{\alpha\beta\}^\pm \right\rangle \equiv \frac{|\alpha\rangle_1 |\beta\rangle_2 \pm |\alpha\rangle_2 |\beta\rangle_1}{\sqrt{2(1 + \delta_{\alpha\beta})}}. \quad (2.10)$$

Usually, the Hamiltonian H is time-independent and collisions can be described by stationary scattering states. To solve the time-independent Schrödinger equation $H|\Psi\rangle = E_{tot}|\Psi\rangle$ we introduce a basis of so-called channel states, based on the above two-body internal states and spherical harmonics $|l m_l\rangle$ for the angular part of the orbital motion. For collisions between distinguishable atoms these are labeled $|l m_l \alpha\beta\rangle$. In the case of indistinguishable bosons (fermions) the channel states are labeled $|l m_l \{\alpha\beta\}^+\rangle$ for even (odd) l , and $|l m_l \{\alpha\beta\}^-\rangle$ for odd (even) l . Note that

all states have the proper permutation symmetry. In equations that are valid for all three bases the general form $|l m_l \{\alpha\beta\}\rangle$ is used. Now, $\langle \vec{r} | \Psi \rangle$ is expanded in terms of the channel states:

$$\langle \vec{r} | \Psi \rangle = \sum_{\{\alpha\beta\}} \sum_{l, m_l} \frac{u_{lm_l\{\alpha\beta\}}(r)}{r} i^l Y_{lm_l}(\hat{r}) |\{\alpha\beta\}\rangle. \quad (2.11)$$

The notation $\{\alpha\beta\}$ under the sum symbol means that the sum should be taken over all different combinations of α and β . Only in the case of distinguishable atoms this is identical to separate sums over α and β . In the other cases $\{\alpha\beta\}$ and $\{\beta\alpha\}$ are identical. Also note that $|\{\alpha\alpha\}^-\rangle = 0$ so that the corresponding terms can be left out of the summation. Substituting expression (2.11) into the Schrödinger equation and projecting onto each of the channel states gives the following system of coupled differential equations for the radial wave functions $u_{lm_l\{\alpha\beta\}}(r)$:

$$\left[-\frac{\hbar^2}{2\mu} \frac{d^2}{dr^2} + \frac{l(l+1)\hbar^2}{2\mu r^2} + \varepsilon_\alpha + \varepsilon_\beta - E_{tot} \right] u_{lm_l\{\alpha\beta\}}(r) = - \sum_{\{\alpha'\beta'\}} \sum_{l', m'_l} C_{lm_l\{\alpha\beta\}, l'm'_l\{\alpha'\beta'\}}(r) u_{l'm'_l\{\alpha'\beta'\}}(r), \quad (2.12)$$

in which the coupling matrix is defined by

$$C_{lm_l\{\alpha\beta\}, l'm'_l\{\alpha'\beta'\}}(r) = i^{l'-l} \langle l m_l \{\alpha\beta\} | V^c | l' m'_l \{\alpha'\beta'\} \rangle. \quad (2.13)$$

These equations are referred to as the coupled-channels equations. The energies ε_α and ε_β are the internal energies of the separate atoms: $(V_1^{hf} + V_1^Z) |\alpha\rangle = \varepsilon_\alpha |\alpha\rangle$ and $(V_2^{hf} + V_2^Z) |\beta\rangle = \varepsilon_\beta |\beta\rangle$. Due to symmetries of the physical system the total system of coupled-channels equations (2.12) can be divided into many mutually uncoupled systems that contain only a few channels. First, the projection of the total angular momentum $\vec{\mathcal{F}} = \vec{l} + \vec{F} = \vec{l} + \vec{f}_1 + \vec{f}_2$ on the magnetic field axis is conserved since an arbitrary rotation of the total system around this axis is a symmetry operation. Secondly, because V^c does not depend on \hat{r} , the orbital angular momentum quantum numbers l and m_l are conserved. And finally, conservation of $m_{\mathcal{F}}$ and m_l also implies that transitions between channel states with different m_F are not allowed. The simplified coupled-channels equations are

$$\left[-\frac{\hbar^2}{2\mu} \frac{d^2}{dr^2} + \frac{l(l+1)\hbar^2}{2\mu r^2} + \varepsilon_\alpha + \varepsilon_\beta - E_{tot} \right] u_{\{\alpha\beta\}}^l(r) = - \sum_{\substack{\{\alpha'\beta'\} \\ m_{f_1} + m_{f_2} = m_F}} C_{\{\alpha\beta\}, \{\alpha'\beta'\}}(r) u_{\{\alpha'\beta'\}}^l(r) \quad (2.14)$$

with

$$C_{\{\alpha\beta\},\{\alpha'\beta'\}}(r) = \langle \{\alpha\beta\} | V^c | \{\alpha'\beta'\} \rangle . \quad (2.15)$$

The subscript m_l has been dropped from the radial wave functions because they are independent of this quantum number. The quantum number l is now written as a superscript to indicate that it is conserved. Note that $C_{\{\alpha\beta\},\{\alpha'\beta'\}}$ is different for odd and even l when the colliding atoms are identical bosons or fermions. For zero magnetic field \mathcal{F} and F are also good quantum numbers and the problem can be even further simplified. This fact is used in section 4 of chapter 7.

The coupled-channels equations alone do not completely determine the radial wave functions $u_{\{\alpha\beta\}}^l(r)$. They must be combined with the boundary conditions

$$\begin{cases} u_{\{\alpha\beta\}}^l(0) = 0 \\ u_{\{\alpha\beta\}}^l(r) \underset{r \rightarrow \infty}{\sim} i \sqrt{\frac{\mu}{2\pi\hbar^2 k_{\alpha\beta}}} \left[\hat{h}_l^-(k_{\alpha\beta}r) - S_{\{\alpha\beta\},\{\gamma\delta\}}^l(E) \hat{h}_l^+(k_{\alpha\beta}r) \right] & \text{if } \{\alpha\beta\} = \{\gamma\delta\} \\ u_{\{\alpha\beta\}}^l(r) \underset{r \rightarrow \infty}{\sim} i \sqrt{\frac{\mu}{2\pi\hbar^2 k_{\alpha\beta}}} S_{\{\alpha\beta\},\{\gamma\delta\}}^l(E) \hat{h}_l^+(k_{\alpha\beta}r) & \text{if } \{\alpha\beta\} \neq \{\gamma\delta\}, \end{cases} \quad (2.16)$$

for a certain choice of entrance state $\{\gamma\delta\}$. Here, \hat{h}_l^- and \hat{h}_l^+ are the Riccati-Hankel functions representing incoming and outgoing waves: $\hat{h}_l^\pm(kr) \underset{r \rightarrow \infty}{\sim} e^{\pm i(kr - l\frac{\pi}{2})}$. Implicitly, we have defined the asymptotic magnitude of the momentum in channels with internal state $|\{\alpha\beta\}\rangle$ as

$$\hbar k_{\alpha\beta} = \sqrt{2\mu(E_{tot} - \varepsilon_\alpha - \varepsilon_\beta)}, \quad (2.17)$$

where the square root is positive real (open channels) or positive imaginary (closed channels; \hat{h}_l^+ becomes an exponentially vanishing function). The relative kinetic energy $E \equiv \hbar^2 k^2 / 2\mu = E_{tot} - \varepsilon_\gamma - \varepsilon_\delta$ in the incident channel is the collision energy that is important for thermal averaging and the threshold behavior discussed in the next section. Also, we have introduced the elements of the S -matrix from which the elastic and inelastic collision rates can be calculated (only the elements for the open channels have a physical meaning). The asymptotic behavior of the radial wave function in the entrance channel can also be written as

$$u_{\{\gamma\delta\}}^l(r) \underset{r \rightarrow \infty}{\sim} \sqrt{\frac{2\mu}{\pi\hbar^2 k}} e^{i\eta_{\{\gamma\delta\}}^l(k)} \sin \left[kr - l\frac{\pi}{2} + \eta_{\{\gamma\delta\}}^l(k) \right], \quad (2.18)$$

where $\eta_{\{\gamma\delta\}}^l$ is the phase shift induced by the interaction and related to the elastic S -matrix element by $S_{\{\gamma\delta\},\{\gamma\delta\}}^l = e^{2i\eta_{\{\gamma\delta\}}^l}$. If there is only one open channel in the

system of coupled-channels equations (elastic scattering), the associated phase shift is real, $|S_{\{\gamma\delta\},\{\gamma\delta\}}^l|^2 = 1$ and the problem is similar to the simple scattering of two particles without internal states. But as soon as there are more than one open channels, $\eta_{\{\gamma\delta\}}^l$ becomes a complex number.

The solutions of (2.14) and (2.16) are denoted by the vectors $\underline{u}_{\{\gamma\delta\}}^l(r; E)$ with all radial wave functions $u_{\{\alpha\beta\}}^l(r)$ coupled to entrance-channel wave function $u_{\{\gamma\delta\}}^l(r)$ (i.e. with the same l and m_F) as components. It is these vectors that we compute in our numerical calculations. To that end we write Eq. (2.14) in the matrix notation

$$\frac{d^2}{dr^2} \underline{u}(r) = \frac{2\mu}{\hbar^2} \tilde{\underline{C}}(r) \underline{u}(r), \quad (2.19)$$

where the columns of \underline{u} represent a complete set of linearly independent solution vectors. The tilde on the coupling matrix indicates that it contains also the diagonal energy and centrifugal terms on the left hand side of Eq. (2.14). This equation is integrated using a modified Numerov method [25], a $O(\hbar^6)$ two-step method. Due to exponential growth of the solutions in locally closed channels for which $\tilde{C}_{\{\alpha\beta\},\{\alpha\beta\}}(r) > 0$, the boundary conditions at the origin can be fulfilled by starting the integration from left to right with $\underline{u}(r_s) = 0$ and $\underline{u}(r_s + h) = \underline{I}$ for sufficiently small r_0 . The desired solutions $\underline{u}_{\{\gamma\delta\}}^l(r; E)$ and the S -matrix are found by connecting to the result of an inward integration started at large r with a diagonal \underline{u} -matrix containing Hankel-like radial wave functions.

To show the relation of the solution vectors $\underline{u}_{\{\gamma\delta\}}^l(r; E)$ to some well-known expressions from scattering theory we define (in coordinate representation) the partial waves

$$\langle \vec{r} | \Psi_{\{\gamma\delta\}}^{lm_l+}(E) \rangle \equiv \sum_{\{\alpha\beta\}} \left[\underline{u}_{\{\gamma\delta\}}^l(r; E) \right]_{\{\alpha\beta\}} \frac{1}{r} i^l Y_{lm_l}(\hat{r}) | \{\alpha\beta\} \rangle, \quad (2.20)$$

in which the sum is taken over the components of \underline{u} . Due to the choice of the leading factors in the boundary conditions (2.16) the partial waves are energy-normalized:

$$\langle \Psi_{\{\gamma\delta\}}^{lm_l+}(E) | \Psi_{\{\gamma'\delta'\}}^{l'm_l'+}(E') \rangle = \delta_{ll'} \delta_{m_l m_l'} \delta_{\{\gamma\delta\} \{\gamma'\delta'\}} \delta(E - E'). \quad (2.21)$$

Evaluating the sum

$$\frac{1}{\sqrt{\mu \hbar k_{\gamma\delta}}} \sum_{l, m_l} \left| \Psi_{\{\gamma\delta\}}^{lm_l+}(E) \right\rangle Y_{lm_l}(\hat{k}), \quad (2.22)$$

which is equivalent to the well-known expansion of a plane wave in terms of spherical harmonics, then gives the three-dimensional scattering state $|\Psi_{\{\gamma\delta\}}^+(\vec{k})\rangle$. For distinguishable atoms it has the familiar asymptotic behavior

$$\langle \vec{r} | \Psi_{\gamma\delta}^+(\vec{k}) \rangle \underset{r \rightarrow \infty}{\sim} \frac{1}{(2\pi\hbar)^{3/2}} \left[e^{i\vec{k}\cdot\vec{r}} |\gamma\delta\rangle + \sum_{\alpha, \beta} f_{\alpha\beta, \gamma\delta}(\hat{r}; \vec{k}) \frac{e^{ikr}}{r} |\alpha\beta\rangle \right] \quad (2.23)$$

with

$$f_{\alpha\beta,\gamma\delta}(\hat{r}; \vec{k}) = \sum_l (2l+1) \frac{S_{\{\alpha\beta\},\{\gamma\delta\}}^l(E) - 1}{2ik} P_l(\hat{r} \cdot \vec{k}), \quad (2.24)$$

comprising an incident plane wave describing the relative motion of two atoms in internal states $|\gamma\rangle$ and $|\delta\rangle$ and scattered waves of atoms in these same internal states or other hyperfine states. For identical atoms $|\Psi_{\{\gamma\delta\}}^+(\vec{k})\rangle$ is proportional to the (anti)symmetrized version of (2.23).

To apply the above theory to actual experiments in dilute gases we must make the transition from the microscopic picture of the S -matrix to the macroscopic picture of a trapped gas containing atoms (possibly of different species) in different internal states $|\gamma\rangle$ with partial densities n_γ . From a quantum Boltzmann equation it can be derived [1] that the time evolution of the partial densities is governed by

$$\frac{d}{dt} n_\gamma = \sum_\delta \sum_{\{\alpha\beta\}} (1 + \delta_{\gamma\delta}) (G_{\alpha\beta \rightarrow \gamma\delta} n_\alpha n_\beta - G_{\gamma\delta \rightarrow \alpha\beta} n_\gamma n_\delta), \quad (2.25)$$

in which the rate coefficients are given by

$$\begin{aligned} G_{\gamma\delta \rightarrow \alpha\beta}(B, T) &= \left\langle \frac{1}{1 + \delta_{\gamma\delta}} v \sigma_{\alpha\beta,\gamma\delta}(v) \right\rangle_{\text{th}} \\ &= \left\langle v \frac{\pi}{k^2} \sum_l (2l+1) \left| S_{\{\alpha\beta\},\{\gamma\delta\}}^l(E) - \delta_{\{\alpha\beta\}\{\gamma\delta\}} \right|^2 \right\rangle_{\text{th}}. \end{aligned} \quad (2.26)$$

The notation $\langle \cdot \rangle_{\text{th}}$ stands for a thermal average over the collision velocity $\vec{v} = \hbar \vec{k} / \mu$ and $\sigma_{\alpha\beta,\gamma\delta}(v)$ is the angle-integrated cross section. Equation (2.26) is the appropriate expression for exothermal transitions ($\varepsilon_\gamma + \varepsilon_\delta > \varepsilon_\alpha + \varepsilon_\beta$) where $\left| S_{\{\alpha\beta\},\{\gamma\delta\}}^l(E) \right|^2$ can be interpreted as a transition probability, and is also valid for the elastic rate coefficients $G_{\gamma\delta \rightarrow \gamma\delta}$. It is sufficient to consider only these processes because the rate coefficients of any process and its reverse are related by [1]

$$G_{\alpha\beta \rightarrow \gamma\delta}(B, T) = G_{\gamma\delta \rightarrow \alpha\beta}(B, T) e^{-(\varepsilon_\gamma + \varepsilon_\delta - \varepsilon_\alpha - \varepsilon_\beta) / k_B T}, \quad (2.27)$$

when the translational degrees of freedom of the atoms are in thermal equilibrium.

The rate equation (2.25) describes the time evolution of partial densities assuming that all atoms stay in the trap. Often, however, exchange collisions in a cold gas lead to the loss of both colliding atoms from the trap and one is interested in the total decay rate. In the common case that the trap is loaded with atoms that are all in the same internal state $|\gamma\rangle$, this decay is described by

$$\frac{d}{dt} n_\gamma = -G_{\text{tot}}(B, T) n_\gamma^2 \quad (2.28)$$

with

$$G_{tot}(B, T) = \sum_{\{\alpha\beta\}} (2 - \delta_{\gamma\alpha} - \delta_{\gamma\beta}) G_{\gamma\gamma \rightarrow \alpha\beta}, \quad (2.29)$$

where the sum is over all possible decay channels, i.e. with the same m_F value as $|\gamma\gamma\rangle$ and reached via an exothermal transition. This follows directly from Eq. (2.25) neglecting endothermal transitions (we assume that $k_B T < \text{internal energy differences}$). Mostly (but not always [27]), exchange decay rate coefficients are so large that stability against them is an important requirement on a hyperfine state to be appropriate for trapping in a magnetic trap, apart from it being low-field seeking. In the case of sodium (see Fig. 2.1), for example, only the doubly polarized state $|f = 2, m_f = 2\rangle$ and the state $|f = 1, m_f = -1\rangle$ can be used. The first state is stable against exchange collisions because the corresponding two-atom hyperfine state is the only one with $m_F = 4$ and the collision proceeds purely along the triplet potential. The two-body state corresponding to the latter state is not the only one with $m_F = -2$ but there are no energetically accessible states with that m_F value. The states $|f = 1, m_f = 0\rangle$, $|f = 1, m_f = 1\rangle$ and $|f = 2, m_f = -2\rangle$ do not decay either for similar reasons but are high-field seeking. Recently, an optical trap has been used to hold Na condensates [28]. Optical traps have the advantage that the requirement with respect to the low-field seeking property does not play a role. As a consequence all $f = 1$ states can be trapped.

Finally, it is important to draw attention to the fact that the above expressions for the rate coefficients were derived for a thermal gas. In a Bose-Einstein condensate two-body rate coefficients are reduced by a factor of two (in general: n -body rates are reduced by a factor $n!$) [29]. Also, the low-temperature limit will apply so that

$$G_{\gamma\delta \rightarrow \alpha\beta}^{BEC}(B) = \frac{1}{2} \lim_{T \rightarrow 0} G_{\gamma\delta \rightarrow \alpha\beta}(B, T). \quad (2.30)$$

2.3 Scattering Properties in the Ultracold Limit

With decreasing temperature the de Broglie wavelength of the atoms becomes larger and larger with respect to the interaction range, causing the number of partial waves that contribute to scattering processes to decrease as well. In the ultracold limit only the spherically symmetric s -wave with $l = 0$ contributes (except for fermions in identical internal states; the antisymmetry requirement does not allow s -waves in that case and virtually no collisions will take place). Moreover, the $l = 0$ phase shifts simply vary as $\eta_{\{\gamma\delta\}}^0(k) = -k a_{\{\gamma\delta\}}$ as $k \rightarrow 0$, where $a_{\{\gamma\delta\}}$ is the (s -wave) scattering length defined by [30]

$$a_{\{\gamma\delta\}} \equiv - \lim_{k \rightarrow 0} \frac{\tan \left[\eta_{\{\gamma\delta\}}^0(k) \right]}{k}. \quad (2.31)$$

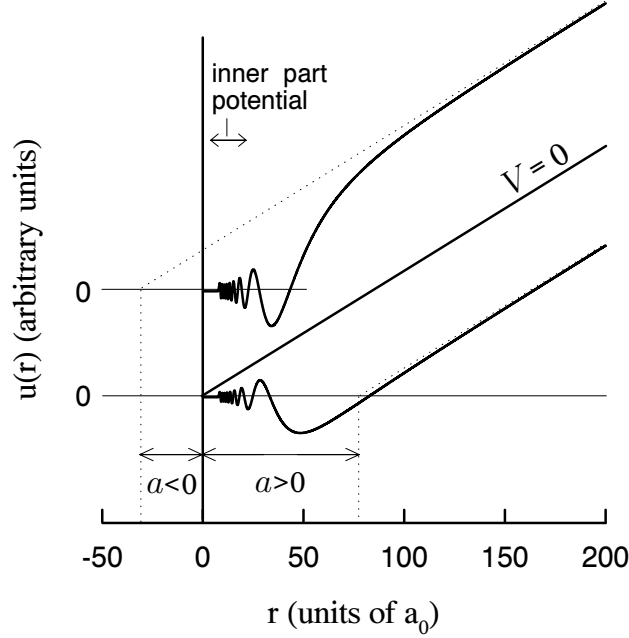


Figure 2.3 Radial scattering wave functions $u(r)$ at very low collision energy for two different model potentials with negative and positive scattering length a and for the case without interaction ($V = 0$). The scattering length can be found by extrapolating the solution at large distances to the r -axis. For clarity the r -axis has been shifted upwards for the radial wave function with negative a .

Instead of $a_{\{\gamma\gamma\}}$ we will write a_γ . The scattering length is primarily used to characterize elastic scattering processes for which it is a real number. As was mentioned before, it is an important parameter in the context of Bose-Einstein condensates. From Eq. (2.26) it follows that the elastic cross section for atoms in identical internal states, essential for evaporative cooling, approaches

$$\sigma_\gamma \equiv \sigma_{\gamma\gamma,\gamma\gamma} \rightarrow 8\pi a_\gamma^2 \quad (2.32)$$

in the low energy limit. The factor 8 instead of the usual 4 occurs due to identical particle symmetry. Note that the rate coefficients for elastic scattering vanish as $T^{1/2}$ for low temperatures.

Figure 2.3 illustrates the properties of a radial wave function at very low collision energy for the case of one-channel scattering (e.g. the collisions between Na $|f=2, m_f=2\rangle$ atoms discussed near the end of the previous section). It shows the wave function for two different model potentials (the *ab initio* triplet potential for Na multiplied by two different constants) with two different scattering lengths a : one positive and one negative.

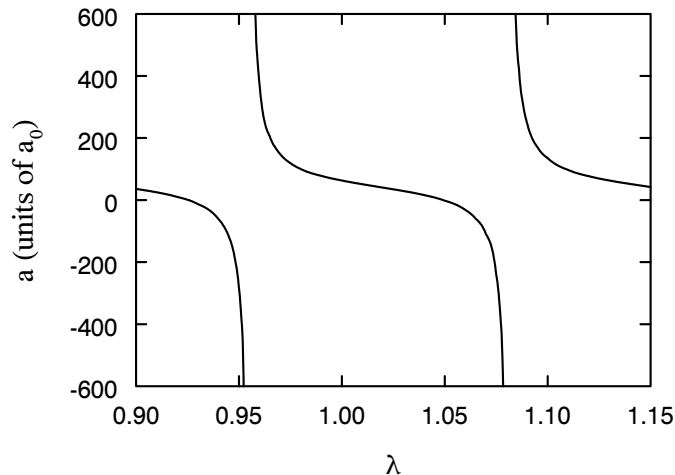


Figure 2.4 Scattering length a as a function of the parameter λ for the model potential $\lambda V(r)$ where $V(r)$ is the Na triplet potential. The scattering length goes through $-\infty$ and $+\infty$ when an additional level is added to the bound states supported by the potential.

tive. At short range the wave function undergoes a large number of oscillations due to the deep potential well. At long range it is proportional to $\sin(kr + \eta^0) = \sin k(r - a)$. The effect of the potential is simply to shift the point of origin of the asymptotic sine wave over a distance a ; for positive a it is the same as for a hard wall at $r = a$. The wave function for the case without interaction is also drawn for comparison.

It is illustrative to consider the behavior of a when one gradually increases the depth of the potential well. To that end Fig. 2.4 shows a for the model potential $\lambda V(r)$, where $V(r)$ is the above-mentioned Na triplet potential, as a function of λ . The scattering length varies between $-\infty$ and $+\infty$. The singularities occur each time that an additional level is added to the bound states supported by the potential.

Inelastic collisions have very different threshold properties than elastic ones. As long as the internal energy of the separated atoms in the exit channel $|\{\alpha\beta\}\rangle$ is lower than for the entrance channel $|\{\gamma\delta\}\rangle$ (exothermal transition), the s -wave S -matrix element varies as [31]

$$S_{\{\alpha\beta\},\{\gamma\delta\}}^0(E) \sim k^{1/2}, \quad \text{as } k \rightarrow 0 \quad (\varepsilon_\gamma + \varepsilon_\delta > \varepsilon_\alpha + \varepsilon_\beta). \quad (2.33)$$

Thus, the cross section for inelastic exothermal collisions varies as $\sigma_{\alpha\beta,\gamma\delta}(v) \sim 1/k$ in the very low energy limit and becomes arbitrarily large. The associated rate coefficient $G_{\gamma\delta \rightarrow \alpha\beta}(B, T)$, however, approaches a nonvanishing constant as $T \rightarrow 0$. If, on the other hand, the internal energies of entrance channel and exit channel are identical (e.g. in the case of zero magnetic field where all one-atom hyperfine states with the

same f value are degenerate: see Fig. 2.1), the S -matrix element varies as

$$S_{\{\alpha\beta\},\{\gamma\delta\}}^0(E) \sim k, \quad \text{as } k \rightarrow 0 \quad (\varepsilon_\gamma + \varepsilon_\delta = \varepsilon_\alpha + \varepsilon_\beta). \quad (2.34)$$

In that case the cross section approaches a constant and $G_{\gamma\delta \rightarrow \alpha\beta}(B, T)$ vanishes as $T^{1/2}$ as $T \rightarrow 0$.

The use of the scattering length can be extended to collisions with open inelastic channels. It is then complex: $a_{\{\gamma\delta\}} = a_{\{\gamma\delta\}}^R + ia_{\{\gamma\delta\}}^I$. From the unitarity of the S -matrix it follows that

$$\begin{aligned} \sum_{\{\alpha\beta\} \neq \{\gamma\delta\}} \left| S_{\{\alpha\beta\},\{\gamma\delta\}}^0(E) \right|^2 &= 1 - \left| S_{\{\gamma\delta\},\{\gamma\delta\}}^0(E) \right|^2 \\ &\rightarrow 4a_{\{\gamma\delta\}}^I k \end{aligned} \quad (2.35)$$

in the low energy limit. Hence

$$\sum_{\{\alpha\beta\} \neq \{\gamma\delta\}} G_{\gamma\delta \rightarrow \alpha\beta}(B, T) \rightarrow \frac{4\pi\hbar}{\mu} a_{\{\gamma\delta\}}^I, \quad \text{as } T \rightarrow 0. \quad (2.36)$$

This sum is similar to the rate coefficient $G_{tot}(B, T)$ defined in the previous section, apart from the factors $(2 - \delta_{\kappa\mu} - \delta_{\kappa\nu})$ that differentiate between processes in which two, one or no atoms are lost from the trap. As long as the imaginary part of a complex scattering length is not too large, its real part is still a good parameter to characterize elastic collision events.

2.4 The Accumulated Phase Method

In section 2.1 we mentioned the coupling region where the exchange interaction V_E is comparable (differing by a factor of order 10 or less) to the internal energy differences caused by the hyperfine and Zeeman interaction. Let the r -interval (r_1, r_2) denote this region. For $r > r_2$ the coupling between the two-atom hyperfine states is negligible and the radial motion is adiabatic. For $r < r_1$ the motion is also adiabatic, but with S as a good quantum number. Consequently, a complete set of linearly independent solutions of the coupled-channels equations up to $r = r_1$ can be represented by the diagonal matrix $\underline{\underline{u}}'(r) = \text{diag}(u_i(r))$ in the basis of adiabatic two-body internal states $|i\rangle_{2b}$. The subscript $2b$ is added to avoid confusion with 1-body internal states. Moreover, for $r < r_1$, the radial wave functions $u_i(r)$ are almost identical for different energies E_{tot} (both in the continuum and in the discrete spectrum), provided these energies are all within a range that is smaller than the depth of the singlet and triplet potentials at r_1 (of order 10 K). The same is true for different values of l near $l = 0$. These criteria are fulfilled by the entire ranges of E_{tot} and l values relevant for cold collisions and the highest two-atom bound states. Thus the insufficiently accurate inner parts of the

potentials $V_S(r)$ and $V_T(r)$ can be replaced by two boundary conditions at $r_0 \leq r_1$, one for the singlet wave function and one for the triplet wave function, with a simple dependence on energy and orbital angular momentum. This greatly simplified our analyses of experiments.

In our approach the boundary conditions take the form of the accumulated phases $\phi_S(E, l)$ and $\phi_T(E, l)$ of the rapidly oscillating radial wave functions $\psi_S(r)$ and $\psi_T(r)$ in a pure singlet and a pure triplet channel without internal energy. These phases are defined by the WKB expression

$$\psi_{S/T}(r_0) = A \frac{\sin \left[\int^{r_0} k(r) dr \right]}{\sqrt{k(r_0)}} \equiv A \frac{\sin \left[\phi_{S/T}(E, l) \right]}{\sqrt{k(r_0)}}, \quad (2.37)$$

in which $k(r)$ is the local radial wave number:

$$k^2(r) = \frac{2\mu}{\hbar^2} \left[E - V_{S/T}(r) - \frac{\hbar^2 l(l+1)}{2\mu r^2} \right]. \quad (2.38)$$

In these equations the dependence of k on S , E and l has been omitted in the notation for simplicity. The validity of the WKB approximation is not a prerequisite for the method: we could have specified each boundary condition in terms of a logarithmic derivative of the radial wave function. The accumulated phase may be considered as a convenient parametrization of the logarithmic derivative. Its convenience stems from the fact that it can be accurately expanded in terms of a Taylor series in E and $l(l+1)$, cut off after the second order terms:

$$\begin{aligned} \phi_{S/T}(E, l) = \phi_{S/T}(0, 0) &+ \frac{\partial \phi_{S/T}}{\partial E} E + \frac{\partial \phi_{S/T}}{\partial [l(l+1)]} l(l+1) \\ &+ \frac{1}{2} \frac{\partial^2 \phi_{S/T}}{\partial E^2} E^2 + \frac{\partial^2 \phi_{S/T}}{\partial E \partial [l(l+1)]} E l(l+1), \end{aligned} \quad (2.39)$$

valid for all relevant E and l . The second derivative with respect to $l(l+1)$ can be set to zero. The remaining second and mixed derivatives, which are the least sensitive to errors in the inner parts of V_S and V_T are determined from the best available *ab initio*, RKR or IPA potential. In our work on Na the first-order derivatives and $\phi_{S/T}(0, 0)$ are fitted to experimental data. In the latest determination of Rb interaction parameters, carried out by Vogels *et al.* [32], only $\phi_{S/T}(0, 0)$ was fitted. If the range of energies needed in a calculation is of the order of 1 K or less, which is often the case in cold-atom physics, the expansion (2.39) can even be limited to its linear part. In contrast, the logarithmic derivative shows the typical tangent-shaped excursions through infinity each time a radial node passes the point $r = r_0$.

The adiabatic potentials $V_i(r)$ felt by the adiabatic internal states $|i\rangle_{2b}$ follow from

$$\begin{aligned} \left[V^{hf+} + \sum_{j=1}^2 V_j^Z + V^c(r) + \frac{\hbar^2 l(l+1)}{2\mu r^2} \right] |i\rangle_{2b} &= V_i(r) |i\rangle_{2b} \\ &= \left[\varepsilon_i + V_{S/T}(r) + \frac{\hbar^2 l(l+1)}{2\mu r^2} \right] |i\rangle_{2b} . \end{aligned} \quad (2.40)$$

Whether the singlet or triplet potential applies is determined by the S quantum number of $|i\rangle_{2b}$. Note that ε_i is independent of r . The operator

$$V^{hf+} \equiv \frac{a_1^{hf}}{2\hbar^2} \vec{S} \cdot \vec{i}_1 + \frac{a_2^{hf}}{2\hbar^2} \vec{S} \cdot \vec{i}_2 , \quad (2.41)$$

which equals $\frac{a^{hf}}{2\hbar^2} \vec{S} \cdot \vec{I}$ for indistinguishable atoms, is the part of the total hyperfine interaction $\sum_{j=1}^2 V_j^{hf}$ that is diagonal in S . The part that is not diagonal in S is negligible for $r < r_1$ because of the large singlet-triplet energy separation. The only difference between the adiabatic potential $V_i(r)$ and the potential (including centrifugal barrier) in Eq. (2.38) is ε_i . The boundary condition for the radial wave function $u_i(r)$ in channel $|i\rangle_{2b}$ for total energy E_{tot} is therefore given by

$$u_i(r_0) = A \frac{\sin \left[\phi_{S/T}(E_{tot} - \varepsilon_i, l) \right]}{\sqrt{k_i(r_0)}} . \quad (2.42)$$

Now, to solve the coupled-channels equations, the solution matrix $\underline{\underline{u}}'(r)$ in the adiabatic basis is transformed to a matrix $\underline{\underline{u}}(r)$ in the basis of asymptotic hyperfine states, and the Schrödinger equation (2.19) is integrated for $r > r_0$.

2.5 Feshbach Resonances

Feshbach resonances were introduced in section 1.2 as a promising tool to tune the scattering length. The basic idea is illustrated in Fig. 2.5. The upper panel shows the scattering length $a_{1,1}$ for collisions between two Na atoms in the $|\kappa\rangle = |f=1, m_f=1\rangle$ hyperfine state as a function of magnetic field strength, obtained from coupled-channels calculations. The lower panel shows the field-dependent threshold energy $2\varepsilon_\kappa(B)$ for this entrance channel (the total energy where zero collision energy scattering takes place), and the field-dependent energies of two bound states, which are solutions of the same coupled-channels equations with $l=0$ and $m_F=2$. Near the field strength B_0 where a bound-state energy equals the threshold energy, $a_{1,1}(B)$ displays a dispersive feature:

$$a(B) = a_\infty \left(1 - \frac{\Delta}{B - B_0} \right) . \quad (2.43)$$

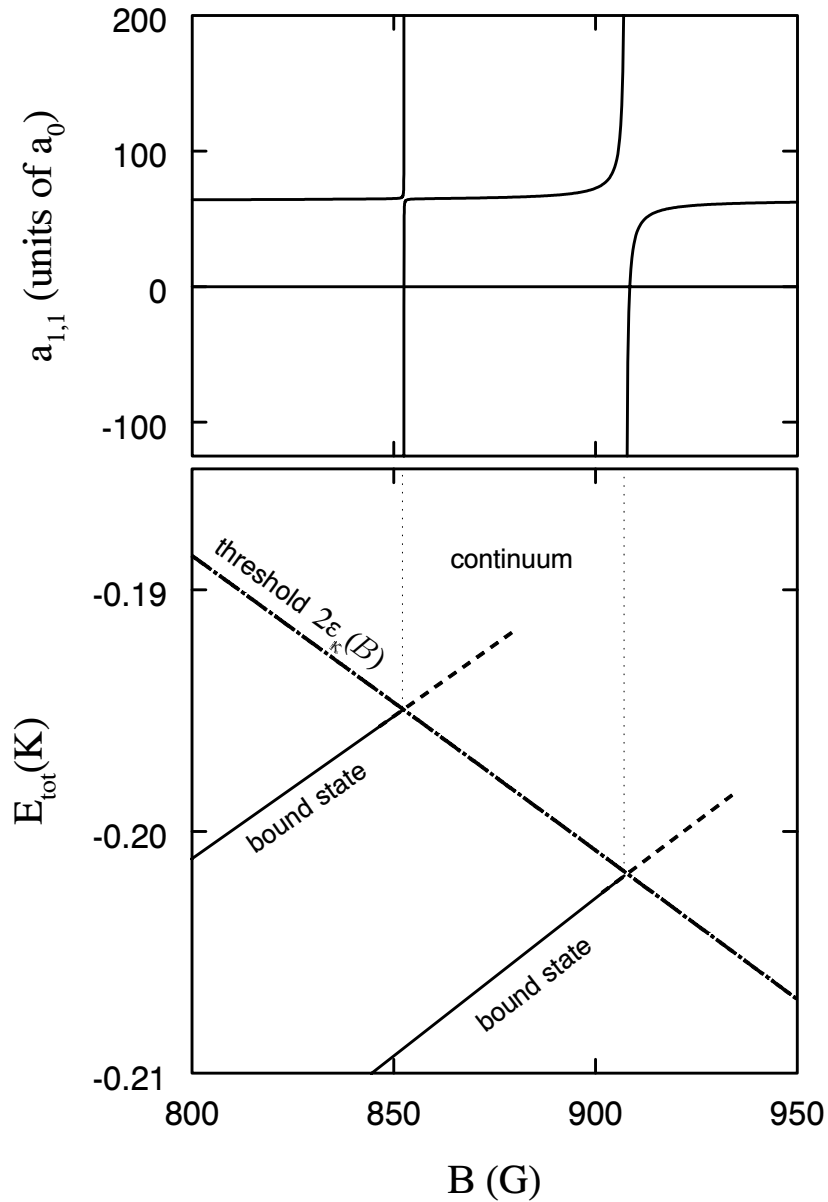


Figure 2.5 Feshbach resonances for collisions of two Na atoms in the hyperfine state $|\kappa\rangle = |f=1, m_f=1\rangle$. The lower panel shows the field-dependent threshold energy $2\epsilon_{\kappa}(B)$ for this entrance channel, and the field-dependent energies of two bound states. The upper panel shows the scattering length $a_{1,1}$ for these collisions as a function of the magnetic field strength B , obtained from coupled-channels calculations. Near the field strengths where a bound-state energy equals the threshold energy, $a_{1,1}(B)$ displays a dispersive feature. For the 907 G resonance the sign of the scattering length is changed within a field range of 1 G.

Exactly at B_0 the scattering length is infinite. The absolute value of the field width Δ specifies the range of magnetic field strength for which the sign of a is different than for the off-resonant value a_∞ . At $B_0 + \Delta$ the scattering length passes through zero. Above threshold, Feshbach resonances occur when $E_{tot}(B) = E + 2\varepsilon_\kappa(B)$ is approximately equal to the energy on the extrapolation of one of the bound-state curves, causing the elastic collision rate to go through a maximum and a minimum (or vice versa) as a function of B . Thus, applying a static magnetic field to a Bose-Einstein condensate in a dilute atomic gas enables an experimentalist to control the effective interactions between the atoms in that gas. In an experiment designed to study the collapse of a condensate by suddenly changing the scattering length from positive to negative, the ratio Δ/B_0 governs the degree of field control that is needed and should be as large as possible.

To give the reader some insight in the origin of Feshbach resonances, we give a brief outline of their mathematical description, specializing to the formalism for s -wave scattering of two atoms explained in the previous sections. For a more detailed treatment we refer to the literature [30, 33]. The first step is splitting the coupled-channels equations describing $l = 0$ collisions for the entrance channel $|\{\gamma\delta\}\rangle$ (in the above example for Na, $|\{\gamma\delta\}\rangle = |\kappa\kappa\rangle$) into two uncoupled subsystems: one containing the open channels and one containing the closed channels. The associated Hilbert spaces are denoted by \mathcal{P} and \mathcal{Q} , respectively. We also introduce the operators P and Q that project on these spaces. Next, the coupled-channels equations for the \mathcal{P} space are solved with the usual boundary conditions (2.16), giving the result

$$\langle r | \psi_{\{\gamma\delta\}}^+ \rangle \equiv \sum_{\{\alpha\beta\} \text{ in } \mathcal{P}} [\underline{u}_{\{\gamma\delta\}}^P(r)]_{\{\alpha\beta\}} |\{\alpha\beta\}\rangle. \quad (2.44)$$

The coupled-channels equations for the \mathcal{Q} space are solved with bound-state boundary conditions, resulting in the bound states

$$\langle r | \phi_m \rangle \equiv \sum_{\{\alpha\beta\} \text{ in } \mathcal{Q}} [\underline{u}_m^Q(r)]_{\{\alpha\beta\}} |\{\alpha\beta\}\rangle, \quad (2.45)$$

with energies E_m . In the language of Feshbach resonance theory $|\psi_{\{\gamma\delta\}}^+\rangle$ and $|\phi_m\rangle$ are eigenstates of $H_{PP} \equiv PH^0P$ and $H_{QQ} \equiv QH^0Q$, where H^0 is the $l = 0$ radial Hamiltonian. If the total energy E_{tot} is close enough to one particular bound-state energy E_b the dynamics in the \mathcal{Q} space are dominated by the one state $|\phi_b\rangle$. Reintroducing the coupling between \mathcal{P} and \mathcal{Q} into the problem results in this bound state becoming a quasibound state and acquiring a finite width Γ , and in its energy undergoing a so-called resonance shift Δ_{res} . For the S -matrix element for the transition to channel

$|\{\alpha\beta\}\rangle$ one finds the expression

$$S_{\{\alpha\beta\},\{\gamma\delta\}}^0 = S_{\{\alpha\beta\},\{\gamma\delta\}}^P - 2\pi i \frac{\langle \psi_{\{\alpha\beta\}}^- | H_{PQ} | \phi_b \rangle \langle \phi_b | H_{QP} | \psi_{\{\gamma\delta\}}^+ \rangle}{E_{tot} - E_b - \Delta_{res} + \frac{i}{2}\Gamma}, \quad (2.46)$$

containing the well-known Breit-Wigner denominator. The minus sign in $|\psi_{\{\alpha\beta\}}^- \rangle$ indicates an outgoing instead of an incoming plane wave in the boundary conditions. We see that apart from the direct term $S_{\{\alpha\beta\},\{\gamma\delta\}}^P$ resulting from coupling within \mathcal{P} -space alone, the amplitude of the outgoing wave in channel $|\{\alpha\beta\}\rangle$ will include a term arising from coupling of the incoming wave in channel $|\{\gamma\delta\}\rangle$ to the bound state in \mathcal{Q} -space followed by coupling of this state to channel $|\{\alpha\beta\}\rangle$. The coupling operator $H_{PQ} \equiv PH^0Q = H_{QP}^\dagger$ is effectively proportional to the exchange interaction V_E . If there is only one open channel, which is often the case, we can write

$$S_{\{\gamma\delta\},\{\gamma\delta\}}^0 = S_{\{\gamma\delta\},\{\gamma\delta\}}^P \left(1 - \frac{i\Gamma}{E_{tot} - E_b - \Delta_{res} + \frac{i}{2}\Gamma} \right), \quad (2.47)$$

and $\Gamma = \Gamma_{\{\gamma\delta\}} = 2\pi \left| \langle \phi_b | H_{QP} | \psi_{\{\gamma\delta\}}^+ \rangle \right|^2$. Now, for a certain collision energy E , the resonance condition

$$E = E_b(B) + \Delta_{res}(B, E) - \varepsilon_\gamma(B) - \varepsilon_\delta(B) \equiv \varepsilon_{res}(B, E), \quad (2.48)$$

where ε_{res} is the resonance energy with respect to threshold, can be fulfilled by tuning B . From this condition it is clear that a curve representing $E_b(B) + \Delta_{res}(B, E)$ should in fact be used instead of the extrapolation of the bound-state curve in Fig. 2.5. On the scale of this figure, however, these are approximately identical. An interesting difference between the two near threshold will be demonstrated below.

In the low energy limit $\Gamma_{\{\gamma\delta\}} = Ck$ with $C > 0$, and close to a resonance field strength B_0 we can write

$$\varepsilon_{res}(B) \equiv \varepsilon_{res}(B, 0) = (\mu_{free} - \mu_{qb})(B - B_0), \quad (2.49)$$

in which μ_{free} and μ_{qb} are the effective magnetic moments of the free two-atom system and the quasibound state considered; in other words $\mu_{free} - \mu_{qb}$ is approximately proportional to the difference in slope of the crossing lines in Fig. 2.5. Setting $S_{\{\gamma\delta\},\{\gamma\delta\}}^0 = e^{-2ika}$ and $S_{\{\gamma\delta\},\{\gamma\delta\}}^P = e^{-2ika_\infty}$ then leads to the dispersive behavior (2.43) of $a(B)$ with

$$\Delta = \frac{C}{a_\infty(\mu_{free} - \mu_{qb})}. \quad (2.50)$$

The quantities C and a_∞ can usually be considered constant over the resonance. It should be emphasized that the resonance field strength B_0 always corresponds exactly

to the field strength where the energy of a real bound state of the total system equals the threshold energy. This can be seen from the threshold relation between the binding energy $E_{bind} \equiv \hbar^2 \kappa_b^2 / 2\mu$ of the highest $l = 0$ bound state (near a resonance this is the state about to cross the threshold) and the scattering length [30]: $\kappa_b = 1/a$. In combination with the dispersive behavior of $a(B)$ near B_0 this leads to the conclusion that the bound-state energy curves bend quadratically toward the threshold curve as a function of B just before they touch it.

Sometimes, more than one bound state in \mathcal{Q} -space has an energy close to E_{lot} near a resonant field strength. Then it becomes necessary to include a Breit-Wigner-like term for each of these states in expression (2.46). The additional quasibound states can induce a significant change in the background scattering length that is otherwise determined by interactions in \mathcal{P} -space alone, and cause interferences between resonances. This situation will come up in chapters 4 and 5 which deal with a Feshbach resonance in ^{85}Rb .

Finally, it is important to distinguish Feshbach resonances from potential resonances. The latter occur in potential scattering where only the translational dynamics of the colliding atoms is involved. In practice they arise for partial waves with $l > 0$ when a quasibound state occurs inside the centrifugal barrier. As explained above, the quasibound state of a Feshbach resonance has an internal structure orthogonal to that of the combined scattering partners so that it can only occur in multi-channel scattering and also for $l = 0$.

2.6 Photoassociation

The principle of cold photoassociation was already briefly explained in section 1.2: excitation of a colliding pair of cold atoms by a laser photon leads to the formation of an electronically excited bound molecular state, followed by spontaneous decay back to free atoms. The relative velocity of the atoms after decay will be practically identical to that before decay (Franck-Condon principle). And since the average velocity in the deep excited-state potential is relatively large (the atoms undergo many vibration cycles before decaying), the free atoms will have enough translational energy to leave the trap in which the process takes place. The decrease of density by this trap loss can be detected, for instance, by measuring the fluorescence from the atoms in the trap. In the simple case that the ground-state dynamics can be described with one radial wave function $u_g(r)$ (e.g. one-channel s -wave scattering), the same Franck-Condon principle is responsible for the excitation probability being approximately proportional to $|u_g(r)|^2$ with r near the classical outer turning point of the excited state where the velocity of the atoms is low and thus comparable to that before excitation. This

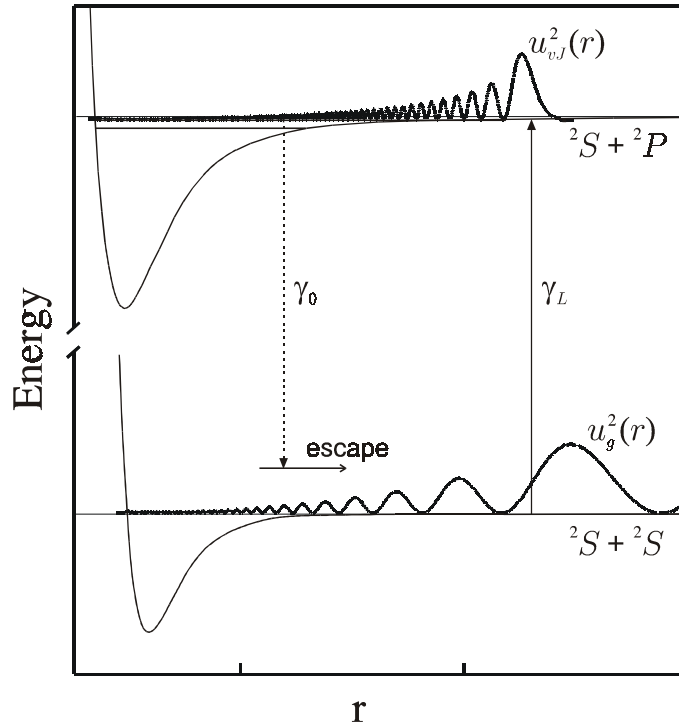


Figure 2.6 Cold-atom photoassociation. A colliding pair of atoms, described by the scattering wave function $u_g(r)$, is excited by a laser field into an electronically excited bound molecular state with radial wave function $u_{v,J}(r)$ at a rate γ_L . This state then decays back at a rate γ_0 to free atoms. Due to the large average velocity in the excited-state potential, these have enough translational energy to leave the trap in which the process takes place. The decrease in atomic density in the trap due to this loss is detected. For clarity energies are not shown to scale.

enables one to map out the nodal structure of this wave function along a laser frequency axis [20]. The whole process is illustrated in Fig. 2.6.

Obviously a theoretical description of photoassociation requires knowledge of the excited bound states apart from the description of the ground-state dynamics treated in the previous sections. The electronic structure of the excited states can, like that for two ground-state atoms, be determined by means of a Born-Oppenheimer procedure. The excited alkali atom states that occur in this thesis are all associated with the ${}^2S + {}^2P$ separated-atom limits. These states have been studied by Movre and Pichler [34]. In the radial range of outer turning points of the uppermost rovibrational levels of the Born-Oppenheimer potential curves – which are the ones observed in the experiments – the excited states have a relatively simple electronic structure

determined by only a few basis states coupled by the fine-structure interaction of the excited atom and the interatomic resonant electric dipole interaction proportional to $1/r^3$. The rovibrational levels are labeled by v , the vibrational quantum number, and by J , where $\vec{J} = \vec{l} + \vec{L} + \vec{S}$ and \vec{L} is the electronic orbital angular momentum (for Li the electronic spin-orbit coupling is so weak that \vec{S} does not couple to $\vec{N} = \vec{l} + \vec{L}$ as usual; this results in rovibrational levels labeled by v and N : Hund's case b). Each level consists of a number of bound states labeled by additional quantum numbers (in particular those related to the nuclear spins), possibly split in energy by the hyperfine and Zeeman interactions. The expression for the photoassociation rate coefficient should contain an incoherent sum over all excited states that are approximately resonant at the frequency ω_L of the photoassociation laser. Often, this sum involves precisely all states that belong to one rovibrational level.

In chapters 4 and 5 of this thesis we study a photoassociation process in ^{85}Rb . By a careful choice of excited state we are there able to avoid the above-mentioned hyperfine and Zeeman splitting, so that all excited states that contribute to the photoassociation signal are degenerate and have a simple structure. We have also analyzed a photoassociation experiment for Li where the Zeeman and hyperfine splitting were absent. In view of these experimental conditions, we will limit the following discussion to the case of degenerate excited states with energy E_{vJ} . The rate at which these states are formed during collisions of two atoms in hyperfine states $|\gamma\rangle$ and $|\delta\rangle$ is given (in energy units) by the width for laser excitation

$$\gamma_{L,\{\gamma\delta\}} = \frac{\pi I_L}{\varepsilon_0 c} \sum_{l, m_l} \sum_{\beta} \left| \left\langle \Phi_{\beta}^{vJ} \left| (\vec{d}_1 + \vec{d}_2) \cdot \vec{\sigma} \right| \Psi_{\{\gamma\delta\}}^{l m_l +}(E) \right\rangle \right|^2, \quad (2.51)$$

where \vec{d}_1 and \vec{d}_2 are the electric dipole operators of atoms one and two, $\vec{\sigma}$ is the polarization vector of the photoassociation laser and I_L its intensity. The partial waves $|\Psi_{\{\gamma\delta\}}^{l m_l +}(E)\rangle$, describing the ground-state dynamics, are defined by Eq. (2.20). They are coupled by the laser field to the electronically excited bound states $|\Phi_{\beta}^{vJ}\rangle$, where v and J label the resonant rovibrational level in one of the Born-Oppenheimer potentials, and β labels all other quantum numbers. The width $\gamma_{L,\{\gamma\delta\}}$ contains overlap integrals of the excited bound-state radial wavefunction $u_{vJ}(r)$ and the ground-state radial wavefunctions $u_{\{\alpha\beta\}}^l(r)$. Just like for the ground-state Born-Oppenheimer potentials, the inner part of the excited-state potentials is not as accurately known as its above-mentioned simple long-range part. Therefore, the wave function $u_{vJ}(r)$ is computed by inward integration for the experimental level energy E_{vJ} . Moreover, due to application of the accumulated phase method the functions $u_{\{\alpha\beta\}}^l(r)$ are not available for $r < r_0$. Fortunately, the overlap integrals are completely dominated by the r -region near the classical turning point associated with $u_{vJ}(r)$ (as can be seen from Fig. 2.6), so that the integration can be limited to the long-range interval $r > r_0$ without any effect on

the result.

From the width $\gamma_{L,\{\gamma\delta\}}$ for excitation and the natural linewidth γ_0 of the laser-coupled excited-state level, representing the rate at which the excited bound states belonging to this level decay back to free atoms, the rate coefficient $K_{\{\gamma\delta\}}$ for photoassociation losses can be calculated. To first order in the laser intensity I_L one finds [18,35]

$$K_{\{\gamma\delta\}}(B, T, \omega_L) = \left\langle v \frac{\pi}{k^2} \frac{\gamma_0 \gamma_{L,\{\gamma\delta\}}}{(E + \hbar\omega_L - E_{vJ})^2 + \frac{1}{4}\gamma_0^2} \right\rangle_{\text{th}}. \quad (2.52)$$

To see if the approximation to first order in I_L applies in a certain experiment one usually checks if the photoassociation rate varies linearly with laser intensity. The rate coefficient $K_{\{\gamma\delta\}}$ can be used in the same way as the inelastic collision rate coefficients $G_{\gamma\delta \rightarrow \alpha\beta}$.

References

- [1] H.T.C. Stoof, J.M.V.A. Koelman, and B.J. Verhaar, Phys. Rev. B **38**, 4688 (1988).
- [2] J.P.H.W. van den Eijnde, Ph. D. thesis, Eindhoven University, The Netherlands, 1984 (unpublished).
- [3] B. Shizgal, J. Chem. Phys. **58**, 3424 (1973).
- [4] L.H.A. Leunissen, internal report, Eindhoven University, The Netherlands, 1992 (unpublished).
- [5] M. Marinescu, H.R. Sadeghpour, and A. Dalgarno, Phys. Rev. A **49**, 982 (1994).
- [6] Z.-C. Yan, J.F. Babb, A. Dalgarno, and G.W.F. Drake, Phys. Rev. A **54**, 2824 (1996).
- [7] A. Derevianko, W.R. Johnson, M.S. Safronova, and J.F Babb, Phys. Rev. Lett. **82**, 3589 (1999).
- [8] B.M. Smirnov and M.I. Chibisov, Zh. Eksp. Teor. Fiz. **48**, 939 (1965) [Sov. Phys. JETP **21**, 624 (1965)].
- [9] G. Hadinger and G. Hadinger, J. Mol. Spectr. **175**, 441 (1996).
- [10] R. Rydberg, Z. Physik **73**, 326 (1931); *ibid.* **80**, 514 (1931); O. Klein, Z. Physik **76**, 226 (1932); A.L.G. Rees, Proc. Phys. Soc. (London) **59**, 998 (1947).
- [11] C.R. Vidal and H. Scheingraber, J. Mol. Spectr. **56**, 93 (1977).
- [12] A.J. Moerdijk, W.C. Stwalley, R.G. Hulet, and B.J. Verhaar, Phys. rev. Lett. **72**, 40 (1994); A.J. Moerdijk, B.J. Verhaar and A. Axelsson, Phys. Rev. A **51**, 4852 (1995).
- [13] E.R.I. Abraham, W.I. McAlexander, C.A. Sackett, and R.G. Hulet, Phys. Rev. Lett. **74**, 1315 (1995).
- [14] A. Crubellier, O. Dulieu, F. Masnou-Seeuws, M. Elbs, H. Knöckel, and E. Tiemann, Eur. J. Phys. D **6**, 211 (1999).

-
- [15] C.C. Tsai, R.S. Freeland, J.M. Vogels, H.M.J.M. Boesten, B.J. Verhaar, and D.J. Heinzen, *Phys. Rev. Lett.* **79**, 7 (1997).
- [16] S. Inouye, M.R. Andrews, J. Stenger, H.-J. Miesner, D.M. Stamper-Kurn, and W. Ketterle, *Nature* **392**, 151 (1998).
- [17] Ph. Courteille, R.S. Freeland, D.J. Heinzen, F.A. van Abeelen, and B.J. Verhaar, *Phys. Rev. Lett.* **81**, 69 (1998).
- [18] J.R. Gardner, R.A. Cline, J.D. Miller, D.J. Heinzen, H.M.J.M. Boesten, and B.J. Verhaar, *Phys. Rev. Lett.* **74**, 3764 (1995).
- [19] H.M.J.M. Boesten, C.C. Tsai, J.R. Gardner, D.J. Heinzen, and B.J. Verhaar, *Phys. Rev. A* **55**, 636 (1997); H.M.J.M. Boesten, C.C. Tsai, B.J. Verhaar, and D.J. Heinzen, *Phys. Rev. Lett.* **77**, 5194 (1996); H.M.J.M. Boesten, C.C. Tsai, D.J. Heinzen, A.J. Moonen, and B.J. Verhaar, *J. Phys. B* **32**, 287 (1999).
- [20] E.R.I. Abraham, W.I. McAlexander, J.M. Gerton, R.G. Hulet, R. Côté, and A. Dalgarno, *Phys. Rev. A* **53**, R3713 (1996).
- [21] E. Tiesinga, C.J. Williams, P.S. Julienne, K.M. Jones, P.D. Lett, and W.D. Phillips, *J. Res. Natl. Inst. Stand. Technol.* **101**, 505 (1996).
- [22] I. Schmidt-Mink, W. Müller, and W. Meyer, *Chem. Phys.* **92**, 263 (1985).
- [23] D.D. Konowalow, M.E. Rosenkrantz, and M.L. Olson, *J. Chem. Phys.* **72**, 2612 (1980).
- [24] M. Gutowski, *J. Chem. Phys.* **110**, 4695 (1999).
- [25] J. Raynal, in *Computing as a Language of Physics*, edited by A. Salam (IAEA, Vienna, 1972), p. 292.
- [26] B.J. Verhaar, J.M.V.A. Koelman, H.T.C. Stoof, O.J. Luiten, and S.B. Crampton, *Phys. Rev. A* **35**, 3825 (1987); *ibid.* **38**, 3535 (1988).
- [27] D.S. Hall, M.R. Matthews, C.E. Wieman, and E.A. Cornell, *Phys. Rev. Lett.* **81**, 1543 (1998).
- [28] D. M. Stamper-Kurn, M. R. Andrews, A. P. Chikkatur, S. Inouye, H.-J. Miesner, J. Stenger, and W. Ketterle, *Phys. Rev. Lett.* **80**, 2027 (1998).
- [29] Yu. Kagan, B.V. Svistunov, and G.V. Shlyapnikov, *Pis'ma Zh. Eksp. Teor. Fiz.* **42**, 169 (1985) [*JETP Lett.* **42**, 209 (1985)].
- [30] C.J. Joachain, *Quantum Collision Theory* (North-Holland, New York, 1972).
- [31] E.P. Wigner, *Phys. Rev.* **73**, 1002 (1948).
- [32] J.M. Vogels, R.S. Freeland, C.C. Tsai, B.J. Verhaar, and D.J. Heinzen, accepted for publication in *Phys. Rev. A*
- [33] H. Feshbach, *Theoretical Nuclear Physics*, (Wiley, New York, 1992).
- [34] M. Movre and G. Pichler, *J. Phys. B* **10**, 2631 (1997).
- [35] R. Napolitano, J. Weiner, P.S. Julienne, and C.J. Williams, *Phys. Rev. Lett.* **73**, 1352 (1994).

3

Time-Dependent Feshbach Resonance Scattering and Anomalous Decay of a Na Bose-Einstein Condensate

F.A. van Abeelen and B.J. Verhaar

Published in Phys. Rev. Lett. **83**, 1550 (1999)

We study Feshbach resonance scattering in a time-dependent magnetic field. We explain the extremely rapid decay observed in a recent experiment investigating Feshbach resonances in a Na Bose-Einstein condensate. In our picture, the decay is stimulated by the formation of a molecular condensate of quasibound atom pairs. Another essential element is the concept of a global and a local resonance lifetime. The predicted decay rates are large, about 5 orders of magnitude larger than typical dipole decay rates and 1 order larger than typical exchange decay rates. We point out the possible role of a Josephson-like oscillation between the atomic condensate and a long-range molecular condensate.

3.1 Introduction

A remarkable aspect of the recently realized Bose-Einstein condensates in dilute alkali and hydrogen atomic gases [1] is the prominent role of atom-atom interactions. For instance, the linear dimensions of a trapped condensate may be several times larger than for the quantum mechanical ground state in the trap potential [2], i.e. the state of the condensate without interactions. Other examples are the spin domain structure recently observed in a spinor condensate [3], an amazing and counter-intuitive phenomenon for a dilute system, and the fascinating recent four-wave mixing experiment [4]. There is reason to expect that interactions will also be important for future developments in the direction of coherent matter waves. The fact that such waves can interact may well be one of the most important advantages of atom lasers compared to optical lasers.

Unlike previously studied degenerate systems such as ^4He , the new quantum liquids can be understood quantitatively on the basis of first principles. Most of their properties can be expressed with the aid of a single interaction parameter: the scattering length a . Interestingly, this parameter can be experimentally modified. A promising

way to do this relies on the strong variation of a that occurs if a Feshbach resonance is tuned through zero energy by varying an external magnetic field [5]. Such resonances have been observed in Na [6] and in ^{85}Rb [7, 8]. In the Na experiment the scattering length was seen to vary dispersively as a function of the magnetic field as predicted:

$$a(B) = a_\infty \left(1 - \frac{\Delta}{B - B_0} \right), \quad (3.1)$$

where a_∞ is the off-resonant scattering length and Δ characterizes the width of the resonance as a function of B . Feshbach resonances thus offer the possibility to study quantum liquids and coherent matter in widely varying circumstances with positive, negative and zero values of a in a single experiment. In particular, it should be possible to see the predicted [9], but still unobserved collapse of a condensate if its scattering length is suddenly shifted to a sufficiently negative value.

Cold atom Feshbach resonances are exceptional also in another sense. For practically realizable time-varying fields, it is possible to change the properties of a scattering process significantly while it is going on. It is the purpose of this Letter to point out that this was in fact an important element in a recent experiment by Stenger *et al.* [10] at MIT. In an attempt to realize a maximum variation of a in an optically trapped Na Bose-Einstein condensate, they observed a strong decay of the condensate when a resonance was approached or crossed with the external magnetic field. The experiment consisted of runs of two types: (1) Runs in which the magnetic field was changed adiabatically from an off-resonant value to a value near a resonance field strength without crossing the resonance; (2) runs in which a resonance was crossed with high ramp speed, beginning and ending with off-resonant fields. A mechanism for the type 1 observations has been proposed by Timmermans *et al.* [11] and will be briefly recapitulated later in this paper. We will focus on the anomalous decay in the second type of experiment. As pointed out by Stenger *et al.*, the experimental data suggest decay rates far larger than expected for any of the known two-body and three-body mechanisms. We will present a new picture based on time-dependent Feshbach resonance scattering.

3.2 Anomalous Decay in Type 2 Runs

Feshbach resonances arise when the total energy of a pair of colliding atoms matches the energy of a quasibound two-atom state, leading to the resonant formation of this state during the collision [12]. Figure 4.2 in chapter 4 [13] shows an example of the enhancement of the collisional wavefunction near a resonance, reflecting the increased amplitude of the admixed quasibound state. Magnetic tuning is possible if the pair of free atoms and the quasibound state have different magnetic moments $\mu_{free} - \mu_{qb} = \Delta\mu \neq 0$, giving rise to different Zeeman dependencies. Figure 3.1 shows the crossings of two Na quasibound states with the collision threshold at $B = 853$ and 907 G. The

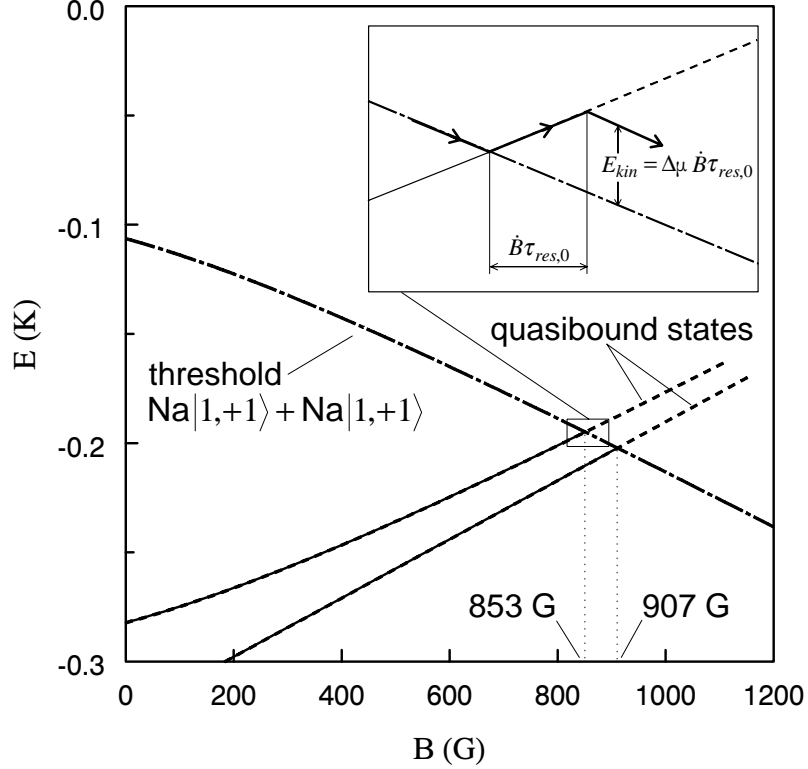


Figure 3.1 Crossing of quasibound two-atom states with Na + Na collision threshold at $B = 853$ and 907 G, due to different Zeeman dependencies of the quasibound states and the state of free atoms. Inset: Schematic illustration of proposed loss mechanism.

corresponding resonances were observed [10] in a condensate of atoms in the lowest hyperfine state $|f, m_f\rangle = |1, +1\rangle$, with $\vec{f} = \vec{s} + \vec{v}$ the total atomic spin. First, we will focus on the resonance at 853 G.

In our picture the extremely rapid loss of the atomic condensate in the high ramp speed experiments is due to the fact that the formation and the decay of the resonance state occur at two different field values as a consequence of the delay caused by the resonance lifetime $\tau_{res,0}$. Whereas outside the resonance the energy of each of the two atoms follows adiabatically the single-atom Zeeman dependence (see schematic inset in Fig. 3.1), this energy decrease is interrupted during the lifetime of the resonance by a rate of change of energy, different by $\Delta\mu \dot{B}$. The result is a significantly increased kinetic energy of the free two-atom state arising from the decay of the quasibound state. This increase can be estimated as $\Delta\mu \dot{B} \tau_{res,0} \approx k_B [0.5 \text{ to } 3.5 \mu\text{K}]$ (the Boltzmann constant k_B will be omitted in all equations below where energy is expressed in Kelvins). Because it is larger than the mean-field energy in the condensate, the accelerated atoms are

counted as lost from the condensate when the remaining number of atoms is determined after the sweep [14]. In short, the quasibound pairs start to be formed from the atomic condensate, stimulated by a bosonic stimulation factor, and form a “molecular” condensate [15]. On the other hand, their decay back to the atomic condensate is almost completely suppressed due to the above kinetic energy gain. Instead, a very rapid decay takes place to a noncondensed atom fraction, which is effectively observed as a loss process. The possibility that the resonantly formed quasibound atom pairs form a condensate was previously suggested by Timmermans *et al.* [11]. In contrast to their proposal, however, a crucial element of our description is the above decay to a noncondensed atom fraction.

Interestingly, for the above estimate of the kinetic energy it is not the usual “global” resonance lifetime $\tau_{res} = \hbar/\gamma$ (where γ is the decay width) that is relevant but the, often much shorter, “local” lifetime $\tau_{res,0} = \hbar/\gamma_0$. This is the lifetime associated with the formation or decay of the resonance in the radial region ($r \lesssim 24$ atomic units a_0) where the quasibound state is coupled to the incoming channel via the exchange interaction. It follows from the energy dependence of the local phase shift δ_0 of the radial wavefunction at $r \approx 24 a_0$ near resonance. With $e^{2i\delta_0} = e^{2i\delta_{0,bg}} [1 - i\gamma_0/(E - \epsilon_{res} + \frac{i}{2}\gamma_0)]$ [12] we find $\tau_{res,0} = 1.4 \mu\text{s}$ (calculated using the interaction parameters derived in chapter 7 [16]). In this formula $\delta_{0,bg}$ is the background value of the local phase shift, ϵ_{res} is the resonance energy and $E \approx 1$ nK the typical kinetic energy for an atom in the condensate. The local lifetime is much shorter than the global lifetime $\tau_{res} = \hbar/\gamma(E) \sim E^{-\frac{1}{2}}$ of order 1 ms, associated with the energy dependence of the phase shift at a much larger distance ($r > 1000 a_0$). In contrast to an intermediate radial range where quantum reflection takes place [17], a wave packet propagates in the regions at small and large r without significant reflection, so that meaningful concepts of phase shift and delay time are possible. Understandably, the global lifetime is the resonance lifetime that mostly occurs in expressions for resonance phenomena. In our case it is much longer than the local lifetime due to strong quantum reflection.

3.3 Two-State Model

We calculate the atom loss fraction after the field ramp by considering the atom pairs in their quasibound state as a molecular Bose-Einstein condensate, described by a coherent field $\phi_2(\vec{x}, t)$ in addition to the field $\phi_1(\vec{x}, t)$ describing the atomic condensate. The evolution of the double-condensate system is described by a two-state model, governed by a pair of coupled Gross-Pitaevskii equations [11, 18]:

$$\begin{aligned} i\hbar\dot{\phi}_1 &= U_0|\phi_1|^2\phi_1 + 2\alpha\phi_1^*\phi_2, \\ i\hbar\dot{\phi}_2 &= (\epsilon_{res} - \frac{i}{2}\gamma_0)\phi_2 + \alpha\phi_1^2, \end{aligned} \quad (3.2)$$

with uniform amplitudes $\phi_{1,2} = \sqrt{n_{1,2}} \exp(i\theta_{1,2})$ over the volume of the condensate. Here $U_0 = 4\pi\hbar^2 a_\infty/m$ is the off-resonant strength of the atomic condensate self-energy and the α terms describe the process that converts atoms into molecules. In our simulations we omit the influence of the interactions between the molecules during their short lifetime and between those molecules and atoms. The coupling parameter is given by $\alpha = (\frac{1}{2}U_0\Delta\mu\Delta)^{1/2}$, while $\epsilon_{res}(t) - \frac{i}{2}\gamma_0 = [B(t) - B_0]\Delta\mu - \frac{i}{2}\gamma_0$ is the complex energy of the quasibound state relative to threshold including its decay width. In view of that large decay width, we treat ϕ_2 by the method of elimination of fast variables, expressing it as $\phi_2(t) = -\alpha\phi_1^2/(\epsilon_{res} - \frac{i}{2}\gamma_0)$. We then end up with an equation for $\phi_1(t)$ only:

$$i\hbar\dot{\phi}_1 = \left(U_0 - \frac{2\alpha^2}{\epsilon_{res}(t) - \frac{i}{2}\gamma_0} \right) |\phi_1|^2 \phi_1 = U |\phi_1|^2 \phi_1, \quad (3.3)$$

with initial condition $\phi_1(-\infty) = \sqrt{n_i}$. Apparently, the influence of the resonance during the field ramp has effectively the form of a Breit-Wigner contribution to the condensate self-energy. The off-resonant strength U_0 changes into $U = 4\pi\hbar^2 a/m$, with a complex scattering length of the form (3.1) with B_0 replaced by $B_0 + \frac{i}{2}\Delta B$, where $\Delta B = \gamma_0/\Delta\mu$. The quantity ΔB characterizes the local width of the resonance as a function of the field. It is approximately equal to twice the width parameter Δ of Eq. (3.1) in the circumstances of the experiment. More generally, the ratio $\Delta/\Delta B$ is related to the transmission through the quantum reflection region and depends on a_∞ . The imaginary part of U describes the decay of the atomic condensate: $\dot{n}_1 = -G(t)n_1^2$, with the rate coefficient $G(t) = \frac{2\alpha^2}{\hbar}\gamma_0/(\epsilon_{res}^2 + \frac{1}{4}\gamma_0^2)$. Its maximum value is $8\alpha^2/\hbar\gamma_0 = 4U_0\Delta/\hbar\Delta B \approx 2 \times 10^{-10} \text{cm}^3\text{s}^{-1}$, independent of \dot{B} . To our knowledge, this value for the instantaneous rate of decay observed in the MIT experiment represents the largest inelastic rate for a cold atom process ever observed, at least 1 order of magnitude larger than typical exchange decay rates ($G_{exch} \approx 10^{-11} \text{cm}^3\text{s}^{-1}$) and 5 orders larger than typical dipolar decay rates ($G_{dip} \approx 10^{-15} \text{cm}^3\text{s}^{-1}$). Note that the physics of our picture is very similar to that of *exchange* relaxation in the vicinity of a Feshbach resonance (forbidden in our case). In chapter 6 [19] we predict for that process in ${}^6\text{Li}-{}^7\text{Li}$ collisions a relaxation rate with a quantum limit magnitude, at least 10^3 larger than the typical exchange value.

Integrating the rate equation we obtain the fraction of atoms lost from the condensate for a given ramp speed:

$$\frac{n_i - n_f}{n_i} = \frac{n_i \int G(t) dt}{1 + n_i \int G(t) dt} \equiv \frac{p(\dot{B})}{1 + p(\dot{B})}, \quad (3.4)$$

where $p(\dot{B}) = \pi(U_0 n_i/\hbar) \cdot (2\Delta/\dot{B})$. Apparently, the loss is determined by the non-

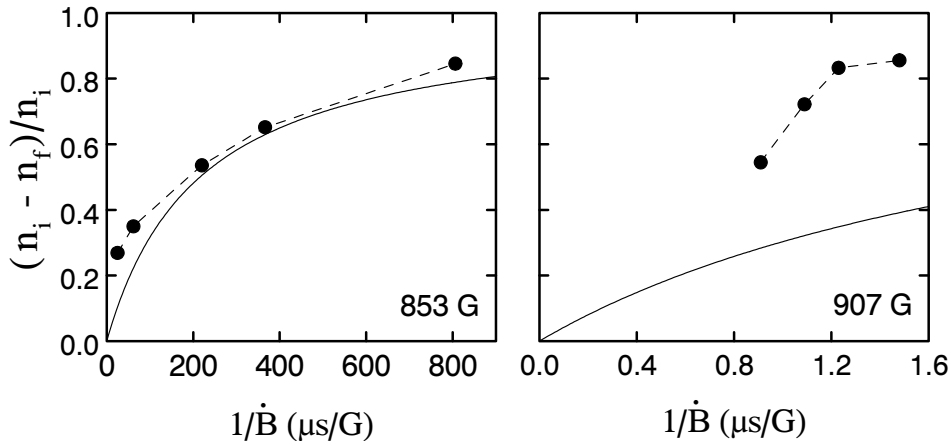


Figure 3.2 Predicted (solid lines) and measured (dots connected by dashed lines) fraction of lost atoms after crossing the Feshbach resonance as a function of inverse ramp speed for the resonances at 853 and 907 G.

resonant change of the condensate phase θ_1 during the crossing of the resonance. Note that the two-state model predicts the loss fraction to depend on n_i and \dot{B} only via the combination n_i/\dot{B} . The specific properties of the resonance come in only via Δ as was already implicitly assumed in Ref. [10]. While a fast time dependence of the magnetic field is needed for the resonant loss process, the loss decreases with increasing \dot{B} due to the shorter time in which the resonance is crossed.

3.4 Results

In Fig. 3.2 we present the loss fraction for $\tau_{res,0}$ equal to the calculated value $1.4 \mu\text{s}$ ($\gamma_0 = 5.3 \mu\text{K}$, $\Delta = 0.0091 \text{ G}$). We obtain rather good agreement with experiment for $n_i = 7.0 \times 10^{14} \text{ cm}^{-3}$. This (uniform) initial density agrees with the experimental value $5.2 \times 10^{14} \text{ cm}^{-3}$ for the mean initial density within the combined experimental ($\pm 5\%$ statistical, $\pm 20\%$ systematic) [14] and theoretical error bars.

In the case of the 853 G resonance, the quasibound state and the free two-atom state are very weakly coupled. The coupling is more than a factor 100 stronger for the other resonance at 907 G. Fig. 3.2 shows the loss fraction following from the previous expressions for the calculated value $\tau_{res,0} = 0.012 \mu\text{s}$ ($\gamma_0 = 646 \mu\text{K}$, $\Delta = 1.05 \text{ G}$) at the experimental mean density $n_i = 5.7 \times 10^{14} \text{ cm}^{-3}$ [14]. Clearly, for both resonances the order of magnitude of the loss rate is correctly described, confirming the basic mechanism. For the 907 G resonance, however, the theoretical prediction shows a difference with experiment. We believe that this is due to the fact that for the highest experimental \dot{B} values the time dependence of the scattering process is incompletely described in

our two-state model. In particular, the finite time needed for the transmission of a wave packet through the quantum reflection region and for the multiple reflections between this region and the origin may play a role, since it turns out to be comparable to the time in which the resonance is crossed with the magnetic field. This suggests that in this regime the time-dependent resonance phenomenon in a condensate is too involved to be described in terms of a combination of an atomic and a molecular condensate wavefunction.

Instead, a description with a pair condensate wavefunction $\phi(\vec{x}_1, \vec{x}_2, t)$ in analogy to the independent-pair description for fermionic systems [20] would seem appropriate. This requires a generalization of the coupled Gross-Pitaevskii equations. Remarkably, we found that a simple extension of the above coupled Eqs. (3.2) with an extra coupling term in both equations produced by an additional reflection, describes qualitatively the behavior of the observed loss fraction for a delay time due to reflection of about 10 μs . The situation of the quantum reflection region separating two condensates (a condensate of free atoms and a “long-range molecular” condensate) with an initial removal of atom pairs on one side during the crossing of the resonance, is reminiscent of the Josephson effect [2]. In this picture, two types of molecular condensate play a role: The “long-range” condensate of atom pairs in the initial spin state with interatomic distances up to the quantum reflection region and the “short-range” condensate of quasibound pairs in the admixed spin state. The latter is only indirectly coupled with the atomic condensate via the long-range molecular condensate. The excess loss observed experimentally would be caused by the additional resonance absorption of the inward atom flux arising from the first Josephson oscillation. The fall-off of this excess loss at low $1/\dot{B}$ would be due to an arrival at $24 a_0$ with a 10 μs delay of the order of the inverse Josephson frequency, too late to be in full resonance with the quasibound state.

3.5 Two-Step Three-body Decay in Type 1 Runs

We now turn to the experimental data for the runs of type 1. In this case, the fast-sweep two-body decay mechanism is absent and most of the loss occurs after the field ramp. We follow the treatment by Timmermans *et al.* [11] (see also Ref. [21]), which we recapitulate using the latest Na parameters (see chapter 7 [16]). They explain the loss as a two-step process: the formation of quasibound pairs during the adiabatic field change, followed by stabilizing collisions of such pairs with third Na atoms with rate coefficient G_{stab} . The density of quasibound pairs follows directly from the static off-resonant equivalent of Eq. (3.2) without γ_0 , as well as from an explicit wavefunction calculation: $n_2 = (\alpha^2/\epsilon_{res}^2)n_1^2$. Assuming that all three atoms are lost, we have the

rate equation

$$\dot{n}_1 = -3G_{stab} \left[\frac{\alpha}{\Delta\mu(B - B_0)} \right]^2 n_1^3. \quad (3.5)$$

Note that this equation is valid for fields smaller and larger than B_0 . An approximate determination of the effective two-body relaxation constant G_{stab} is possible using Fig. 2 of Ref. [10]. We find good agreement with experiment with $G_{stab} = 4 \times 10^{-10} \text{ cm}^3\text{s}^{-1}$ for the 907 G resonance and $G_{stab} = 1 \times 10^{-11} \text{ cm}^3\text{s}^{-1}$ for the 1195 G resonance, both with an order of magnitude in the range 10^{-9} to $10^{-11} \text{ cm}^3\text{s}^{-1}$ estimated by Timmermans *et al.* [11] on the basis of calculations for $\text{H}_2 + \text{He}$ collisions. For the 907 G we can thus compare the decay width $\gamma_{stab} = \hbar G_{stab} n_1$ to γ_0 . We find γ_{stab} to be smaller by a factor of order 100 and thus negligible in runs of type 2.

3.6 Conclusions

We have given an explanation for the losses in the MIT high ramp speed experiment. As a next step, a more detailed understanding on the basis of an extended version of the Gross-Pitaevskii equations would be important, since it should then be possible to make reliable further predictions. For instance, a high ramp speed experiment with a tailored time dependence might lead to the “permanent” formation of a molecular condensate. If followed by a suitable stimulated Raman pulse, this could be converted to a more strongly bound state [15, 18]. The resonance at 1195 G seems to be particularly interesting for this purpose. There, the energy of the quasibound state decreases with increasing magnetic field, so that a simple fast sweep from low to high field tends to create condensed molecules rather than atoms with increased kinetic energy. A fast sweep from high to low field across the 853 G or 907 G resonance would have a similar effect but has the disadvantage of reducing the condensate fraction when the field is turned on. The dependence on field ramp direction is typical for the fast-sweep two-body mechanism and absent in the 3-body mechanism proposed by Timmermans *et al.* Additional high ramp speed observations should be of great importance to test the above n_i/\dot{B} dependence of the loss for the 853 G resonance, while time-resolved measurements might detect the Josephson-like current-phase effects expected for the 907 G resonance.

References

- [1] M.H. Anderson *et al.*, Science **269**, 193 (1995); K. Davis *et al.*, Phys. Rev. Lett. **75**, 3969 (1995); C.C. Bradley *et al.*, *ibid.* **78**, 985 (1997); D.G. Fried *et al.*, Phys. Rev. Lett. **81**, 3811 (1998).
- [2] F. Dalfovo, S. Giorgini, L.P. Pitaevskii, and S. Stringari, Rev. Mod. Phys. **71**, 463 (1999).

-
- [3] J. Stenger, S. Inouye, D.M. Stamper-Kurn, H.-J. Miesner, A.P. Chikkatur, and W. Ketterle, *Nature* **396**, 345 (1998).
 - [4] L. Deng, E.W. Hagley, J. Wen, M. Trippenbach, Y. Band, P.S. Julienne, J.E. Simsarian, K. Helmerson, S.L. Rolston, and W.D. Phillips, *Nature* **398**, 218 (1999).
 - [5] E. Tiesinga, B.J. Verhaar, and H.T.C. Stoof, *Phys. Rev. A* **47**, 4114 (1993); E. Tiesinga, A.J. Moerdijk, B.J. Verhaar, and H.T.C. Stoof, *ibid.* **46**, R1167 (1992).
 - [6] S. Inouye, M.R. Andrews, J. Stenger, H.-J. Miesner, D.M. Stamper-Kurn, and W. Ketterle, *Nature* **392**, 151 (1998).
 - [7] Ph. Courteille, R.S. Freeland, D.J. Heinzen, F.A. van Abeelen, and B.J. Verhaar, *Phys. Rev. Lett.* **81**, 69 (1998).
 - [8] J. L. Roberts, N. R. Claussen, James P. Burke, Jr., Chris H. Greene, E. A. Cornell, and C. E. Wieman, *Phys. Rev. Lett.* **81**, 5109 (1998).
 - [9] Yu. Kagan, E.L. Surkov, and G.V. Shlyapnikov, *Phys. Rev. Lett.* **79**, 2604 (1997).
 - [10] J. Stenger, S. Inouye, M.R. Andrews, H.-J. Miesner, D.M. Stamper-Kurn, and W. Ketterle, *Phys. Rev. Lett.* **82**, 2422 (1999).
 - [11] E. Timmermans, P. Tommasini, R. Côté, M. Hussein, A. Kerman, *Phys. Rev. Lett.* **83**, 2691 (1999).
 - [12] C.J. Joachain, *Quantum Collision Theory* (North-Holland, New York, 1972).
 - [13] F.A. van Abeelen, D.J. Heinzen and B.J. Verhaar, *Phys. Rev. A* **57**, R4102 (1998).
 - [14] W. Ketterle and J. Stenger, *Priv. commun.*
 - [15] P.S. Julienne, K. Burnett, Y. B. Band, and W. C. Stwalley, *Phys. Rev. A* **58**, R797 (1998).
 - [16] F.A. van Abeelen and B.J. Verhaar, *Phys. Rev. A* **59**, 578 (1999).
 - [17] P.S. Julienne and F.H. Mies, *J. Opt. Soc. Am. B* **6**, 2257 (1989).
 - [18] D.J. Heinzen, P.D. Drummond, and K.V. Kheruntsyan (to be published).
 - [19] F.A. van Abeelen and B.J. Verhaar, *Phys. Rev. A* **55**, 4377 (1997).
 - [20] A. deShalit and H. Feshbach, *Theoretical Nuclear Physics, Part 1: Nuclear Structure* (Wiley, New York, 1974).
 - [21] M. W. Reynolds, I. Shinkoda, R. W. Cline, and W. N. Hardy, *Phys. Rev. B* **34**, 4912 (1986).

4

Photoassociation as a Probe of Feshbach Resonances in Cold-Atom Scattering

F.A. van Abeelen, D.J. Heinzen, and B.J. Verhaar

Published in Phys. Rev. A **57**, R4102 (1998)

We investigate theoretically the influence of magnetically tunable Feshbach collision resonances on the photoassociation spectra of ultracold atoms. As an example we consider recently predicted resonances for ^{85}Rb atoms. For excitation to the $^{85}\text{Rb}_2 0_g^-(S_{1/2}+P_{1/2})$ electronic state, we predict that the photoassociation rate is resonantly enhanced by at least two orders of magnitude. We find that photoassociation could serve as a useful probe for studying Feshbach resonances in ultracold collisions. In turn, these resonances should be very important to Bose-condensed gases, and more generally, to coherent atom optics.

4.1 Introduction

After the first observations of Bose-Einstein condensation (BEC) in dilute, ultracold gases of alkali-metal atoms [1–3], rapid progress has been made in observing and understanding the properties of Bose condensates. Atomic interactions have been found to play a crucial role. Their effect may be accounted for in a mean-field model by a self-energy $4\pi\hbar^2 n(\vec{r})a/m$, where a is the two-body scattering length, m the mass of the atoms, and n their density. In spite of the importance of interactions, in many respects the range of accessible interaction strengths has been rather limited. For example, an important natural scaling parameter for the interaction strength is $\eta = 1.57(N^{1/6}a/a_{HO})^{2/5}$, where a_{HO} is the spread of the zero-point wave function of the trapped atoms and N is their number [4]. For positive scattering length gases, only a very narrow range for η near the value 0.4 has been realized. A negative scattering length gas has also been explored [3], but again under rather limited circumstances. The experiment confirms predictions [5] that condensates can form only if the attractive mean-field energy is less than the spacing of the trap levels. For larger interaction energies the condensate presumably collapses [5], but the physics of such a collapse is as yet unclear.

In order to more fully understand the effect of atomic interactions on dilute Bose condensates, it would clearly be desirable to be able to tune the scattering length to an arbitrary value. This would allow studies of BEC in very strong or weak interaction limits, and it might also be possible to study the dynamics of the collapse of a condensate induced by a sudden switch of the sign of a . A proposal to produce such variations of the scattering length with magnetic-field-induced Feshbach resonances was published some years ago [6]. Feshbach resonances are scattering resonances which arise when the total energy of a pair of colliding atoms matches the energy of a quasibound two-atom state, leading to the resonant formation of this state during the collision. Magnetic tuning of the resonance is possible if the magnetic moments of the free and quasibound states are different, and this allows for tuning of the scattering length. A concrete example of this was predicted recently for the case of a ^{85}Rb gas sample in the highest level ($|f, m_f\rangle = |2, -2\rangle$) of the $f = 2$ lower hyperfine manifold [7]. According to this prediction, based on a previous analysis of measured bound $^{85}\text{Rb}_2$ levels [8], a can be given an arbitrary positive or negative value by changing the strength of the magnetic field around a certain resonance value for each of three Feshbach resonances. All of these are in the range where the atoms can be trapped in a static magnetic trap.

The potential importance of these scattering resonances is not necessarily restricted to single-species Bose condensation. For instance, they could allow tuning of the relative interaction strengths between and within species in a multicomponent Bose condensate. Feshbach resonances might play a role in minimizing interactions within the lasing species in an atom laser. Resonant interactions between coherent beams of atoms might be important, and could occur at a nonzero and sharply defined value of the relative kinetic energy.

Experimental studies of these collision resonances are clearly desirable, in order to determine the quantum numbers of the resonances, the field values at which resonances occur as a function of collision energy, and the resonance widths. We propose a method to observe and study Feshbach resonances based on cold-atom photoassociation [9].

4.2 Photoassociation as a Probe of Feshbach Resonances

In the photoassociation (PA) process, a photoassociation laser optically excites two colliding ground-state atoms into a bound electronically excited molecular state. We predict a dramatic increase of the PA signal for magnetic field strengths in the vicinity of a Feshbach resonance; the resonant formation of the quasibound two-atom state increases the penetration of the colliding atoms to the distance range where the optical excitation occurs. This enhancement of the PA signal should serve as a clear-cut signal for the occurrence of a Feshbach resonance at the experimental field strength. To be concrete, we consider the specific example of the predicted Feshbach resonances of

^{85}Rb [7], but many of the conclusions of this analysis should apply more generally.

An alternative method to observe and study Feshbach resonances would be through their impact on the thermalization of an ultracold gas [10], or on the properties of a Bose-condensed gas. However, photoassociation has certain advantages over studies of gas properties that should make this technique of some interest. First, studies of gas properties at many different field values are rather cumbersome and difficult to carry out. In contrast to this, photoassociation provides a very rapid and direct signature of a collision resonance. This could be particularly important when searching for a very narrow resonance. Further, the analysis of gas thermalization experiments becomes very complicated once the elastic collisions are energy dependent and no longer purely s -wave. With photoassociation, selecting the 0_g^- electronic state connected to the $S_{1/2} + P_{1/2}$ separated-atom limit as the final state circumvents this problem. This state has total electronic angular momentum quantum number $j = 0$ and, therefore, imposes the selection rule $l = J$ for the partial wave l of the ground-state collision that can give rise to the formation of a given excited two-atom rotational state J [11]. Thus, one can study all partial waves separately. Finally, the laser frequency is an extra parameter available experimentally that allows one to study the energy dependence of the resonance phenomenon through careful analysis of the PA line shapes. In fact, scanning both the laser frequency and the magnetic field makes for an ideal new kind of spectroscopy for exploring the structure of the region between the lowest and highest hyperfine-split dissociation limits. One would expect similar resonances in other partial-wave channels at higher temperatures and in other hyperfine entrance channels if the atoms are not polarized.

4.3 Numerical Calculation of the Signal

To illustrate the usefulness of the photoassociation method for the detection and study of field-induced resonances, we calculate the expected PA signal for the broadest of the three predicted ^{85}Rb resonances, which is also predicted to occur at the lowest field strength, i.e., 142 G. We consider a specific temperature (0.3 mK) for the ^{85}Rb gas sample and a linearly polarized PA laser beam propagating in the direction of the magnetic field. For the sake of definiteness we consider the excitation of a specific vibrational level of the lower 0_g^- state with a $J = 0$ level energy at -3.365 cm^{-1} with respect to the barycenter of the $S_{1/2} + P_{1/2}$ dissociation limit. Due to the $l = J$ selection rule, the Feshbach resonance considered should only show in the PA signal for the excitation of $J = 0$ rovibrational levels. Finally, we assume low enough laser intensities that saturation effects can be neglected.

Since the 0_g^- excited state is purely triplet, in the calculation of the PA intensity only the part $P_{S=1}\psi_c$ of the ground-state collisional wave function ψ_c contributes to

the optical matrix element. Here, $P_{S=1}$ is a projection operator on the triplet spin subspace, while ψ_c describes both the relative motion of the atoms and the electronic and nuclear spin dynamics, and is energy normalized. $P_{S=1}\psi_c$ follows from a coupled-channels calculation and is a linear combination of $|S, m_S, I, m_I\rangle$ components:

$$P_{S=1}\psi_c = \sum_{m_S, I, m_I} u_{S=1, m_S, I, m_I}(r; E) |S = 1, m_S, I, m_I\rangle, \quad (4.1)$$

subject to the requirements of Bose symmetry ($l+S+I = 1+I = \text{even}$) and conservation of spin angular momentum about the field direction ($m_S+m_I = -4$). The partial width γ_L for the laser excitation is then given by

$$\gamma_L(E) = \frac{\pi I_L}{\varepsilon_0 c} \sum_{I, m_I} \left| \sum_{m_S} \int_0^\infty u_f(r) \langle j, m_j = 0, 0 | [\vec{d}_1 + \vec{d}_2] \cdot \vec{\sigma}_L | S = 1, m_S \rangle u_{S=1, m_S, I, m_I}(r; E) dr \right|^2, \quad (4.2)$$

with E the collision energy, I_L the laser intensity, $\vec{\sigma}_L$ its polarization vector, $u_f(r)$ the radial wave function of the final state, and \vec{d}_1 and \vec{d}_2 the atomic electric dipole operators. Compared to Eq. (3) of Ref. [11] a coherent sum over m_S and an incoherent sum over I, m_I have been added. This simple treatment of the nuclear spin is possible because of the selection of the 0_g^- state, which avoids a complicated “hyperfine spaghetti” structure of the PA spectrum. The second-order Zeeman broadening of the 0_g^- state is negligible compared to the width γ_0 due to spontaneous decay, despite the relatively strong magnetic field.

Figure 4.1 shows the laser frequency dependence of the expected PA signal in arbitrary units, for a number of B values close to the resonance field value and two nonresonant fields. The abscissa is the laser detuning Δ_L relative to the energy difference between the asymptotic ground hyperfine state and the above-mentioned final vibrational level. We find a dramatic resonance enhancement close to $B = 143$ G; the PA maximum grows to a value at least two orders larger than the nonresonant background value. A gradual shift of the maximum to the right combined with an almost constant width at half maximum, is noticeable for increasing field values. The width of the peaks corresponds approximately to γ_0 .

To illustrate the origin of the increased PA maximum, in Figs. 4.2(a) and 4.2(b) we show the radial wave functions for the hyperfine components $|f_1, m_{f1}, f_2, m_{f2}\rangle$ of ψ_c for $E = 0.3$ mK and two values of B : one close to the resonance value and one further off. The resonant enhancement of the penetration, due to the admixture of the quasibound two-atom state in ψ_c , is clearly visible in the form of a large increase of the spin components that are formed by the promotion of one or both atoms from

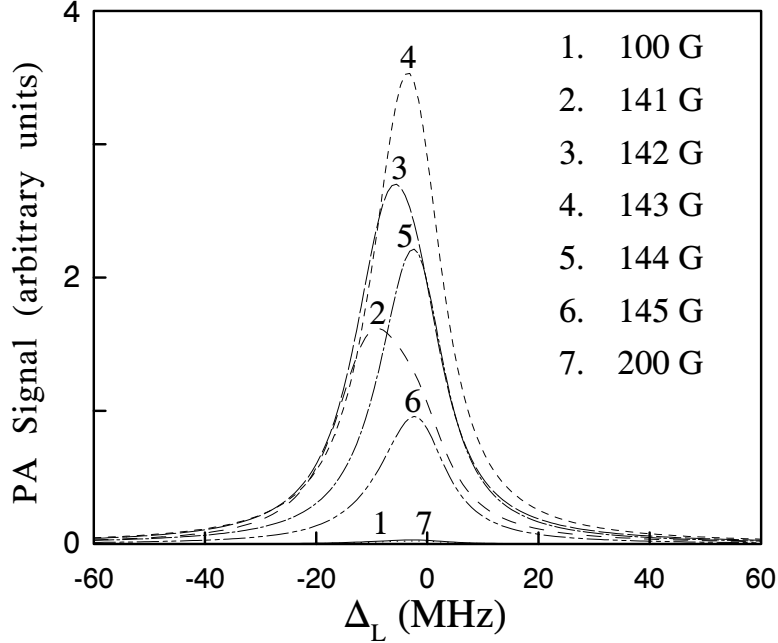


Figure 4.1 Calculated photoassociation signal as a function of laser frequency for the ^{85}Rb Feshbach resonance in arbitrary units, for five B values near the resonance field value and two values further off.

the lower hyperfine manifold $f = 2$ to $f = 3$. The shift in the location of the PA maximum is due to the approach of the total energy at resonance to the threshold of the $|f_1, m_{f1}, f_2, m_{f2}\rangle = |2, -2, 2, -2\rangle$ incident channel, reducing the resonant collisional kinetic energy ε_{res} and thus increasing the resonant laser frequency. This is consistent with the predicted pattern of the $a(B)$ dependence [7]: a decrease to $-\infty$, followed by a decrease from $+\infty$ for increasing B , pointing to a quasibound state that crosses the threshold from above (see Fig. 4.3).

4.4 An Analytical Model

A more detailed investigation of the partial width γ_L for the laser excitation enables a qualitative explanation of all the main features of Fig. 4.1. In Fig. 4.4 we show the dependence of γ_L on the collision energy E for a value of B close to the resonance field. A clear resonance behavior is visible superposed on a nonresonant background. The resonant part is described approximately by a Breit-Wigner-like factor $(\Gamma/2\pi)/[(E - \varepsilon_{res})^2 + \frac{1}{4}\Gamma^2]$ with $\Gamma(B)$ the resonance width. Figure 4.4 also shows a Breit-Wigner fit to $\gamma_L(E)$. The width turns out to be at most of order 0.2 mK. We

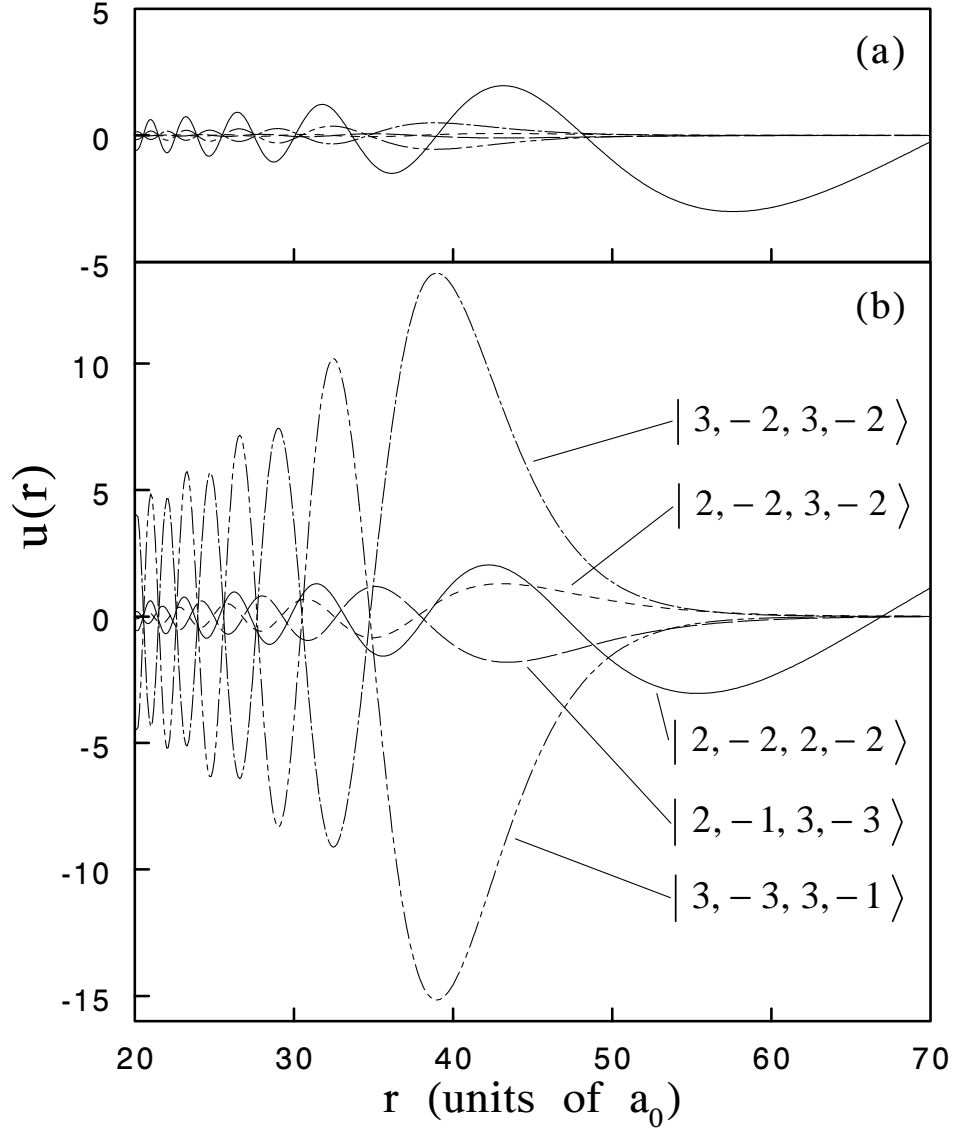


Figure 4.2 Radial wave functions $u(r)$ for the hyperfine components $|f_1, m_{f_1}, f_2, m_{f_2}\rangle$ of the ground-state collisional wave function, for collision energy $E = 0.3$ mK (with amplitude $(ka_0)^{-1/2}$ for $r \rightarrow \infty$, where k is the asymptotic wave number). (a) Field far from resonance ($B = 100$ G). (b) Field close to resonance ($B = 143$ G). Resonant admixture of a quasibound two-atom state enhances the interior wave functions.

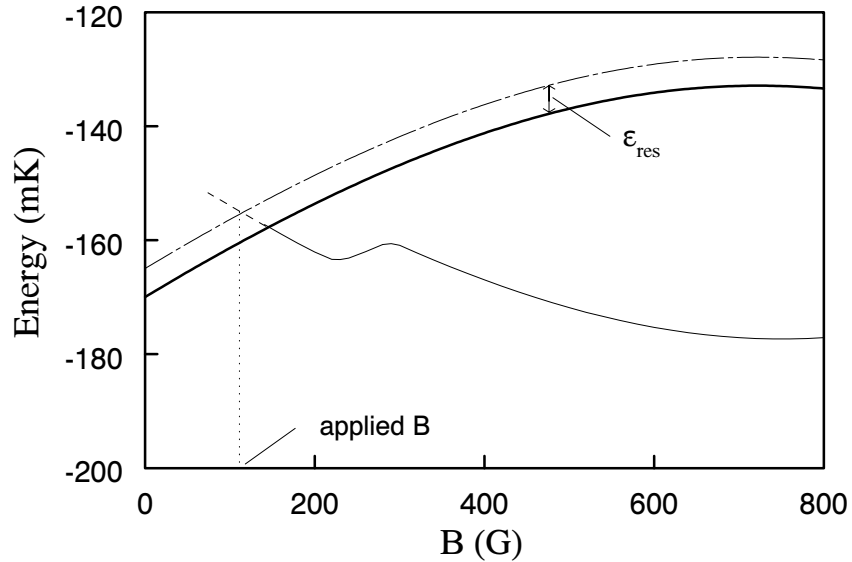


Figure 4.3 Bound-state energy (thin solid line) and entrance channel threshold (thick line) as a function of the magnetic field strength B . The dashed extrapolation of the bound-state curve is a symbolic representation of a quasibound state embedded in the continuum. A Feshbach resonance occurs when the total energy (threshold plus kinetic energy; dashed-dotted line) equals the quasibound-state energy at the applied magnetic field. For clarity the figure shows a situation where the resonant kinetic energy ϵ_{res} is higher than the energies that contribute to the PA signal at experimental temperatures.

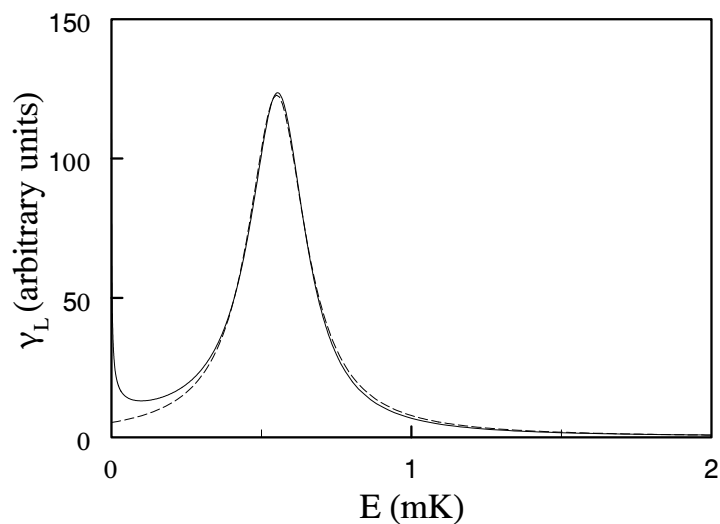


Figure 4.4 Dependence of partial width γ_L (solid line) for laser excitation on collision energy E close to resonance and a Breit-Wigner fit to this curve (dashed line).

find that $\varepsilon_{res}(B)$ shows approximately a linear B dependence, as one would expect for a state that crosses the threshold to become bound. It is interesting to note, however, that the crossing ($\varepsilon_{res} = 0$) appears to occur at a field somewhat larger than where the scattering length becomes infinite ($B = 142$ G), due to interference of the resonance with the background for small ε_{res} .

Retaining only the Feshbach resonance contribution to γ_L and describing it by the above Breit-Wigner form, the photoassociation rate constant

$$K(T, B, \omega_L) = \left\langle v \frac{\pi}{k^2} \frac{\gamma_0 \gamma_L}{[E + \Delta_L]^2 + \frac{1}{4} \gamma_0^2} \right\rangle_{\text{th}}, \quad (4.3)$$

with the brackets $\langle \cdot \rangle_{\text{th}}$ standing for a thermal average over the collision velocity v and the associated wave number k , factorizes into the E integral

$$T^{-3/2} \int_0^\infty dE e^{-E/k_B T} \frac{1}{[E + \Delta_L]^2 + \frac{1}{4} \gamma_0^2} \frac{\Gamma/2\pi}{[E - \varepsilon_{res}]^2 + \frac{1}{4} \Gamma^2} \quad (4.4)$$

and a factor K_0 independent of T , B and ω_L . Γ is sufficiently small compared to the two remaining energy scales $k_B T$ and γ_0 occurring in the integral (4.4), for a qualitative description in which we approximate the Feshbach resonance energy dependence by a Dirac δ function and obtain

$$K(T, B, \omega_L) = K_0 T^{-3/2} e^{-\varepsilon_{res}/k_B T} \frac{1}{[\varepsilon_{res} + \Delta_L]^2 + \frac{1}{4} \gamma_0^2}. \quad (4.5)$$

Eq. (4.5) describes the qualitative features of the PA signals with $141 \text{ G} < B < 143 \text{ G}$ displayed in Fig. 4.1: (1) A shift of the signals from $\Delta_L = 0$ over $\varepsilon_{res}(B)$ in the negative Δ_L direction; (2) a width approximately equal to the spontaneous emission rate γ_0 ; (3) a decrease in magnitude of the PA maximum with increasing resonance energy above threshold. The decrease of the signal with increasing B above 143 G can be ascribed to the gradual disappearance of the resonance below threshold.

4.5 Conclusions

We conclude that magnetic-field induced Feshbach resonances will be readily observable in a photoassociation experiment carried out on a ^{85}Rb gas sample. We predict a strong enhancement of the PA signal, with a dependence on the laser frequency and the magnetic field that can be qualitatively understood by considering the limit of a vanishing width of the Feshbach resonance. The laser detuning at the maximum of the PA signal immediately gives the resonant kinetic energy at the experimental field. The observation of the PA spectral peak for varying B could enable the first experimental demonstration of the shift of a Feshbach resonance into the continuum, starting from a bound two-atom state that crosses the threshold of the elastic scattering channel. An

interesting alternative possibility to study this phenomenon could be realized via a two-photon experiment, where two atoms in the $|f_1 = 3, m_{f_1} = -3\rangle + |f_2 = 3, m_{f_2} = -3\rangle$ entrance channel collide in the presence of two laser fields of frequency ω_1 and ω_2 that enable a two-photon transition to the above-mentioned bound state. Again, varying the magnetic field, the latter could be tuned to above the threshold.

For these reasons, photoassociation spectroscopy appears well suited as a probe of Feshbach resonant collisions, and more generally as a spectroscopic probe of the structure of the region between the lowest and highest hyperfine-split two-atom dissociation limits. Such scattering resonances should provide new opportunities to study Bose-Einstein condensates with a wider range of interaction strengths, and may have other applications in atom optics. We finally note that very precise measurements of the magnetic field values at which the collisions are resonant could more precisely determine interatomic potentials.

Acknowledgment

D.J. Heinzen acknowledges support from the R.A. Welch Foundation, the National Science Foundation, and the NASA Microgravity Research Division.

References

- [1] M.H. Anderson, J.R. Ensher, M.R. Matthews, C.E. Wieman, and E.A. Cornell, *Science* **269**, 198 (1995).
- [2] K.B. Davis, M.-O. Mewes, M.R. Andrews, N.J. van Druten, D.S. Durfee, D.M. Kurn, and W. Ketterle, *Phys. Rev. Lett.* **75**, 3969 (1995).
- [3] C.C. Bradley, C.A. Sackett, and R.G. Hulet, *Phys. Rev. Lett.* **78**, 985 (1997); *ibid.* **75**, 1687 (1995).
- [4] S. Giorgini, L. P. Pitaevskii, and S. Stringari, *Phys. Rev. Lett.* **78** 3987 (1997).
- [5] Yu. Kagan, E.L. Surkov, and G.V. Shlyapnikow, *Phys. Rev. Lett.* **79**, 2604 (1997).
- [6] E. Tiesinga, A.J. Moerdijk, B.J. Verhaar, and H.T.C. Stoof, *Phys. Rev. A* **46**, R1167 (1992); E. Tiesinga, B.J. Verhaar, and H.T.C. Stoof, *Phys. Rev. A* **47**, 4114 (1993).
- [7] J. M. Vogels, C. C. Tsai, R. S. Freeland, S. J. J. M. F. Kokkelmans, B. J. Verhaar, and D. J. Heinzen, *Phys. Rev. A* **56**, R1067 (1997).
- [8] C. C. Tsai, R. S. Freeland, J. M. Vogels, H. M. J. M. Boesten, B. J. Verhaar, and D. J. Heinzen, *Phys. Rev. Lett.* **79**, 1245 (1997).
- [9] D.J. Heinzen in *Atomic Physics 14*, Proceedings of the Fourteenth International Conference on Atomic Physics, Boulder, CO, 1994, edited by D.J. Wineland, C.E. Wieman, and S.J. Smith, AIP Conf. Proc. No. **323** (AIP, New York, 1995), pp. 211-218.
- [10] N. R. Newbury, C. J. Myatt, and C. E. Wieman, *Phys. Rev. A* **51**, R2680, (1995).

- [11] J. R. Gardner, R. A. Cline, J. D. Miller, D. J. Heinzen, H. M. J. M. Boesten, and B. J. Verhaar, *Phys. Rev. Lett.* **74**, 3764 (1995).

5

Observation of a Feshbach Resonance in Cold-Atom Scattering

Ph. Courteille, R. S. Freeland, D. J. Heinzen, F.A. van Abeelen, and B.J. Verhaar

Published in Phys. Rev. Lett. **81**, 69 (1998)

We probe s -wave collisions of laser-cooled ^{85}Rb $|f = 2, m_f = -2\rangle$ atoms with Zeeman-resolved photoassociation spectroscopy. We observe that these collisions exhibit a magnetically tunable Feshbach resonance, and determine that this resonance tunes to zero energy at a magnetic field of 164 ± 7 G. This result indicates that the self-interaction energy of an ^{85}Rb Bose-Einstein condensate can be magnetically tuned. We also demonstrate that Zeeman-resolved photoassociation spectroscopy provides a useful new tool for the study of ultracold atomic collisions.

5.1 Introduction

The observation of Bose-Einstein condensation (BEC) in dilute, magnetically trapped alkali gases has created exciting new opportunities for studies of macroscopic quantum phenomena [1–7]. An important aspect of dilute gas BEC is that two-body interactions dominate, and give rise to a condensate self-energy proportional to the two-body scattering length a . The self-energy strongly influences most of the important properties of a condensate, including its stability, formation rate, size and shape, and collective excitations. There has been considerable interest in finding ways to experimentally modify the scattering length, because that could make possible studies of a BEC with a very strong, very weak, positive, negative, or even time-dependent interaction strength, all within a single experiment. One promising proposal to do this relies on the strong variation of a that occurs if a Feshbach collision resonance is tuned through zero energy [8]. Such a tunable resonance could be induced optically, but this method introduces undesired effects of optical spontaneous emission into the condensate [9, 10]. Magnetically tunable Feshbach resonances that arise from the coupling between different spin channels in an atomic collision can also result in a tunable value of a [8, 11, 12]. A previous search for this type of resonance [13] did not detect one. Interest in this topic increased with a prediction of a zero-energy Feshbach resonance in collisions of ^{85}Rb $|f = 2, m_f = -2\rangle$ atoms [12]. In this paper, we report the observation of this reso-

nance, which we find tunes to zero energy at a magnetic field of 164 ± 7 G. From the observed position and width of the resonance, we are able to precisely determine ^{85}Rb interaction parameters. Our work, along with a recent report of a similar resonance in an atomic ^{23}Na BEC [14], constitute the first observations of this important cold collision phenomenon.

5.2 Experimental Method

In order to detect this resonance, we use photoassociation spectroscopy [15] to probe the collisions of laser-cooled ^{85}Rb atoms in a magnetic field. The concept of the experiment is illustrated in Fig. 5.1. To be concrete, we specialize to our particular case. Free, ground-state ^{85}Rb atoms collide in the $|f = 2, m_f = -2\rangle + |f = 2, m_f = -2\rangle$ entrance channel. Here, $f = 2$ or 3 is the hyperfine state (combined electron and nuclear spin) of an atom and m_f is the spin projection quantum number of that atom. The entrance channel has a total angular momentum projection quantum number $M_F = -4$, equal to the sum of the two atomic m_f values. It is coupled to other $M_F = -4$ channels at small internuclear distance by the electronic exchange interaction. The other $M_F = -4$ potential curves all correlate to the higher energy $f = 2 + f = 3$ or $f = 3 + f = 3$ dissociation limits. They support multichannel quasibound states at positive energies, where we take the zero of energy to be the threshold of the entrance channel. If the energy of the incoming atoms matches the energy of one of these states, a Feshbach resonance occurs in which a large wave-function amplitude builds up in the quasibound state. The resonance energy can be tuned to zero with a magnetic field because the quasibound state and threshold energy Zeeman shift at different rates. In that case the resonance strongly affects ultracold collisions. In order to detect the resonance, we drive photoassociation transitions to the excited $^{85}\text{Rb}_2 0_g^-$ bound molecular vibrational state at an energy 5.9 cm^{-1} below the $5^2S_{1/2} + 5^2P_{1/2}$ dissociation limit [16]. As discussed below, we are able to isolate a single component of the spectrum which originates from the s -wave, $M_F = -4$, collisional resonance state. Its transition rate is proportional to the square of the wave-function overlap between the collisional state and the excited state, and therefore shows an enhancement when the Feshbach resonance is tuned near zero energy.

We detect the photoassociation with a trap loss method [16–19]. About 10^4 ^{85}Rb atoms are transferred from a magneto-optical trap into a far-off resonance optical dipole force trap (FORT) [20], created by a 1.7 W, 835 nm wavelength laser beam focussed to a waist of $20 \mu\text{m}$. The atoms are laser cooled to a temperature between 30 and $100 \mu\text{K}$, and have a density between 10^{11} and 10^{12} cm^{-3} . We then switch on a magnetic field B and allow it to stabilize for 300 ms. After this, we continuously illuminate the atoms with a near-resonance laser beam that optically pumps them into

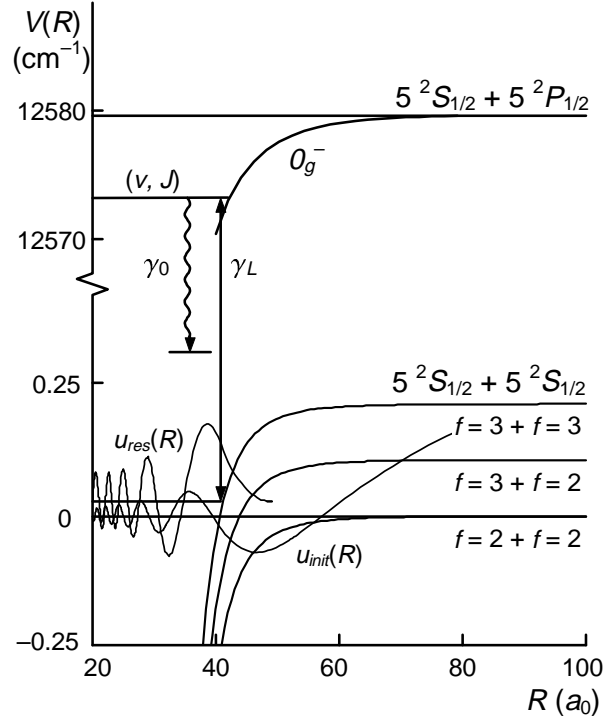


Figure 5.1 Photoassociation method for detecting a Feshbach resonance in collisions of ultracold ^{85}Rb $|f=2, m_f=-2\rangle$ atoms. The entrance channel wave function $u_{init}(R)$ couples to a quasibound state with wave function $u_{res}(R)$. A laser field induces photoassociation of this state to an excited, bound $0_g^-(v, J)$ molecular state at a rate γ_L , which then decays back to free atoms at a rate γ_0 . As a magnetic field is varied, the quasibound state tunes through zero energy, producing a Feshbach resonance for ultracold collisions. The resulting enhancement of $u_{res}(R)$ produces an enhancement of γ_L that we detect with a trap loss method.

their $f=2$ ground hyperfine state, and with a tunable probe (PA) laser beam which induces the photoassociation transitions. In some cases we also apply an additional near-resonance σ^- -polarized (OP) laser to pump the atoms into their $m_f=-2$ state. After an additional 700 to 1000 ms, we switch off these laser beams and the magnetic field, and probe the atoms remaining in the trap with laser-induced fluorescence. The photoassociation rate is detectable as reduced atomic fluorescence, because most pairs of atoms which absorb a PA laser photon return to the ground state by spontaneous emission as free atoms with a kinetic energy that is too high to remain in the trap. In the plots below, we show this measured fluorescence signal vs PA laser frequency, inverted so that photoassociation-induced trap loss produces upward going peaks.

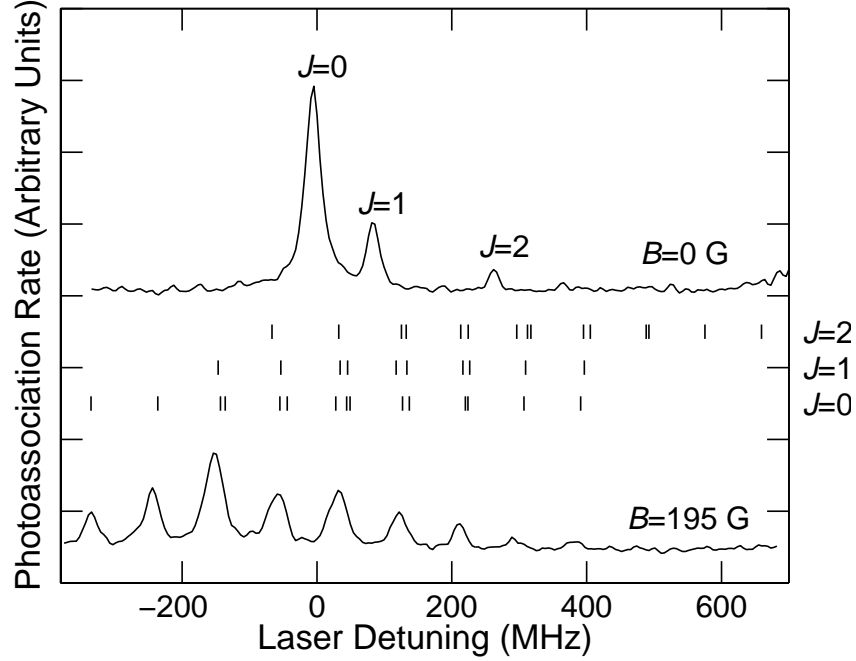


Figure 5.2 $^{85}\text{Rb}_2$ photoassociation spectra for excitation from lower ($f = 2 + f = 2$) hyperfine state collisions to a single excited vibrational level, at a laser intensity of 20 W/cm^2 . Upper curve: spectrum at zero magnetic field. Lower curve: spectrum at a magnetic field of 195 G. Each of the zero-field components splits into 10 or 15 distinct components due to Zeeman splitting of the ground-state atoms; calculated splittings are shown by the vertical dashed marks. The successive peaks in the lower spectrum correspond mainly to $J = 0$, and (from left) $M_F = -4, -3, -2, -1, 0, 1, \text{ and } 2$.

5.3 Observation of a Feshbach Resonance

A typical spectrum, recorded with the OP laser beam off and with no magnetic field, is shown in Fig. 5.2. We observe a simple spectrum that arises from the 0_g^- excited state $J = 0, 1, \text{ and } 2$ rotational levels. Fig. 5.2 also shows the spectrum with the OP laser beam off and with $B \approx 195 \text{ G}$. In this case, the $f = 2 + f = 2$ dissociation limit Zeeman splits into 15 different limits for the even partial waves, and 10 different limits for the odd partial waves, which correspond to the various possible combinations of the two atomic m_f quantum numbers. Without optical pumping all of these combinations are populated. The excited state does not show a significant Zeeman splitting. Because some of the splittings are not resolved, the $J = 0$ rotational peak splits into 9 Zeeman components corresponding to $M_F = -4, \dots, +4$. The leftmost peak in the spectrum arises only from $|f = 2, m_f = -2\rangle + |f = 2, m_f = -2\rangle$ ($M_F = -4$) collisions. Further, this peak arises only from s -wave collisions because the selection rule $J = l$ is obeyed

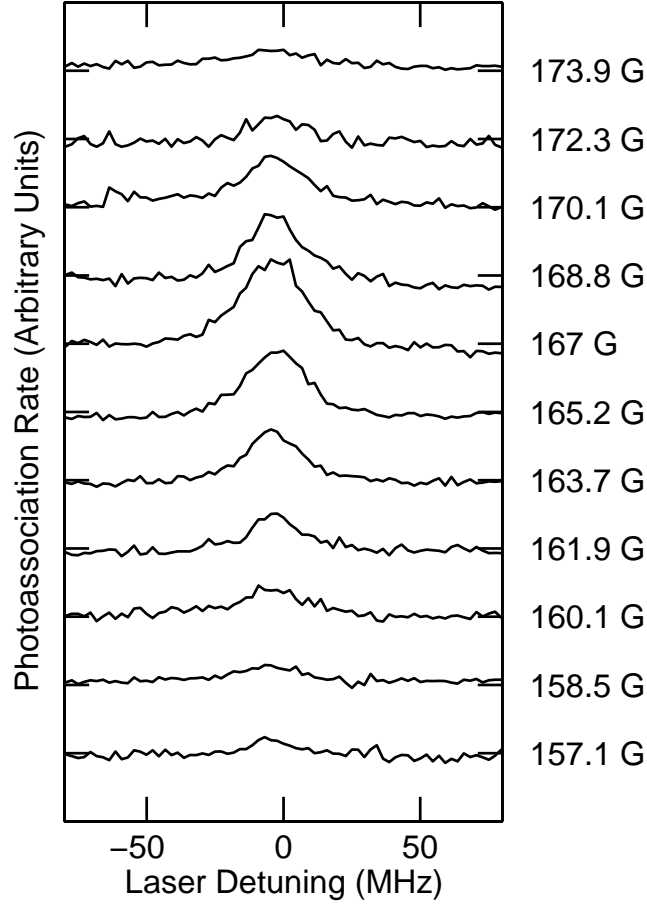


Figure 5.3 Photoassociation spectra showing the $J = 0$, $M_F = -4$ peak at a succession of magnetic field values, with a laser intensity of 0.1 W/cm^2 . The relative Zeeman shift of the successive peaks is removed so that they appear at the same laser tuning.

for this transition, where l is the orbital angular momentum of the initial state [16]. Therefore the leftmost peak probes exclusively the desired collision channel.

In Fig. 5.3, we show repeated scans over the $J = 0$, $M_F = -4$ peak at many different field values. The data clearly show the effect of the Feshbach resonance. For these scans we also turn on the OP laser beam, which enhances the intensity of the $M_F = -4$ peak by a factor of 5. The PA laser intensity $I = 0.1 \text{ W/cm}^2$. As the magnetic field is increased, the signal emerges from the noise, reaches a maximum strength near 167 G, and then disappears again into the noise. The field magnitude is calibrated using the Zeeman-resolved spectra. Our interpretation of this enhancement as a Feshbach resonance is supported by several factors. First, previous studies of

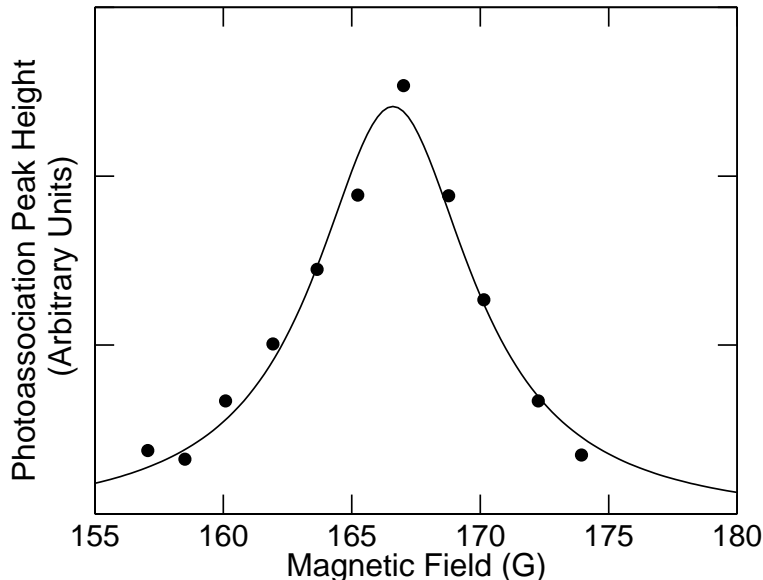


Figure 5.4 Height of the photoassociation peaks shown in Fig. 5.3, as a function of magnetic field, showing clearly the Feshbach resonance. The solid curve shows a Lorentzian fit to the data.

ultracold Rb collisions have fairly strongly constrained its ground-state interaction potentials [4, 13, 16–19, 21, 22], and allowed for predictions of this resonance [12, 22]. We observe a resonance in the correct channel near the predicted field. Finally, we observe these photoassociation peaks at an anomalously low laser intensity, at which other features in the spectrum are not visible. This can occur only with resonance enhancement of the rate γ_L due to the enhanced wave-function amplitude.

In Fig. 5.4, we plot the heights of the photoassociation peaks, determined from Lorentzian fits, as a function of magnetic field. We find that this curve is also well fit by a Lorentzian line shape, which yields a resonance field $B_{0,PA}(I)$ and a width (FWHM) $\Delta B_{PA}(I)$. Theoretical calculations along the lines of chapter 4 [23] show that departures from Lorentzian line shapes should be small for our conditions. We find that optical power broadening is significant. In order to account for this, we repeat the measurements at laser intensities I ranging from 0.1 to 0.54 W/cm², and plot $B_{0,PA}(I)$ and $\Delta B_{PA}(I)$ vs I . $B_{0,PA}(I)$ varies by less than 1.5 G over this range, and $\Delta B_{PA}(I)$ varies from about 8 G to about 15 G. By fitting these data, we determine zero-intensity intercepts of $B_{0,PA} = 166.6 \pm 6$ G and $\Delta B_{PA} = 5.9 \pm 2.1$ G. The error in $B_{0,PA}$ is mainly due to errors in the magnetic field calibration. We searched for and did not find any additional Feshbach resonances in the field range between 100 G and 195 G.

5.4 Determination of ^{85}Rb Interaction Parameters

In order to further analyze these results, we have calculated the resonance field $B_{0,PA}$ and width ΔB_{PA} using an accurate model for the atomic Rb interaction potentials and photoassociation process, as described in chapter 4 [23]. These quantities depend most sensitively on the Rb_2 ground-state Van der Waals interaction coefficient C_6 , and the two parameters $v_{DS}(\text{mod } 1)$ and $v_{DT}(\text{mod } 1)$. v_{DS} and v_{DT} correspond to the (fractional) number of bound states in the lowest singlet and triplet $^{85}\text{Rb}_2$ molecular potential wells, respectively. Further, near our parameter range the position of the resonance depends mostly on C_6 and on the sum $v_{DS}(\text{mod } 1) + v_{DT}(\text{mod } 1)$, whereas its width depends mostly on the difference $v_{DS}(\text{mod } 1) - v_{DT}(\text{mod } 1)$. Taking a fixed $C_6 = 4550$ a.u. [18] we determine from our measured value of $B_{0,PA}$ that $v_{DS}(\text{mod } 1) + v_{DT}(\text{mod } 1) = -0.082 \pm 0.011$. Allowing for a 50 a.u. uncertainty in C_6 increases the uncertainty of $v_{DS}(\text{mod } 1) + v_{DT}(\text{mod } 1)$ to ± 0.016 . From the measured value of ΔB_{PA} , we determine $v_{DS}(\text{mod } 1) - v_{DT}(\text{mod } 1) = 0.058 \pm 0.016$. (We rule out an opposite sign for $v_{DS} - v_{DT}$ because it conflicts with previous measurements [19].) Combining these results, we determine $v_{DS}(\text{mod } 1) = -0.012$ and $v_{DT}(\text{mod } 1) = -0.070$, with uncertainties for both their sum and difference of ± 0.016 .

The best previous determination of these quantities followed from our measurements of the highest bound levels of the $^{85}\text{Rb}_2$ molecule [19]. Taking again a fixed $C_6 = 4550$ a.u., those measurements yield $v_{DS}(\text{mod } 1) = -0.006 \pm 0.008$ and $v_{DT}(\text{mod } 1) = -0.047 \pm 0.006$. Plotting the allowed regions in the $v_{DS} - v_{DT}$ plane at fixed C_6 for both the Feshbach and the bound-state measurements, we find that they nearly contact each other near the point corresponding to the lower limits for both the Feshbach resonance width and resonance field. The difference between the parameters derived from the two experiments is somewhat larger than would be expected from their respective uncertainties; a possible explanation is that errors in the bound-state measurements due to line-shape effects were underestimated. The uncertainty in C_6 also increases the uncertainties of the parameters derived from the bound-state experiment [19], but it does not significantly change the level of agreement between the two experiments because their allowed $v_{DS} - v_{DT}$ regions display similar shifts with C_6 .

Based on our Feshbach resonance measurements, we calculate the scattering length $a_{2,-2}$ for collisions of ^{85}Rb $|f=2, m_f=-2\rangle$ atoms as a function of field strength, shown in Fig. 5.5. The resonance in the scattering length has the dispersive form $a_{2,-2} = a_{2,-2}^0 [1 - \Delta/(B - B_0)]$. For the same parameters that yield the observed values of $B_{0,PA}$ and ΔB_{PA} , we find that $a_{2,-2}^0 = -295 \pm 80 a_0$, $\Delta = 8.2 \pm 3.8$ G, and $B_0 = 164 \pm 7$ G. B_0 is a few Gauss lower than $B_{0,PA}$ due to the fact that close to the crossing of the Rb_2 bound state and the $|f=2, m_f=-2\rangle + |f=2, m_f=-2\rangle$ threshold, the PA phenomenon is influenced to a significant extent by interference of

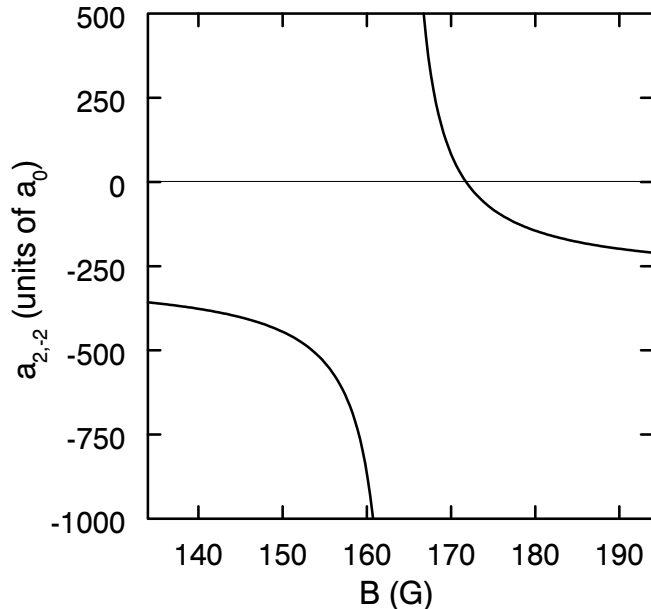


Figure 5.5 Calculated field dependence of scattering length $a_{2,-2}$, corresponding with the resonance field value and width observed in this experiment.

the Feshbach resonance and the strong background (potential) scattering associated with the large background value of $a_{2,-2}$. The measured resonance field is in moderate disagreement with our previous prediction of 142 ± 10 G [12], which was based on the bound-state measurements [19], for the reasons discussed above.

5.5 Conclusions

In summary, we have detected a zero-energy Feshbach resonance in collisions of ^{85}Rb $|f = 2, m_f = -2\rangle$ atoms at a magnetic field of 164 ± 7 G. Our method, based on Zeeman-resolved photoassociation spectroscopy of ultracold atoms, allows us to search for resonances in any hyperfine, Zeeman, and partial wave channel by simply looking for an enhancement of the appropriate spectral component as the magnetic field is tuned. This method may therefore prove more generally useful as a new probe of ultracold atomic collisions. ^{85}Rb $|f = 2, m_f = -2\rangle$ atoms can be magnetically trapped, and are expected to exhibit a very low two-body inelastic collision rate [22]. Evaporative cooling of this isotope is somewhat difficult due to a suppression of its elastic cross section at temperatures above $10 \mu\text{K}$ [22, 24, 25], but it is feasible [25]. Therefore it should be possible to study a magnetically trapped ^{85}Rb BEC with an adjustable scattering length. One attractive feature of this resonance is that its ratio Δ/B_0 , which governs the degree of magnetic field control needed to stably produce a very large

scattering length, is relatively large. Two and three body collisional loss rates are also enhanced by a Feshbach resonance [14, 22], and this may limit the tuning range achievable in practice. A further interesting possibility is that it should be possible to form a mixed ^{87}Rb - ^{85}Rb condensate, with the ^{87}Rb and cross-species scattering length positive [17, 22], and the ^{85}Rb scattering length tunable. Other Feshbach resonances in both single and multicomponent gases could play important roles in many future BEC and coherent atom optics experiments.

Acknowledgments

We gratefully acknowledge useful discussions with Carl Wieman and Chris Greene, including a preliminary indication of a resonance field value from experiments at JILA. Work at Texas was supported by the R. A. Welch Foundation, the National Science Foundation, and the NASA Microgravity Research Division.

References

- [1] M.H. Anderson, J.R. Ensher, M.R. Matthews, C.E. Wieman, and E.A. Cornell, *Science* **269**, 198 (1995).
- [2] K.B. Davis, M.-O. Mewes, M.R. Andrews, N.J. van Druten, D.S. Durfee, D.M. Kurn, and W. Ketterle, *Phys. Rev. Lett.* **75**, 3969 (1995).
- [3] C.C. Bradley, C.A. Sackett, and R.G. Hulet, *Phys. Rev. Lett.* **78**, 985 (1997).
- [4] C.J. Myatt, E.A. Burt, R.W. Ghrist, E.A. Cornell, and C.E. Wieman, *Phys. Rev. Lett.* **78**, 586 (1997)
- [5] U. Ernst, A. Marte, F. Schreck, J. Schuster and G. Rempe, *Europhys. Lett.* **41**, 1 (1998).
- [6] L. V. Hau, B. D. Busch, C. Liu, Z. Dutton, M. M. Burns, and J. A. Golovchenko, *Phys. Rev. A* **58**, R54 (1998).
- [7] D. J. Han, R. H. Wynar, Ph. Courteille, and D. J. Heinzen, *Phys. Rev. A* **57**, R4114 (1998).
- [8] E. Tiesinga, A. J. Moerdijk, B. J. Verhaar, and H. Stoof, *Phys. Rev. A* **46**, R1167 (1992); E. Tiesinga, B. J. Verhaar, and H. Stoof, *Phys. Rev. A* **47**, 4114 (1993).
- [9] P. O. Fedichev, Yu. Kagan, G. V. Shlyapnikov, and J. T. M. Walraven, *Phys. Rev. Lett.* **77**, 2913 (1996).
- [10] J. L. Bohn and P. S. Julienne, *Phys. Rev. A* **56**, 1486 (1997).
- [11] A. J. Moerdijk, B. J. Verhaar and A. Axelsson, *Phys. Rev. A* **51**, 4852 (1995).
- [12] J. M. Vogels, C. C. Tsai, R. S. Freeland, S. J. J. M. F. Kokkelmans, B. J. Verhaar, and D. J. Heinzen, *Phys. Rev. A* **56**, R1067 (1997).
- [13] N. R. Newbury, C. J. Myatt, and C. E. Wieman, *Phys. Rev. A* **51**, R2680 (1995).
- [14] S. Inouye, M. R. Andrews, J. Stenger, H.-J. Miesner, D. M. Stamper-Kurn, and W. Ketterle, *Nature* **392**, 151 (1998).

-
- [15] D. J. Heinzen, in *Atomic Physics 14*, eds. D.J. Wineland, C.E. Wieman, and S.J. Smith, AIP Conf. Proc. No. 323 (New York, 1995), p. 211.
- [16] J. R. Gardner, R. A. Cline, J. D. Miller, D. J. Heinzen, H. M. J. M. Boesten, and B. J. Verhaar, *Phys. Rev. Lett.* **74**, 3764 (1995).
- [17] H. M. J. M. Boesten, C. C. Tsai, J. R. Gardner, D. J. Heinzen, and B. J. Verhaar, *Phys. Rev. A* **55**, 636 (1997).
- [18] H. M. J. M. Boesten, C. C. Tsai, B. J. Verhaar, and D. J. Heinzen, *Phys. Rev. Lett.* **77**, 5194 (1996).
- [19] C. C. Tsai, R. S. Freeland, J. M. Vogels, H. M. J. M. Boesten, B. J. Verhaar, and D. J. Heinzen, *Phys. Rev. Lett.* **79**, 1245 (1997).
- [20] J. D. Miller, R. A. Cline, and D. J. Heinzen, *Phys. Rev. A* **47**, R4567 (1993).
- [21] S. J. J. M. F. Kokkelmans, H. M. J. M. Boesten, and B. J. Verhaar, *Phys. Rev. A* **55**, R1589 (1997); P. S. Julienne, F. H. Mies, E. Tiesinga, and C. J. Williams, *Phys. Rev. Lett.* **78**, 1880 (1997); J. P. Burke, Jr., J. L. Bohn, B. D. Esry, and Chris H. Greene, *Phys. Rev. A* **55**, R2511 (1997).
- [22] J. P. Burke, Jr., J. L. Bohn, B. D. Esry, and Chris. H. Greene, *Phys. Rev. Lett.* **80**, 2097 (1998); Chris Greene, private communication.
- [23] F. A. van Abeelen, D. J. Heinzen, and B. J. Verhaar, *Phys. Rev. A* **57**, R4102 (1998).
- [24] S. J. J. M. F. Kokkelmans, B. J. Verhaar, K. Gibble, and D. J. Heinzen, *Phys. Rev. A* **56**, R4389 (1997).
- [25] C. Wieman, private communication.

6

Sympathetic Cooling of ${}^6\text{Li}$ Atoms

F.A. van Abeelen, B.J. Verhaar, and A.J. Moerdijk

Published in Phys. Rev. A **55**, 4377 (1997)

We use recently measured cold photoassociation and two-photon data to extract the singlet and triplet accumulated radial phases of interacting ground-state lithium atoms. Using the resulting values we predict scattering lengths, Feshbach resonances and exchange decay rate coefficients for cold collisions between ${}^7\text{Li}$ and ${}^6\text{Li}$ atoms that are of interest for the possibility of sympathetic cooling of ${}^6\text{Li}$ and for the coexistence of the bosonic and fermionic quantum-degenerate phases of ${}^7\text{Li}$ and ${}^6\text{Li}$. In addition, we calculate scattering lengths and exchange decay rate coefficients for cold collisions between identical lithium isotopes in different hyperfine states. These quantities are used to examine the possibilities of coexisting ${}^7\text{Li}$ Bose condensates and of evaporatively cooling coexisting ${}^6\text{Li}$ subsystems.

6.1 Introduction

In recent years cold collisions between ${}^7\text{Li}$ atoms and between ${}^6\text{Li}$ atoms have been studied extensively both experimentally and theoretically. Relatively little attention has been devoted to collisions where a ${}^7\text{Li}$ atom collides with a ${}^6\text{Li}$ atom. Interest in fermion-boson collisions like these, however, is rapidly growing in view of the possibility of cooling a fermionic gas to the Fermi-degenerate regime by contact with an ultracold bosonic gas (sympathetic cooling [1]). Such a cooling method is called for since normal evaporative cooling of a spin-polarized fermionic gas is not efficient due to the absence of s -wave collisions in this case [2]. The efficiency of the sympathetic cooling scheme, on the other hand, does depend on the elastic s -wave cross section $\sigma = 4\pi a^2$ of ${}^7\text{Li}$ - ${}^6\text{Li}$ collisions, where a is the scattering length. As in the single-isotope case we are especially interested in combinations of ${}^7\text{Li}$ and ${}^6\text{Li}$ hyperfine states for which the typically fast exchange decay is forbidden in a static magnetic trap: $|f_1 = 2, m_{f_1} = 2\rangle$ with $|f_2 = \frac{3}{2}, m_{f_2} = \frac{3}{2}\rangle$ and $|f_1 = 1, m_{f_1} = -1\rangle$ with $|f_2 = \frac{1}{2}, m_{f_2} = -\frac{1}{2}\rangle$. In this paper we present calculated a values for the corresponding collision channels.

In addition to sympathetic cooling, the scattering length is also of interest for the description of the effective interaction between the bosonic and fermionic subsystems in a future system of coexisting quantum-degenerate ${}^7\text{Li}$ and ${}^6\text{Li}$ phases in case the above

scheme for sympathetic cooling is successful. In this connection we also address in this paper the topic of the possible existence of Feshbach resonances in the $(1 - 1) + (\frac{1}{2} - \frac{1}{2})$ collision channel. Such a resonance causes a to change sign as a function of the magnetic field strength in the trap and would therefore offer the possibility to change the nature of the effective interactions in a combined quantum-degenerate state.

Another possibility to cool a ${}^6\text{Li}$ gas sample, without contact with evaporatively cooled ${}^7\text{Li}$, could be the use of coexisting ${}^6\text{Li}$ subsystems in the $|\frac{3}{2}, \frac{3}{2}\rangle$ and $|\frac{1}{2}, -\frac{1}{2}\rangle$ hyperfine states, for which s -wave collisions are not forbidden [3]. This system would be analogous to the recently realized coexisting ${}^{87}\text{Rb}$ subsystems in different hyperfine states [1]. A necessary condition for this scheme to work is a small enough exchange decay rate and a sizable scattering length. For this reason we also study these quantities.

As a byproduct of our calculations we also obtain the scattering length and exchange decay rate for collisions of two ${}^7\text{Li}$ atoms in two different hyperfine states, which is important for possible experiments with coexisting $|2, 2\rangle$ and $|1, -1\rangle$ Bose condensates in an ultracold ${}^7\text{Li}$ gas sample [4].

Recent developments, both theoretical and experimental, enable us to base our predictions on improved knowledge of the interaction between ground-state lithium atoms. An important development in theory is the rigorous calculation of the $\text{Li} + \text{Li}$ dispersion coefficients by Yan *et al.* [7]. On the experimental side a measurement of the binding energy of the least-bound ${}^7\text{Li}_2$ triplet $l = 0$ state [8], as well as a recent ${}^7\text{Li} + {}^7\text{Li}$ and ${}^6\text{Li} + {}^6\text{Li}$ cold photoassociation study [9], yield important information that needs to be taken into account.

All results in the present paper have been calculated by the rigorous coupled-channels method. They could also have been obtained in the degenerate internal states (DIS) approximation [5,6]. The shifts in the photoassociation signals (see Figs. 6.1 and 6.2) would result from a calculation including a first-order correction to DIS results [5]. We preferred to carry out the full coupled-channels calculations in view of our interest in Feshbach resonances, which do not show up in the approximate calculations.

In section 6.2 we reexamine the information available on the interaction properties of the ground-state lithium isotopes, using the method of accumulated phases [10,11]. In section 6.3 we present predictions for the mixed ${}^7\text{Li}$ - ${}^6\text{Li}$ collisions and in section 6.4 for the identical-isotope ${}^7\text{Li}$ - ${}^7\text{Li}$ and ${}^6\text{Li}$ - ${}^6\text{Li}$ systems. Our conclusions are given in section 6.5.

6.2 Reexamination of the $\text{Li} + \text{Li}$ Accumulated Phases

We have applied the accumulated phase method to the ground-state triplet potential $V_T(r)$ and singlet potential $V_S(r)$, and the associated partial-wave radial wave

functions. The central idea is to impose a boundary condition on the oscillating radial wavefunction at a radius $r_0 = 18a_0$ in the form of a WKB phase $\phi_{T/S}(E, l) = \phi_{T/S}^0(E, l) + \Delta\phi_{T/S}$, forgetting about the detailed form of the potentials within this boundary, except for variations in the reference phases $\phi_{T/S}^0(E, l)$ with E and $l(l+1)$ which follow accurately from the available potentials [10,12], as described by Moerdijk *et al.* [10,11]. The long-range part of the potentials ($r > 18a_0$) consists of dispersion and exchange parts of the form

$$V_{T/S} = -\frac{C_6}{r^6} - \frac{C_8}{r^8} - \frac{C_{10}}{r^{10}} \pm Ae^{-\alpha r}, \quad (6.1)$$

the only change relative to Refs. [10–12] being the substitution of the rigorous values for the dispersion coefficients which have recently become available [7].

To further improve our knowledge of the Li + Li short-range interaction during cold collisions, we first concentrate on the triplet accumulated phase and compare theoretical predictions for the binding energy of the least-bound $l = 0$ triplet state of ${}^7\text{Li}_2$ ($v = 10$) to the measured value -12.47 ± 0.04 GHz [8], thus establishing the phase correction $\Delta\phi_T$ needed to reproduce it. With a conservative error bar we find $\Delta\phi_T = 0.025 \pm 0.005$ [$a_T({}^7\text{Li}) = -(27.6 \pm 0.8) a_0$, $a_T({}^6\text{Li}) = -(22 \pm 8) \times 10^2 a_0$]. The ${}^7\text{Li}$ triplet scattering length that we calculate agrees with the value given in Ref. [8].

We now turn to the singlet accumulated phase. The most accurate published value for $\Delta\phi_S$ [11] was derived from energy intervals between highly excited singlet rovibrational ${}^7\text{Li}_2$ levels. It is useful to compare the result,

$$-0.02 < \Delta\phi_S < +0.05, \quad (6.2)$$

to recent cold-atom ${}^7\text{Li} + {}^7\text{Li}$ and ${}^6\text{Li} + {}^6\text{Li}$ photoassociation experiments [9]. In these experiments a single $N = 1$ rotational level of the $A^1\Sigma_u^+$ state of Li_2 was optically excited for a number of subsequent vibrational quantum numbers ($v = 65\text{--}76$, $79\text{--}82$ for ${}^7\text{Li}_2$, $v = 62\text{--}72$, $76\text{--}79$ for ${}^6\text{Li}_2$), starting from unpolarized $(f_1, f_2) = (i + \frac{1}{2}, i + \frac{1}{2})$, $(i + \frac{1}{2}, i - \frac{1}{2})$, and $(i - \frac{1}{2}, i - \frac{1}{2})$ ground-state hyperfine channels with $i = \frac{3}{2}$ (1) the nuclear spin of ${}^7\text{Li}$ (${}^6\text{Li}$). These data were analyzed by Abraham *et al.* [9] in the DIS approximation [5,6], assuming essentially that the singlet and triplet parts of the wave function in each incident ground-state hyperfine channel are scattered independently off the singlet and triplet potentials. As a consequence, the analysis yielded a value for the singlet scattering length with a rather large error bar, since each of the three f_1, f_2 combinations under their assumption leads to a different a_S value. For the purpose of this paper we have dropped this assumption and carried out a full coupled-channels analysis taking into account both the singlet and triplet interactions and the atomic hyperfine couplings during a collision. Using the electric-dipole matrix element for the optical transition involved, the long-range $A^1\Sigma_u^+$ atom-atom potential derived in

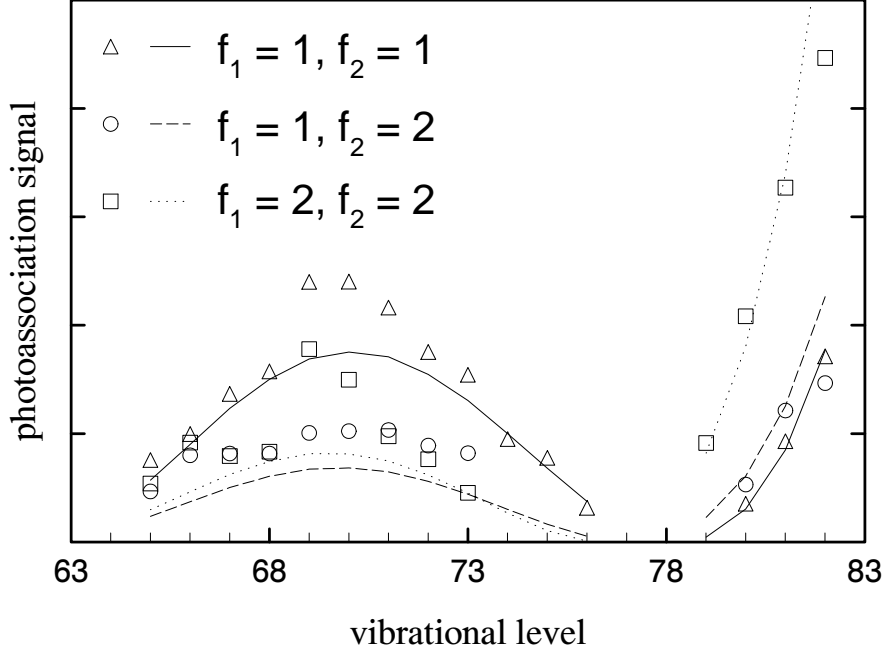


Figure 6.1 Comparison between experimental photoassociation signals (taken from Ref. [9]) for three (f_1, f_2) combinations (triangles, circles and squares) and theoretical predictions (lines) for $\Delta\phi_S = 0$ and $\Delta\phi_T = 0.0275$. The agreement is good.

Ref. [7], and the $A^1\Sigma_u^+$ ($N = 1$) binding energies measured by Abraham *et al.* [13], we have calculated the thermally averaged and m_{f_1}, m_{f_2} averaged photoassociation signal as a function of v for a range of $\Delta\phi_S$ values. We restricted $\Delta\phi_T$ to the range previously derived from the least-bound fully spin stretched ${}^7\text{Li}_2$ state. Comparing with the ${}^7\text{Li}$ photoassociation measurements we thus find the range

$$-0.05 < \Delta\phi_S < +0.08. \quad (6.3)$$

Figure 6.1 illustrates the excellent agreement for $\Delta\phi_S = 0$: the shifts along the v -axis for the three f_1, f_2 combinations are very well described. Figure 6.2 shows that the agreement is much worse for $\Delta\phi_S = -0.1$.

Similarly, the ${}^6\text{Li}$ data lead us to the range

$$-0.1 < \Delta\phi_S < 0. \quad (6.4)$$

Both ranges are consistent with the result (6.2). For the following, we take with a conservative error bar

$$\Delta\phi_S = 0.00 \pm 0.04 [a_S({}^7\text{Li}) = (34 \pm 1) a_0, a_S({}^6\text{Li}) = (45 \pm 1) a_0]. \quad (6.5)$$

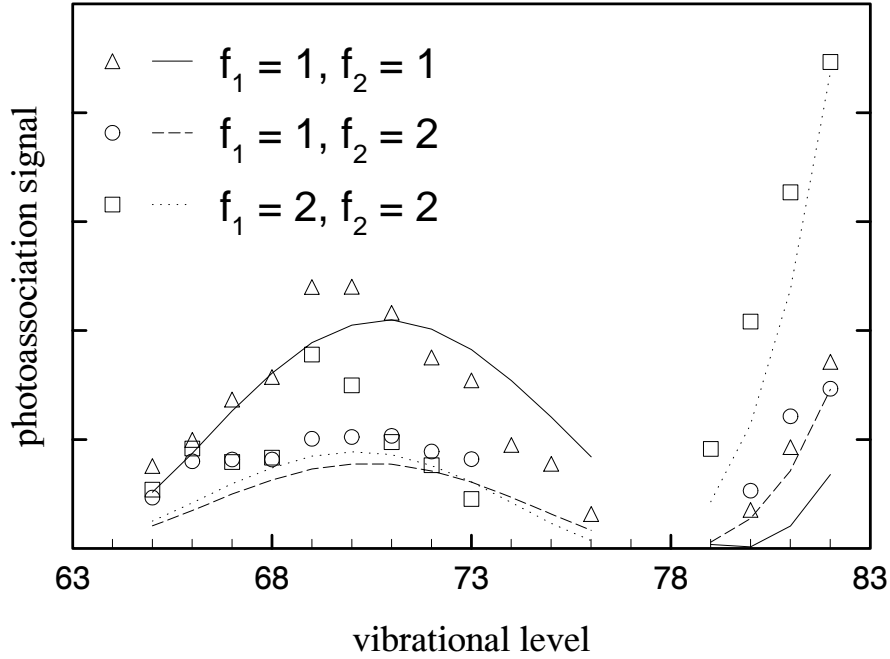


Figure 6.2 Same comparison as in Fig. 6.1, but for $\Delta\phi_s = -0.1$. Experimental signals from Ref. [9]. The lines that connect the theoretical values are shifted to the right relative to the experimental data.

The singlet scattering lengths given in Eq. (6.5) agree well with the DIS values in Ref. [9], but have a considerably higher accuracy than those thanks to our full coupled-channels approach.

With the above accumulated phases we now dispose of the information needed to calculate all relevant ground-state Li + Li cold collision quantities, either for like or for unlike isotopes. In this paper the main interest goes to the mixed boson-fermion system.

6.3 ${}^7\text{Li}$ - ${}^6\text{Li}$ Collisions

Our predictions for the $(22) + (\frac{3}{2} \frac{3}{2})$ and $(1-1) + (\frac{1}{2} - \frac{1}{2})$ scattering lengths for $B = 0$ [$a_{(22)(\frac{3}{2} \frac{3}{2})}$ and $a_{(1-1)(\frac{1}{2} - \frac{1}{2})}$, respectively] are listed in Table 6.1. Note that the former is independent of B . The error bars correspond to the uncertainties in the accumulated triplet and singlet radial phases. Both $a_{(22)(\frac{3}{2} \frac{3}{2})}$ and $a_{(1-1)(\frac{1}{2} - \frac{1}{2})}$ are large so that sympathetic cooling should work efficiently for each of the two trappable combinations of hyperfine states. Also, they are both positive, indicating an effectively repulsive interaction, which may be favorable from the point of view of the stability of the mixed

Table 6.1 Zero magnetic-field values for the real part of the scattering length a and for the zero-temperature total exchange decay rate coefficient G for a number of Li-Li collision channels involving different isotopes and spin states.

Channel	Re a (a_0)	G (10^{-11} cm ³ /s)
${}^7\text{Li}$ (2 2) + ${}^6\text{Li}$ ($\frac{3}{2}$ $\frac{3}{2}$)	40.8 ± 0.2	—
${}^7\text{Li}$ (1 - 1) + ${}^6\text{Li}$ ($\frac{1}{2}$ - $\frac{1}{2}$)	38.0 ± 0.2	—
${}^7\text{Li}$ (2 2) + ${}^6\text{Li}$ ($\frac{1}{2}$ - $\frac{1}{2}$)	34.9 ± 0.4	2.7 ± 0.3
${}^7\text{Li}$ (1 - 1) + ${}^6\text{Li}$ ($\frac{3}{2}$ $\frac{3}{2}$)	38.5 ± 0.2	0.15 ± 0.01
${}^6\text{Li}$ ($\frac{3}{2}$ $\frac{3}{2}$) + ${}^6\text{Li}$ ($\frac{1}{2}$ - $\frac{1}{2}$)	$-(17 \pm 6) \times 10^2$	$\rightarrow 0$
${}^7\text{Li}$ (2 2) + ${}^7\text{Li}$ (1 - 1)	-14 ± 1	2.4 ± 0.2

quantum-degenerate system. More generally, the calculated interisotope scattering lengths are of importance for the solution of the coupled system of generalized Gross-Pitaevskii equations of this mixed quantum-degenerate system.

In Fig. 6.3 the real part of $a_{(1-1)(\frac{1}{2}-\frac{1}{2})}$ is shown as a function of B for $\Delta\phi_T = 0.0275$ and $\Delta\phi_S = -0.01$. The results for other accumulated phases within the error bars do not show significant differences. It turns out that, due to the small ${}^6\text{Li}$ hyperfine splitting, at $B \approx 150$ G the exchange decay channel $(1\ 0) + (\frac{3}{2} - \frac{3}{2})$ opens and $a_{(1-1)(\frac{1}{2}-\frac{1}{2})}$ becomes complex (see dotted and dashed lines in Fig. 6.4). A similar situation cannot arise in the scattering of two identical isotopes. Fortunately, the decay is still forbidden for the experimentally relevant low temperatures and the lower field range where the atoms are trappable in a static magnetic field. The decay rate coefficient $G_{(1-1)(\frac{1}{2}-\frac{1}{2}) \rightarrow (10)(\frac{3}{2}-\frac{3}{2})}$ is also shown in the figure. This rate contains the same information as the imaginary part of $a_{(1-1)(\frac{1}{2}-\frac{1}{2})}$ which is not shown.

The curve for the scattering length contains three resonance features, two of which occur at almost the same field. Unfortunately, none of them occurs in the B range where both ${}^7\text{Li}$ and ${}^6\text{Li}$ atoms are low-field seeking with ${}^6\text{Li}$ putting the strongest restriction on the magnetic field strength: $B < 27$ G. As a result of this the resonances cannot be observed in a static magnetic trap. They might be observable, for instance, in an infrared trap [14] with a static magnetic field superimposed. At resonance 2 (we number the resonances from low to high magnetic field) $a_{(1-1)(\frac{1}{2}-\frac{1}{2})}$ goes through $\pm\infty$, as we would expect for a Feshbach resonance [15]. At the resonances 1 and 3 this is not the case and the scattering length does not change sign. This is only possible due to the presence of an exchange decay channel. The resonances in $a_{(1-1)(\frac{1}{2}-\frac{1}{2})}$ coincide with the maxima in G . At resonance 2, G shows a cusplike behavior; by accurate tuning of the field, G values of more than 10^3 times the typical exchange value ($G_{exch} \approx 10^{-11}$ cm³/s) might arise. The other maxima do not show this behavior, in

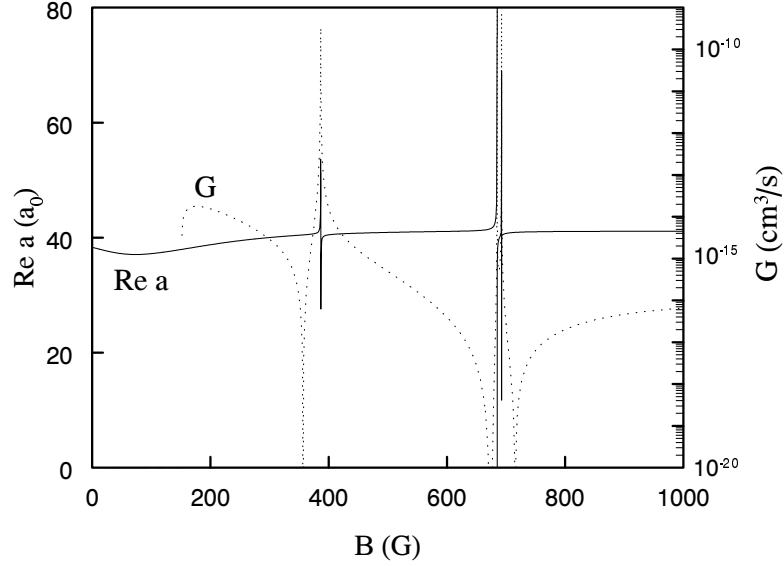


Figure 6.3 Real part of the scattering length a and zero-temperature exchange decay rate coefficient G for $(1 - 1) + (\frac{1}{2} - \frac{1}{2})$ ${}^7\text{Li}-{}^6\text{Li}$ collisions as a function of the magnetic field strength, calculated with $\Delta\phi_S = -0.01$ and $\Delta\phi_T = 0.0275$. The exchange decay channel opens at $B \approx 150$ G.

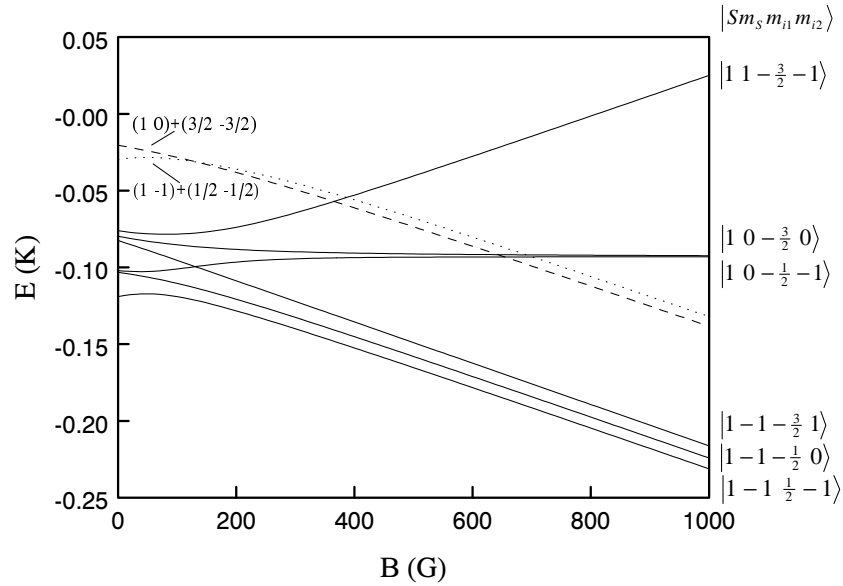


Figure 6.4 Energies of the least-bound triplet $l = 0$ states ($v = 10$) as a function of the magnetic field strength (solid lines) and the threshold energies of the incoming channel (dotted line) and the decay channel (dashed line). Feshbach resonances occur near the intersections.

agreement with the behavior of the scattering length. At the first two resonances the maximum in G is preceded by a G minimum. At resonance 3 the situation is reversed and the maximum is followed by the minimum. Outside the resonance regions the decay rate coefficient is of order 10^{-16} – 10^{-14} , much smaller than the typical exchange decay rate coefficient G_{exch} . This is probably due to the small available phase space in the final channel.

The location of the resonances in Fig. 6.3 can be understood by means of a simple ${}^7\text{Li}$ – ${}^6\text{Li}$ bound-state calculation, neglecting the part of the total hyperfine interaction for the two-atom system coupling the singlet and triplet subspaces, i.e. the part proportional to $\vec{S}_1 - \vec{S}_2$. Figure 6.4 shows the energies of the two-atom bound states with the same value $m_F = m_{f1} + m_{f2} = -\frac{3}{2}$ of the conserved total spin magnetic quantum number as that in the incident channel, as a function of the magnetic field strength. At the B values where a particular bound state crosses the continuum threshold of the incident channel (the dotted curve), it turns into a Feshbach resonance at zero collision energy. The crossings indeed occur at about the field values where the resonances were predicted in the continuum calculation of Fig. 6.3. The difference in nature between resonances 1 and 3 on the one hand and resonance 2 on the other will be the subject of further study.

For completeness, in Table 6.1 we also give the scattering length and total exchange decay rate coefficient for $B = 0$ in the case of ${}^7\text{Li}$ ($2\ 2$) + ${}^6\text{Li}$ ($\frac{1}{2} - \frac{1}{2}$) scattering and ${}^7\text{Li}$ ($1 - 1$) + ${}^6\text{Li}$ ($\frac{3}{2} \frac{3}{2}$) scattering.

6.4 Collisions between Identical Isotopes

We now give the results of calculations of some quantities that are of importance for the alternative sympathetic cooling method described in section 6.1, involving s -wave collisions between ${}^6\text{Li}$ atoms in different hyperfine states. Due to the fact that s -wave scattering is forbidden for two ${}^6\text{Li}$ atoms in identical spin states, exchange decay to the $(\frac{1}{2} \frac{1}{2}) + (\frac{1}{2} \frac{1}{2})$ channel is not possible and only one decay channel remains: $(\frac{3}{2} \frac{1}{2}) + (\frac{1}{2} \frac{1}{2})$. The zero-temperature rate coefficient G to this channel vanishes for $B \rightarrow 0$ because of the zero available phase space in that case. For small B , it is proportional to $B^{1/2}$. In Fig. 6.5 the rate coefficient G is shown as a function of B along with the real part of the scattering length a for $\Delta\phi_S = -0.01$ and $\Delta\phi_T = 0.0275$. For other values of the phase corrections within their error bars, the results are not significantly different. The real part of a changes sign at $B \approx 40$ G, indicating an effective interaction that changes from attractive to repulsive. At small B the absolute value of the scattering length is very large: $a \approx -2 \times 10^3 a_0$ for $B = 0$, see Table 6.1. Together with the vanishing zero-temperature exchange decay rate this would suggest that a mixed ${}^6\text{Li}$ $|\frac{3}{2}, \frac{3}{2}\rangle + {}^6\text{Li}$ $|\frac{1}{2}, -\frac{1}{2}\rangle$ gas sample can be cooled evaporatively. It should be noted, however, that G is still of

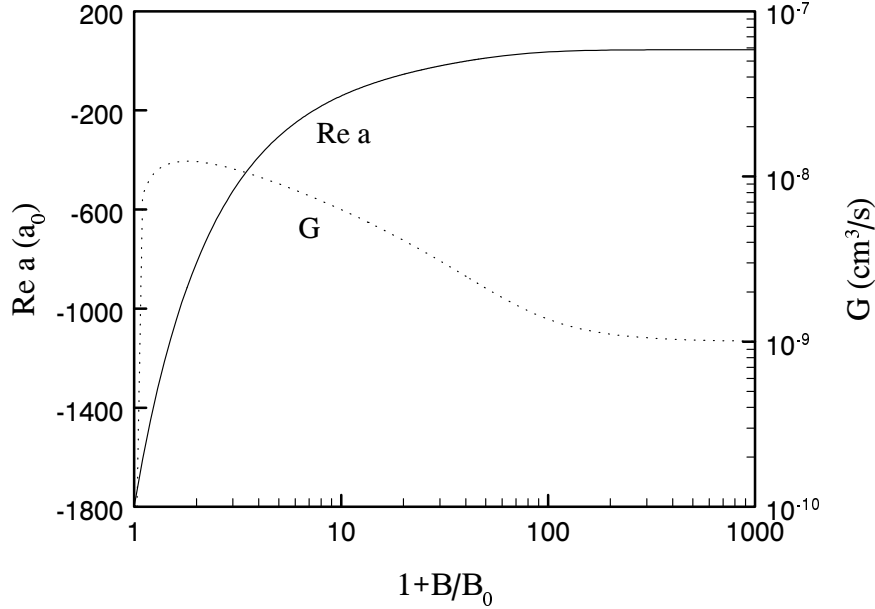


Figure 6.5 Real part of the scattering length a (solid line) and zero-temperature exchange decay rate coefficient G (dotted line) for $(\frac{3}{2} \frac{3}{2}) + (\frac{1}{2} - \frac{1}{2})$ ${}^6\text{Li}$ - ${}^6\text{Li}$ scattering as a function of the magnetic field strength B , calculated with $\Delta\phi_S = -0.01$ and $\Delta\phi_T = 0.0275$. To combine the advantages of a linear field scale for small B and a logarithmic scale for large B we have plotted $1 + B/B_0$ logarithmically with $B_0 = 1$ G.

order 10^{-10} cm^3/s at $B = 0$ for a finite temperature of 10 nK.

In view of the present interest in coexisting Bose condensates we also present predictions for the scattering length a and the exchange decay rate coefficient $G_{(22)(1-1)}$ associated with ${}^7\text{Li} (2 2) + {}^7\text{Li} (1 - 1)$ scattering in a static magnetic field B . The available exchange decay channels in this case are $(2 1) + (1 0)$, $(2 0) + (1 1)$ and $(1 0) + (1 1)$. Figure 6.6 shows the real part of the scattering length as a function of B . In the same figure we present the zero-temperature value of $G_{(22)(1-1)}$ along with the separate contributions from the three decay channels for $\Delta\phi_S = -0.01$. The G values for other choices of $\Delta\phi_S$ within the combined error bar that we found in section 6.2 are not significantly different from those shown in the figure. $\Delta\phi_T$ is set to 0.0275. The real part of a is negative for small and positive for large B , indicating an effective intercondensate interaction that changes from attractive to repulsive as the magnetic field is increased. The partial decay rates to the two $f_1, f_2 = 2, 1$ channels vanish as B approaches zero, as one should expect since these channels have zero available phase space for $B \rightarrow 0$. The partial rate to the $f_1, f_2 = 1, 1$ channel starts from a nonvanishing value and therefore dominates the total rate for the very low B values of

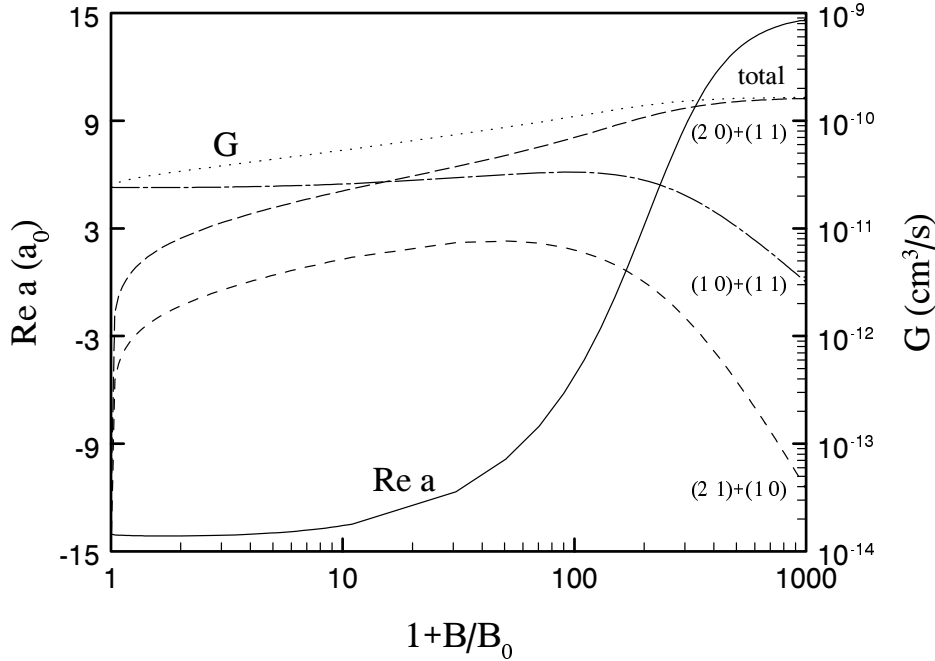


Figure 6.6 Real part of the scattering length a (solid line) and zero-temperature partial (dashed lines) and total (dotted line) decay rate coefficients G for ${}^7\text{Li}$ intercondensate scattering as a function of the magnetic field strength B , calculated with $\Delta\phi_S = -0.01$ and $\Delta\phi_T = 0.0275$. B axis as in Fig. 5.

primary experimental interest. The decay rate coefficient grows with B and is of order $10^{-11} \text{ cm}^3/\text{s}$ at small B , i.e. the typical magnitude for exchange decay rate coefficients. That means that it is much larger than the experimentally observed intercondensate decay rate coefficient for ${}^{87}\text{Rb}$ [$G_{(22)(1-1)} = 2.2(9) \times 10^{-14} \text{ cm}^3/\text{s}$] that made it possible to create overlapping ${}^{87}\text{Rb}$ condensates in the two different hyperfine levels [1]. We conclude that our predicted exchange rate is too large to make observation of ${}^7\text{Li}$ coexisting Bose condensates possible. It thus appears that the situation for ${}^7\text{Li}$ is in this respect comparable to that for ${}^{23}\text{Na}$ [16].

6.5 Conclusions

We conclude that sympathetic cooling of ${}^6\text{Li}$ atoms by contact with evaporatively cooled ${}^7\text{Li}$ atoms should work efficiently. The interisotope interaction in a mixed gas sample is repulsive. We have found Feshbach resonances in the $(1 - 1) + (\frac{1}{2} - \frac{1}{2})$ collision channel, however outside the magnetic-field range where both Li isotopes are low-field seeking. These resonances show unusual characteristics due to the presence

of an exchange decay channel. The exchange decay rate that occurs in the scattering of ${}^6\text{Li}$ atoms in different hyperfine states vanishes if the magnetic field approaches zero at zero temperature. At finite temperatures as low as 10 nK there is, however, still a sizable decay. The zero magnetic-field scattering length, on the other hand, is of order $10^3 a_0$. By calculating the intercondensate exchange decay rate coefficient for ${}^7\text{Li}$ atoms, we have found that coexisting ${}^7\text{Li}$ Bose condensates cannot be observed. In the process of our calculations we have confirmed the reliability of a previously published singlet accumulated phase correction and found a very narrow range for the triplet accumulated phase correction.

Acknowledgment

We gratefully acknowledge very helpful discussions with Claus Zimmermann.

References

- [1] C.J. Myatt, E.A. Burt, R.W. Ghrist, E.A. Cornell, and C.E. Wieman, *Phys. Rev. Lett.* **78**, 586 (1997).
- [2] J.M.V.A. Koelman, H.T.C. Stoof, B.J. Verhaar, and J.T.M. Walraven, *Phys. Rev. Lett.* **59**, 676 (1987).
- [3] H.T.C. Stoof, M. Houbiers, C.A. Sackett, and G.A. Hulet, *Phys. Rev. Lett.* **76**, 10 (1996), have suggested a sympathetic cooling scheme along this line, but based on a different combination of ${}^6\text{Li}$ hyperfine levels.
- [4] R.G. Hulet, private commun.
- [5] B.J. Verhaar, J.M.V.A. Koelman, H.T.C. Stoof, O.J. Luiten, and J.T.M. Walraven, *Phys. Rev. A* **35**, 3825 (1987).
- [6] H.T.C. Stoof, J.M.V.A. Koelman, and B.J. Verhaar, *Phys. Rev. B* **38**, 4688 (1988).
- [7] Z.-C. Yan, J.F. Babb, A. Dalgarno, and G.W.F. Drake, *Phys. Rev. A* **54**, 2824 (1996).
- [8] E.R.I. Abraham, W.I. McAlexander, C.A. Sackett, and R.G. Hulet, *Phys. Rev. Lett.* **74**, 1315 (1995).
- [9] E.R.I. Abraham, W.I. McAlexander, J.M. Gerton, R.G. Hulet, R. Côté, and A. Dalgarno, *Phys. Rev. A* **53**, R3713 (1996).
- [10] A.J. Moerdijk, W.C. Stwalley, R.G. Hulet, and B.J. Verhaar, *Phys. Rev. Lett.* **72**, 40 (1994).
- [11] A.J. Moerdijk and B.J. Verhaar, *Phys. Rev. Lett.* **73**, 518 (1994).
- [12] W.T. Zemke and W.C. Stwalley, *J. Chem. Phys.* **97**, 2053 (1993).
- [13] E.R.I. Abraham, N.W.M. Ritchie, W.I. McAlexander, and R.G. Hulet, *J. Chem. Phys.* **103**, 7773 (1995).
- [14] T. Takekoshi, J.R. Yeh, and R.J. Knize, *Opt. Commun.* **114**, 421 (1995).

- [15] B.J. Verhaar, *Laser Phys.* **4**, 1054 (1994); B.J. Verhaar, in *Atomic Physics 14*, edited by D.J. Wineland, C.E. Wieman, and S.J. Smith (American Institute of Physics Press, New York, 1995), p. 351.
- [16] S.J.J.M.F. Kokkelmans, H.M.J.M. Boesten, and B.J. Verhaar, *Phys. Rev. A* **55**, (1997).

7

Determination of Collisional Properties of Cold Na Atoms from Analysis of Experimental Data

F.A. van Abeelen and B.J. Verhaar

Published in Phys. Rev. A **59**, 578 (1999)

We review the information on the interactions between cold ground-state Na atoms following from Na₂ bound states, a Na photoassociation experiment, and a recent observation of field-induced Feshbach resonances in a Na Bose condensate. We obtain a set of Na interaction parameters that is in excellent agreement with all these experimental data. The existing discrepancy between different values for the scattering length $a_{1,-1}$ of Na atoms in the $|1, -1\rangle$ hyperfine state is resolved. The present interaction parameters enable us to give accurate predictions for the singlet and triplet scattering lengths a_S and a_T , $a_{1,-1}$, scattering lengths for collisions between Na atoms in other hyperfine states, and resonance fields of several yet unobserved Feshbach resonances. We find $a_S = (19.1 \pm 2.1) a_0$, $a_T = (65.3 \pm 0.9) a_0$, and $a_{1,-1}(B = 0) = (55.4 \pm 1.2) a_0$.

7.1 Introduction

In the past few years extensive experimental and theoretical efforts have been put into obtaining scattering lengths and inelastic rate coefficients for collisions between alkali-metal atoms with the highest possible accuracy. The scattering length for two elastically colliding atoms characterizes their interaction in the ultralow-temperature limit and thus plays a crucial role in the properties of Bose-Einstein condensates and in the evaporative cooling process that is used in the creation of these condensates. The inelastic collisional rates are also important for this cooling process and for the lifetime of these condensates.

The scattering lengths $a_{1,-1}$ for ²³Na atoms colliding in the $|f, m_f\rangle = |1, -1\rangle$ and $a_{2,2}$ for atoms in the $|2, 2\rangle$ doubly polarized state ($f = 1$ or 2 is the hyperfine quantum number, i.e., the combined electron and nuclear spin, of an atom and m_f is its projection) were first calculated by Moerdijk and Verhaar [1], based on an analysis of the energy spacings of bound triplet [2] and singlet [3] Na₂ states. They found

$a_{1,-1} = 86_{-22}^{+66} a_0$ and $a_{2,2} = 106_{-30}^{+79} a_0$. The starting point for this analysis were the triplet and singlet potentials given in Table II of Ref. [4] [composed of Rydberg-Klein-Rees (RKR) curves, and analytic inner wall and long-range tail]. An inverted perturbation analysis (IPA) was applied to the singlet potential after one RKR point was shifted to better fit the highest measured vibrational energy spacings. In the same year, Côté and Dalgarno [5] predicted $a_S = 34.9 a_0$ and $a_T = 77.3 a_0$, without error bars, for the singlet and triplet scattering lengths. They also used the RKR curves of Ref. [4], but extended the singlet curve with two spectroscopic data points near the potential minimum and both curves with *ab initio* data points in the short-range region. In addition, they used a different analytical inner wall and long-range tail.

Since then, an analysis by Tiesinga *et al.* [6] of a Na photoassociation experiment led to scattering lengths with much smaller error bars than those of Moerdijk and Verhaar: $a_{1,-1} = (52 \pm 5) a_0$ and $a_{2,2} = (85 \pm 3) a_0$. The fact that two specific rovibrational lines in the photoassociation spectrum that arise from *p*-wave scattering were significantly weaker than neighboring lines enabled them to constrain the position of the last node in the zero-magnetic-field *p*-wave ground-state wave function with total atomic angular momentum quantum numbers $f_1 = f_2 = 1$ and sum $F = 1$. Next, by introducing a smooth change in the inner walls of the above-mentioned RKR potentials, they constructed a family of potentials reproducing the *p*-wave node within these constraints. The ratio of the peaks for the rotational quantum numbers $J = 2$ and $J = 4$ was then used to further constrain the potentials. With the final family of potentials, the scattering lengths were calculated. The changes in the potential were restricted by the requirement that the number of $l = 0$ vibrational levels in both the singlet and triplet potentials was conserved. Contrary to Moerdijk and Verhaar and Côté and Dalgarno, Tiesinga *et al.* did not check the consistency of their final potentials with the energy spacings between the measured bound states.

We notice an apparent discrepancy between the photoassociation data analyzed by Tiesinga *et al.* and the level spacings analyzed by Moerdijk and Verhaar: The ranges that they find for $a_{1,-1}$ do not overlap. This discrepancy is further enhanced by the fact that each prediction for $a_{1,-1}$ is supported by one more direct measurement of $a_{1,-1}$: From the thermalization time of a ^{23}Na gas sample with a temperature of $200 \mu\text{K}$ the value $a_{1,-1} = (92 \pm 25) a_0$ was found [7], whereas a later analysis of time-of-flight measurements of expanding condensates [8] yielded $(42 \pm 15) a_0$.

Valuable additional experimental data recently became available in the form of magnetic field values at which Feshbach resonances occur in the scattering of ultracold ^{23}Na atoms. Feshbach resonances arise when the total energy of a pair of colliding atoms matches the energy of a quasibound two-atom state, leading to the resonant formation of this state during the collision. They give rise to a variation of the scattering length to arbitrary positive or negative values as a function of the applied field strength

around a resonance value [9] and, depending on experimental conditions, to a significant enhancement of inelastic processes [9]. Both these effects were observed in an optically trapped ^{23}Na $|1, 1\rangle$ Bose-Einstein condensate at an external magnetic field of 907 ± 20 G. A second Feshbach resonance was detected at a field strength 54 ± 1 G smaller [10].

In this paper, we show that the fairly large discrepancy between the photoassociation data and the bound-state data can be removed with the use of a set of potential parameters that give an improved description of the interactions between ultracold ground-state ^{23}Na atoms with respect to the former (modified) RKR and IPA potentials. Also, we show agreement between these potential parameters and the measured Feshbach resonance fields, which are then used to restrict the parameters to very narrow ranges and accurately predict scattering lengths and field values for other Feshbach resonances in ^{23}Na - ^{23}Na collisions.

7.2 Method

Rather than using complete singlet ($S = 0$) and triplet ($S = 1$) potentials, we use only the long-range parts and summarize the information in the short-range parts in a boundary condition on the $S = 0$ and $S = 1$ radial wave functions at a suitable interatomic distance $r = r_0 = 16 a_0$, on the basis of which Schrödinger's equation is solved for $r > r_0$. The choice of $r_0 = 16 a_0$ is discussed below. The boundary condition takes the form of a set of phases $\phi_S[E, l(l+1)]$ and $\phi_T[E, l(l+1)]$ of the oscillating singlet and triplet radial wave functions as a function of the energy E and interatomic angular momentum quantum number l [11]. The phases $\phi_S[E, l(l+1)]$ and $\phi_T[E, l(l+1)]$ are expressed as a Taylor series up to second order in the two variables E and $l(l+1)$. The long-range singlet and triplet potentials V_S and V_T are written in the form

$$V_{S/T}(r) = -\frac{C_6}{r^6} - \frac{C_8}{r^8} - \frac{C_{10}}{r^{10}} \mp V_E, \quad (7.1)$$

with the Smirnov-Chibisov [12] exchange part

$$V_E = Ar^{7/2\alpha-1}e^{-2\alpha r}, \quad (7.2)$$

in which we use their recommended ^{23}Na parameters $\alpha = 0.626 a_0^{-1}$ and $A = 1.25 \times 10^{-2}$ a.u. In Ref. [5], Côté and Dalgarno use the same formula for V_E , but with slightly different values for α and A . The dispersion coefficients C_8 and C_{10} are set to the values calculated by Marinescu, Sadeghpour, and Dalgarno [13]. C_8 is varied within 5% uncertainty limits around this center value. An uncertainty interval is not given in Ref. [13], but we believe 5% is a reasonable estimate. C_{10} is kept fixed because small changes in C_{10} hardly play a role for $r \geq 16 a_0$. A recent accurate value of $C_6 = 1561$ a.u. was obtained by Kharchenko, Babb, and Dalgarno [14]; it differs from

a previous value of 1539 a.u. calculated by Marinescu, Dalgarno, and Babb [15] by 22 a.u. We chose $C_6 = 1561 \pm 22$ a.u. in order to take into account this difference.

The main difference between the analysis of the bound states in this paper and that in Ref. [1] is in the choice of the long-range singlet and triplet potentials. In the previous work these were taken from RKR [4] and IPA [1] analyses of separate sets of singlet and triplet bound diatomic states. The quantities that we want to predict, on the other hand, are very sensitive to the difference of the potentials, i.e., the exchange energy. Although the above bound states were the best experimental information available at the time, we believe that a much better description is achieved by taking the exchange energy from theory. The present use of the Smirnov-Chibisov form for $V_E(r)$ greatly improves the exchange energy in the recoupling region where the hyperfine and exchange interactions are comparable and thus leads to significantly more reliable predictions for scattering lengths and exchange decay rates.

Obviously, at $r = r_0$, the exchange interaction V_E must be much larger than the hyperfine splitting Δ_{hf} so that there are indeed uncoupled $S = 0$ and $S = 1$ radial wave functions to put a boundary condition on. This leads us to the requirement $r_0 \leq 17 a_0$ [$V_E(17 a_0) \approx 23\Delta_{hf}$]. A second requirement, which limits the choice of r_0 on the lower side, is the validity of the long-range expression (7.1) beyond r_0 . Further, for a given value of l , the boundary condition on the radial wave functions at $r = r_0$ can only be expressed in terms of phases ϕ_S and ϕ_T with a simple energy dependence as indicated previously, above a certain minimum energy depending on r_0 and l . Consequently, the choice of r_0 limits the energy range, and thus the number of bound states, that can be included in our analysis for each l . Based on the above considerations we have chosen $r_0 = 16 a_0$. This allows us to analyze ten bound states: three singlet states ($v = 60, 61, 62$) for both $l = 13$ and $l = 15$, and two triplet states ($v = 9, 10$) for both $l = 14$ and $l = 16$.

7.3 Bound-States Analysis

The experimental bound state energies in Refs. [2] and [3] were all (singlet and triplet) determined with respect to the minimum of the singlet potential. How far this minimum lies below the dissociation limit was not measured. Therefore, instead of fitting our potential parameters to absolute binding energies, we fit them to the energy spacings between the levels. To be specific, we use the singlet state with $v = 60$ and $l = 13$ as the reference level, and fit to the energy spacings between this state and each of the other nine bound states used in our analysis. All these states and their experimental energies with respect to the reference state are shown in Table 7.1.

The fitting procedure is as follows: For a certain choice of C_6 and C_8 , we simultaneously optimize $\phi_S(0, 0)$ and $\phi_T(0, 0)$ and their first derivatives with respect to E and

Table 7.1 Bound Na₂ states used in our analysis and their experimental energies [2, 3] with respect to the singlet reference state a ($v = 60, l = 13$) with an energy of 6010.9102 cm⁻¹ [3] with respect to the minimum of the singlet potential.

State	v, l	Energy (cm ⁻¹)
Singlet		
a	60,13	0
b	60,15	1.5941
c	61,13	6.3232
d	61,15	7.5855
e	62,13	10.0079
f	62,15	10.9222
Triplet		
A	9,14	-1.2292
B	9,16	0.5748
C	10,14	4.9298
D	10,16	6.5418

$l(l+1)$ with the aid of a least-squares method that minimizes χ^2 for the bound-state energy spacings. The second and mixed derivatives of ϕ_S and ϕ_T are not fitted but determined from the inner parts (up to 16 a_0) of the IPA singlet potential constructed by Moerdijk and Verhaar and the RKR triplet potential of Ref. [4]. The IPA potential is given in Table 7.2. These derivatives are nearly constant over the energy range between the dissociation limit and the lowest of the analyzed bound states. Their average values, listed in Table 7.3, are used in the fitting procedure. The effects of the spread around the average values can be estimated and are taken into account in the form of small errors added to the uncertainties in the fitted parameters that follow from the least-squares fit. The procedure is repeated for different choices of C_6 and C_8 .

The measured singlet bound-state energies are given with a precision of 10^{-4} cm⁻¹ in Ref. [3]. An experimental error is not given but we assume it to be of the order of 10^{-4} cm⁻¹ as well. With our limited set of potential parameters we cannot reproduce the energy spacings between the singlet bound states with that precision. Still, we can attain a very high precision: if we fit the singlet parameters to the singlet bound states alone, we find $\chi^2 = 5$ (six singlet states give five energy spacings) for a standard deviation $\sigma_S = 1.1 \times 10^{-3}$ cm⁻¹ in the level energies. This σ_S is used in the fitting procedure described above. For the triplet bound-state energies, a maximum experimental error of 0.3 cm⁻¹ is quoted in Ref. [2]. The standard deviation σ_T in the triplet energies is

Table 7.2 IPA singlet potential $V_S(r)$ for Na constructed by Moerdijk and Verhaar [1]. The zero of energy is set at the dissociation limit.

r (a_0)	$V_S(r)$ (a.u.)	r (a_0)	$V_S(r)$ (a.u.)	r (a_0)	$V_S(r)$ (a.u.)
4.0	0.00528777909	10.0	-0.00489382935	16.0	-0.00014170279
4.2	-0.00316646188	10.2	-0.00430593832	16.5	-0.00011305197
4.4	-0.00988365626	10.4	-0.00378361262	17.0	-0.00009126498
4.6	-0.01525470849	10.6	-0.00332132572	17.5	-0.00007458045
4.8	-0.01943835505	10.8	-0.00291347319	18.0	-0.00006155216
5.0	-0.02258676589	11.0	-0.00255429652	18.5	-0.00005099525
5.2	-0.02483791285	11.2	-0.00223928667	19.0	-0.00004242869
5.4	-0.02632625682	11.4	-0.00196378261	19.5	-0.00003549124
5.6	-0.02715809476	11.6	-0.00172292402	20.0	-0.00002982550
5.8	-0.02743663688	11.8	-0.00151253077	20.5	-0.00002517682
6.0	-0.02726590589	12.0	-0.00132896983	21.0	-0.00002140900
6.2	-0.02673455863	12.2	-0.00116878475	21.5	-0.00001839211
6.4	-0.02591530524	12.4	-0.00102918491	22.0	-0.00001599623
6.6	-0.02487041455	12.6	-0.00090748310	22.5	-0.00001409149
6.8	-0.02365557413	12.8	-0.00080126123	23.0	-0.00001254739
7.0	-0.02232021881	13.0	-0.00070860189	23.5	-0.00001123357
7.2	-0.02090703144	13.2	-0.00062776365	24.0	-0.00001004234
7.4	-0.01945205624	13.4	-0.00055712727	24.5	-0.00000895033
7.6	-0.01798532416	13.6	-0.00049535746	25.0	-0.00000795411
7.8	-0.01653183110	13.8	-0.00044128347	25.5	-0.00000704977
8.0	-0.01511214019	14.0	-0.00039390246	26.0	-0.00000623340
8.2	-0.01374289558	14.2	-0.00035236374	26.5	-0.00000553975
8.4	-0.01243710395	14.4	-0.00031586009	27.0	-0.00000488726
8.6	-0.01120451049	14.6	-0.00028376027	27.5	-0.00000431031
8.8	-0.01005181286	14.8	-0.00025548354	28.0	-0.00000380471
9.0	-0.00898302404	15.0	-0.00023047246	28.5	-0.00000336602
9.2	-0.00799981879	15.2	-0.00020832174	29.0	-0.00000298995
9.4	-0.00710187927	15.4	-0.00018868915	29.5	-0.00000251290
9.6	-0.00628723166	15.6	-0.00017123267	30.0	-0.00000221302
9.8	-0.00555263317	15.8	-0.00015563663		

Table 7.3 Values of the second and mixed derivatives of the phases ϕ_S and ϕ_T used in the bound-states analysis.

Parameter	Value
$\partial^2 \phi_S / \partial E^2$	$-4.8 \times 10^{-4} \text{ K}^{-2}$
$\partial^2 \phi_S / \partial [l(l+1)]^2$	0
$\partial^2 \phi_S / \partial E \partial l(l+1)$	$1.9 \times 10^{-5} \text{ K}^{-1}$
$\partial^2 \phi_T / \partial E^2$	$-9.7 \times 10^{-4} \text{ K}^{-2}$
$\partial^2 \phi_T / \partial [l(l+1)]^2$	0
$\partial^2 \phi_T / \partial E \partial l(l+1)$	$3.9 \times 10^{-5} \text{ K}^{-1}$

Table 7.4 The five choices of C_6 and C_8 used in our analysis.

Choice	C_6 (a.u.)	C_8 (a.u.)
I	1539	106283
II	1539	117471
III	1561	111877
IV	1583	106283
V	1583	117471

taken to be $\sigma_T = \frac{1}{2} \times 0.3 \text{ cm}^{-1} = 0.15 \text{ cm}^{-1}$. The differences between the theoretical and experimental energy spacings that we find for the fitted parameters with C_6 and C_8 at the middle of their uncertainty intervals are shown in Fig. 7.1. Note that for the triplet states theory and experiment agree within the above standard deviation. The best accuracy in previous calculations of the highest Na₂ bound states was obtained by Côté and Dalgarno [5]. Their accuracies were around 10^{-2} cm^{-1} for the singlet and 0.2 cm^{-1} for the triplet levels.

The $\phi_S(0, 0)$ and $\phi_T(0, 0)$ that we find from the fitting procedure for each choice of C_6 and C_8 are translated into the fractional vibrational quantum numbers at the dissociation limit of the singlet and triplet ²³Na₂ molecular potential wells $v_{DS} = n_{BS} - 1 + \Delta_S$ and $v_{DT} = n_{BT} - 1 + \Delta_T$, respectively. The integer $n_{BS(T)}$ is the number of bound states in the singlet (triplet) potential and $\Delta_{S(T)}$ is the fractional part; $n_{BS} = 66$ and $n_{BT} = 16$. The v_{DS} and v_{DT} intervals that we find for the four choices of C_6 and C_8 where each of these parameters is at the lower or upper limit of its error bar and for the choice of central values (see Table 7.4) are listed in Table 7.5 (in terms of Δ_S and Δ_T), along with the ranges that we find for $\partial \phi_{S(T)} / \partial E(0, 0)$ and $\partial \phi_{S(T)} / \partial l(l+1)(0, 0)$. The values of C_6 and C_8 for each parameter choice are also given in the table. The allowed

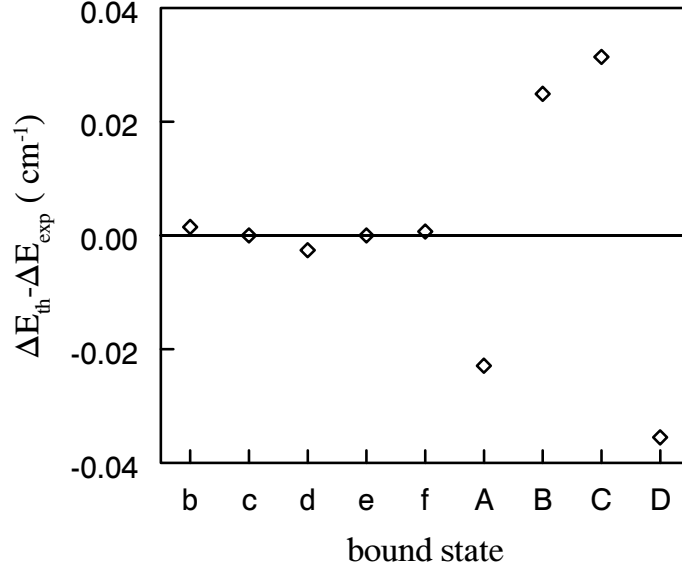


Figure 7.1 Differences between theoretical and experimental (see Table 7.1) bound-state energy spacings found for the fitted potential parameters with C_6 and C_8 at the middle of their uncertainty intervals.

Table 7.5 Singlet (S) and triplet (T) potential parameters resulting from the fit to the bound-state energy spacings in Table 7.1 for the five choices (I–V) of C_6 and C_8 listed in Table 7.4. The phase parameters $\phi_{S(T)}$ have been translated into the corresponding fractional parts $\Delta_{S(T)}$ of $v_{DS(T)}$. The values of $v_{DS(T)}$ itself can be found from $v_{DS(T)} = n_{BS(T)} - 1 + \Delta_{S(T)}$, with $n_{BS} = 66$ and $n_{BT} = 16$. If desired, the values of $\phi_{S(T)}(0, 0)$ can be evaluated by $\phi_{S(T)}(0, 0) \pmod{\pi} = \phi_{thres, S(T)} + \Delta_{S(T)}\pi$. The phases $\phi_{thres, S(T)} \pmod{\pi}$ for which the highest bound state lies at the threshold, are listed in the last column.

Choice	Potential	$\frac{\partial\phi}{\partial E}(0, 0)$ (K ⁻¹)	$\frac{\partial\phi}{\partial l(l+1)}(0, 0)$	Δ	ϕ_{thres}
I	S	0.0989 ± 0.0016	-0.0064 ± 0.0001	0.661 ± 0.005	1.4142
	T	0.126 ± 0.023	-0.008 ± 0.003	0.30 ± 0.18	1.6039
II	S	0.0969 ± 0.0016	-0.0064 ± 0.0001	0.656 ± 0.005	1.3151
	T	0.125 ± 0.023	-0.008 ± 0.003	0.29 ± 0.18	1.5031
III	S	0.0965 ± 0.0016	-0.0063 ± 0.0001	0.669 ± 0.005	1.2616
	T	0.125 ± 0.023	-0.008 ± 0.003	0.30 ± 0.18	1.4494
IV	S	0.0960 ± 0.0016	-0.0063 ± 0.0001	0.682 ± 0.005	1.2084
	T	0.124 ± 0.023	-0.008 ± 0.003	0.32 ± 0.18	1.3960
V	S	0.0941 ± 0.0016	-0.0063 ± 0.0001	0.677 ± 0.005	1.1104
	T	0.123 ± 0.023	-0.008 ± 0.003	0.31 ± 0.18	1.2964

v_{DS} and v_{DT} ranges for other values of C_6 and C_8 can be found by linear interpolation between the given intervals. For each parameter choice the last column of Table 7.5 lists the values of $\phi_S(0,0)$ and $\phi_T(0,0)$ (modulo π) for which $v_{DS(T)} = n_{BS(T)} - 1$, i.e., the highest bound state lies at the threshold. These phase values are denoted as $\phi_{thres,S}$ and $\phi_{thres,T}$. If desired, the phases that correspond to the given Δ_S and Δ_T ranges can be simply evaluated by $\phi_{S(T)}(0,0) \pmod{\pi} = \phi_{thres,S(T)} + \Delta_{S(T)}\pi$. If C_6 is increased, v_{DS} and v_{DT} increase too. This is consistent with the Le Roy formula [16] for binding energies which predicts that the energy spacings between levels decrease with increasing C_6 . All levels must be lowered (and thus v_{DS} and v_{DT} increased) to compensate for this.

We would like to emphasize that the magnitude of the v_{DT} ranges listed in Table 7.5 is directly related to the large error bars in the experimental triplet bound-state energies. They are not due to our method of analyzing the bound states. As an illustration of this, we point to the much smaller v_{DS} ranges in the same table. In this paper we obtain the best accuracy for the singlet parameters for each C_6, C_8 choice from our analysis of the bound states; this singlet accuracy is not further restricted by the remaining experimental data. In fact, it turns out that the uncertainties in $\partial\phi_S/\partial E$ and $\partial\phi_S/\partial l(l+1)$ have negligible effects on the analysis of the remaining data, so that in the following sections we can limit ourselves to fitting $\phi_T(0,0)$ as a function of the C_6, C_8 choice and v_{DS} , $\partial\phi_T/\partial E$, and $\partial\phi_T/\partial l(l+1)$ within the ranges listed in Table 7.5. Only because the range of C_6 is restricted by the remaining data, is the overall error in v_{DS} that we find at the end of this paper smaller than the overall error following from the bound-states analysis alone.

7.4 Photoassociation Data

In the photoassociation experiment analyzed by Tiesinga *et al.* all atoms were pumped into the $3^2S(f=1)$ ground state and no static magnetic field B was applied. For $B=0$ (and neglecting the weak dipole-dipole interactions), the total two-atom electronic angular momentum quantum number F is a good quantum number. Further, the atomic quantum numbers f_1 and f_2 in Na ($f_1=1$)+Na ($f_2=1$) collisions couple to $F=0$ or 2 for even l and $F=1$ for odd l . Therefore, s -wave contributions to the photoassociation data can be represented in terms of two s -wave wave functions Ψ_{s0} and Ψ_{s2} , with $F=0$ and $F=2$, respectively. There is only one p -wave contribution: Ψ_{p1} . Finally, d -waves also contribute to the photoassociation spectrum but we do not need them here.

As mentioned in the introduction, Tiesinga *et al.* were able to constrain the position of the last node in Ψ_{p1} based on the fact that certain rovibrational lines arising from p -wave scattering were significantly weaker than neighboring lines. They found the position of this node to be $(73 \pm 3)a_0$ for a collision energy E_{coll} of 500 μK . The

Table 7.6 Ranges for the fractional parts Δ_{DT} of v_{DT} following from analysis of photoassociation data [6] and observed Feshbach resonances [10], for the five choices of C_6 and C_8 listed in Table 7.4. Ψ_{p1} node, Δ_{DT} range that produces the last node in the p -wave wave function Ψ_{p1} at $(73 \pm 3) a_0$; Ψ_{s0} node, Δ_{DT} range that produces the last node in the s -wave wave function Ψ_{s0} at $(60 \pm 3) a_0$; Ψ_{s2} node, range producing the last node in Ψ_{s2} at $(60 \pm 3) a_0$. The restrictions on the positions of the nodes were taken from Ref. [6]. B_1 , Δ_{DT} range that produces the Feshbach resonance near 907 G at a magnetic field consistent with experiment; $B_1 - B_2$, range producing a difference of Feshbach resonance fields $B_1 - B_2$ consistent with experiment.

Ch.	Ψ_{p1} node	Ψ_{s0} node	Ψ_{s2} node	B_1	$B_1 - B_2$
I	0.3052–0.3495	0.3148–0.4065	0.3593–0.4510	0.3399–0.3600	0.3441–0.3621
II	0.3064–0.3507	0.3157–0.4080	0.3609–0.4519	0.3392–0.3593	0.3434–0.3614
III	0.3052–0.3494	0.3144–0.4061	0.3591–0.4505	0.3427–0.3629	0.3504–0.3676
IV	0.3039–0.3482	0.3125–0.4039	0.3571–0.4484	0.3463–0.3663	0.3573–0.3738
V	0.3051–0.3493	0.3146–0.4060	0.3592–0.4505	0.3455–0.3659	0.3568–0.3733

energy 500 μK is close to the most probable collision energy in the experiment and the photoassociation spectra are therefore most sensitive to the shape of wave functions with this collision energy. In addition, Tiesinga *et al.* showed that the ratio of the $J = 2$ and $J = 4$ peaks is related to the position of the last s -wave node. They gave $(60 \pm 3) a_0$ for this position where they did not differentiate between Ψ_{s0} and Ψ_{s2} . The choice of the precise collision energy is less critical for the s -wave nodes. We take again 500 μK .

With a coupled-channels program we have calculated the positions of the last nodes in Ψ_{p1} , Ψ_{s0} , and Ψ_{s2} as a function of $\phi_S(0, 0)$ and $\phi_T(0, 0)$ for different choices of C_6 , C_8 and with $E_{coll} = 500 \mu\text{K}$. For each of the five choices of C_6 and C_8 introduced in the previous section (see Table 7.4), three v_{DT} intervals are listed in Table 7.6 (in terms of Δ_T): The first gives the v_{DT} range that produces the node in Ψ_{p1} at $(73 \pm 3) a_0$, the second interval gives the v_{DT} range that produces the Ψ_{s0} node at $(60 \pm 3) a_0$, and the last gives the v_{DT} range for the Ψ_{s2} node at $(60 \pm 3) a_0$. A small part of the width of the p -node interval is due to the uncertainty in $\partial\phi_T/\partial l(l+1)$. All listed intervals are for v_{DS} set at the middle of its uncertainty interval following from the bound-states analysis. If v_{DS} is increased or decreased by its uncertainty of 0.005, all v_{DT} intervals move approximately 0.0018 to lower or higher values. Their widths and mutual positions remain unchanged to better than 2%. The results for C_6 , C_8 choices not shown follow from linear interpolation.

To enable a quick comparison, all v_{DT} ranges found in the above analysis of the photoassociation data are also graphically shown in Fig. 7.2, in combination with the v_{DT} ranges from the bound-states analysis. Looking at the p - and s -node intervals, and realizing that the experimentally relevant s -node lies somewhere between the Ψ_{s0} and Ψ_{s2} nodes, there clearly is a strong indication that we have achieved agreement with the photoassociation data. Moreover, this agreement is realized for v_{DS} and v_{DT} values that also agree with the bound-state data.

7.5 Feshbach Resonances

The last two pieces of information that we incorporate in our analysis are the Na $|1, 1\rangle + \text{Na } |1, 1\rangle$ Feshbach resonances measured by Inouye *et al.* [10]. The widest of the two was detected at a magnetic field $B_1 = 907 \pm 20$ G and the second very narrow one $B_1 - B_2 = 54 \pm 1$ G below the first one.

For different choices of our potential parameters, we have calculated the scattering length $a_{1,1}$ for Na $|1, 1\rangle + \text{Na } |1, 1\rangle$ collisions as a function of B and determined where it becomes infinite, thus locating Feshbach resonances [9]. For our five choices of C_6 and C_8 (see Table 7.4), the v_{DT} ranges consistent with the measured field B_1 are listed in Table 7.6 (in terms of Δ_T). The specific choice of v_{DS} in its uncertainty interval has a negligible effect on the allowed v_{DT} values. This is due to the fact that the bound state involved in the Feshbach resonance is almost purely triplet. The uncertainty in $\partial\phi_T/\partial E$, on the other hand, is important (it causes a shift of about ± 7 G in B_1) and contributes to the width of the given v_{DT} interval. Much as expected, changing C_6 within its error limits turns out to cause a significant shift of the v_{DT} range corresponding to the measured B_1 , whereas the effect of changing C_8 is very small: about a ± 0.0003 shift in v_{DT} for a change of $\pm 5\%$ in C_8 .

The v_{DT} intervals that produce a difference of Feshbach resonance fields $B_1 - B_2$ that is consistent with the experiment are also given in Table 7.6, again for each of the five C_6, C_8 choices. Also in this case, results for intermediate C_6, C_8 values can be found by linear interpolation. $B_1 - B_2$ depends mostly on B_0 and C_6 . For $C_6 = 1539$ a.u., $887 \text{ G} < B_0 < 927 \text{ G}$ leads to $53 \text{ G} < B_1 - B_2 < 57 \text{ G}$, where the highest B_0 value corresponds to the lowest $B_1 - B_2$ value. For $C_6 = 1583$ a.u. we get $54 \text{ G} < B_1 - B_2 < 59 \text{ G}$. Since the uncertainty in $\partial\phi_T/\partial E$ has an effect on B_0 , it also has an effect on $B_1 - B_2$ and thus contributes to the width of the v_{DT} ranges that agree with the measured value.

As in section 7.4, for a quick comparison, all v_{DT} ranges found in the above analysis are shown in Fig. 7.2. Overlooking all available data, we conclude that there is complete agreement for C_6 values near the lower end of their uncertainty interval. If C_6 is increased to 1583 a.u., the agreement between the Feshbach resonance fields and the

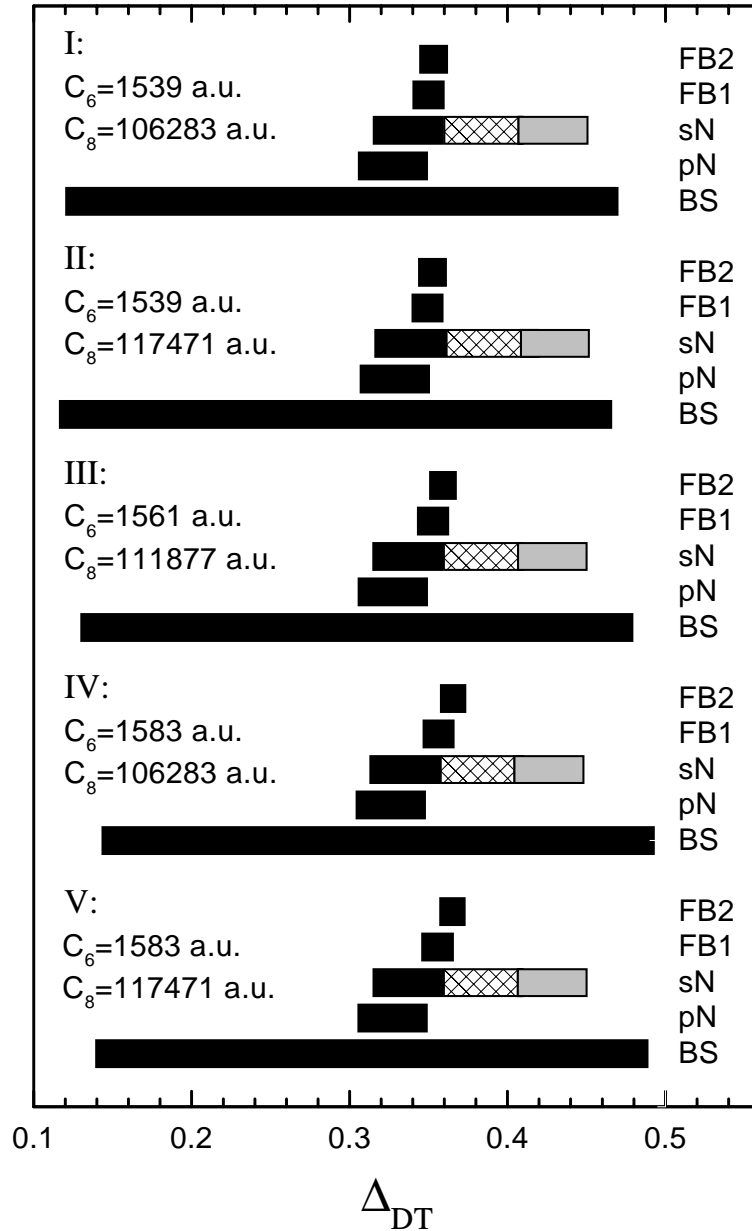


Figure 7.2 Graphical representation of the ranges for the fractional part Δ_{DT} of v_{DT} (see Tables 7.5 and 7.6) resulting from our analysis of various experiments. The numbers I-V refer to the choices of C_6 and C_8 . Each bar represents a Δ_{DT} range. BS, bound-state ranges; pN, Ψ_{p1} node ranges; sN (left-hand range including the hatched part), Ψ_{s0} node ranges; sN (right-hand range including the hatched part), Ψ_{s2} node ranges; FB1, B_1 ranges; FB2, $B_1 - B_2$ ranges. For each C_6, C_8 choice v_{DS} is completely determined by the bound-states analysis.

Table 7.7 Scattering lengths a for all combinations of hyperfine states in the $f = 1$ manifold, evaluated at zero magnetic field.

Channel	a (a_0)
Na $ 1, 1\rangle + \text{Na } 1, 1\rangle$	55.4 ± 1.2
Na $ 1, 1\rangle + \text{Na } 1, 0\rangle$	55.4 ± 1.2
Na $ 1, 1\rangle + \text{Na } 1, -1\rangle$	51.7 ± 1.3
Na $ 1, 0\rangle + \text{Na } 1, 0\rangle$	53.5 ± 1.3
Na $ 1, 0\rangle + \text{Na } 1, -1\rangle$	55.4 ± 1.2
Na $ 1, -1\rangle + \text{Na } 1, -1\rangle$	55.4 ± 1.2

photoassociation data deteriorates. This confirms what one might expect from the two calculations of C_6 by Kharchenko *et al.* [14] and Marinescu *et al.* [15] alone: The value of C_6 should lie between 1539 a.u. and 1561 a.u., rather than above 1561 a.u. Again, the effect of changing C_8 apparently is very small.

7.6 Predictions and Conclusions

Combining all the results of the previous sections as listed in Tables 7.5 and 7.6, we have determined the maximum v_{DS} and v_{DT} ranges that are consistent with all experimental data analyzed in this paper. The overlap between the v_{DT} ranges extracted from the $B_1 - B_2$ data and those extracted from the p -node data turns out to be the limiting factor. We find $v_{DS} = 65.662 \pm 0.012$ and $v_{DT} = 15.348 \pm 0.005$. The corresponding singlet and triplet scattering lengths are $a_S = (19.1 \pm 2.1) a_0$ and $a_T = a_{2,2} = (65.3 \pm 0.9) a_0$. Treating the uncertainties in v_{DS} and v_{DT} as uncorrelated errors, we have also calculated the scattering lengths for all combinations of hyperfine states in the $f = 1$ manifold and for zero magnetic field. The results are listed in Table 7.7. The situation that several scattering lengths have the same value is a result of the fact that for $B = 0$ all s -wave Na ($f_1 = 1$) + Na ($f_2 = 1$) collisions can be represented in terms of Ψ_{s0} and Ψ_{s2} , as discussed in section 7.4. All exchange decay rates for these collisions vanish as $B \rightarrow 0$ and $E \rightarrow 0$ because of zero available phase space. In particular, we find $a_{1,-1} = (55.4 \pm 1.2) a_0$. That is consistent with the value $(52 \pm 5) a_0$ found by Tiesinga *et al.* and the time-of-flight value $(42 \pm 15) a_0$ from Ref. [8]. The thermalization-time value of $a_{1,-1} = (92 \pm 25) a_0$ [7] falls outside the present error bar. The triplet scattering length that we find is significantly smaller than both the values found by Moerdijk and Verhaar and Tiesinga *et al.* This is not very surprising because the long-range part ($r > 16 a_0$) of the triplet potential, for which they both use the tail of the RKR potential from Ref. [4], was improved by us. The fact that our values

Table 7.8 Previous [1] and present values for the resonance fields B_0 of Feshbach resonances in ultracold Na collisions.

Channel	Previous B_0 (G)	Present B_0 (G)
Na $ 1, 1\rangle + \text{Na } 1, 1\rangle$	$900 < B_0 < 1850$	$2035 < B_0 < 2080$
Na $ 1, -1\rangle + \text{Na } 1, -1\rangle$	not reported	$1200 < B_0 < 1285$
Na $ 1, -1\rangle + \text{Na } 1, -1\rangle$	$840 < B_0 < 1340$	$1485 < B_0 < 1520$
Na $ 1, -1\rangle + \text{Na } 1, -1\rangle$	$1480 < B_0 < 2330$	$2620 < B_0 < 2670$

for $a_{1,-1}$ and $a_{2,2}$ are closer together than those of Tiesinga *et al.* can be explained by our different handling of the exchange part of the potentials. Our results for a_S and a_T are also both smaller than the values $a_S = 34.9 a_0$ and $a_T = 77.3 a_0$ found by Côté and Dalgarno, who use a similar treatment of the exchange energy, but the values for the difference $a_T - a_S$ are fairly similar.

We have also used the results of our analysis to predict the locations of an additional Feshbach resonance in the Na $|1, 1\rangle + \text{Na } |1, 1\rangle$ entrance channel and three resonances in the Na $|1, -1\rangle + \text{Na } |1, -1\rangle$ channel. Since all these resonances are related to almost purely triplet quasibound states, their resonance fields depend mostly on v_{DT} , C_6 and $\partial\phi_T/\partial E$. Correlations between these parameters are taken into account. The results are shown in Table 7.8, along with previous predictions by Moerdijk and Verhaar [1] for comparison. The present predictions for the resonance fields are higher than the previous ones. This is in agreement with the lower a_T (higher v_{DT}) that we find in this paper. Except for the resonance near 1200 G in the Na $|1, -1\rangle + \text{Na } |1, -1\rangle$ channel, the bound states that cross the threshold at the predicted magnetic fields have $m_S = +1$; see Fig. 7.3. For the resonance near 1200 G, which was not previously reported, $m_S = -1$ so that a smaller a_T there leads to a lower resonance field.

In conclusion, we have resolved the apparent discrepancy between the Na photoassociation data in Ref. [6] and the singlet and triplet bound-state energies in Refs. [2–4]. Moreover, we have obtained agreement between the above data and the observation of Feshbach resonances in a Na Bose condensate. Combining all these data has enabled us to determine a set of Na interaction parameters with an accuracy that allows precise calculation of Na cold collision properties. A few essential cold collision properties have been presented in this paper, but it is also possible to accurately calculate other properties such as the scattering lengths and exchange decay rate coefficients for arbitrary Na hyperfine states in the $f = 2$ manifold or for collisions between atoms with different f , and the locations of Feshbach resonances in arbitrary entrance channels.

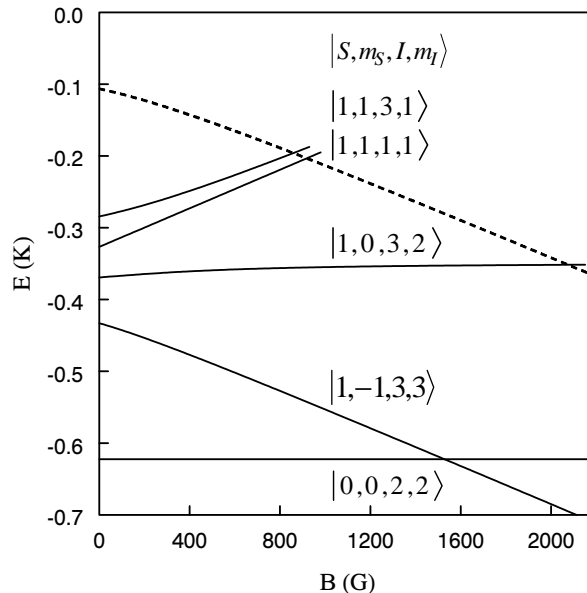


Figure 7.3 Triplet and singlet bound states (solid lines) and the Na $|1, 1\rangle + \text{Na } |1, 1\rangle$ threshold (dashed line) as a function of magnetic field. At $B = 0$, the degeneracy of the triplet state is lifted by the hyperfine interaction. Feshbach resonances occur at the intersections of the bound-state and threshold curves. If v_{DT} is increased, the bound-state curves move to lower energies and thus the resonance fields increase.

Acknowledgment

We acknowledge the help of Johnny Vogels in applying his search code, which he used for the analysis of bound states in ^{85}Rb [17], for the fit of the potential parameters to the experimental bound-state energy spacings.

References

- [1] A.J. Moerdijk and B.J. Verhaar, Phys. Rev. Lett. **73**, 518 (1994); Phys. Rev. A **51**, 4852 (1995).
- [2] Li Li, S.F. Rice, and R.W. Field, J. Chem. Phys. **82**, 1178 (1985).
- [3] R.F. Barrow, J. Verges, C. Effantin, K. Hussein, and J. D'Incan, Chem. Phys. Lett. **104**, 179 (1984).
- [4] W.T. Zemke and W.C. Stwalley, J. Chem. Phys. **100**, 2661 (1994).
- [5] R. Côté and A. Dalgarno, Phys. Rev. A **50**, 4827 (1994).
- [6] E. Tiesinga, C.J. Williams, P.S. Julienne, K.M. Jones, P.D. Lett, and W.D. Phillips, J. Res. Natl. Inst. Stand. Technol. **101**, 505 (1996).

- [7] K.B. Davis, M-O Mewes, M.A. Joffe, M.R. Andrews, and W. Ketterle, Phys. Rev. Lett. **74**, 5202 (1995).
- [8] Y. Castin and R. Dum, Phys. Rev. Lett. **77**, 5315 (1996).
- [9] E. Tiesinga, A.J. Moerdijk, B.J. Verhaar, and H.T.C. Stoof, Phys. Rev. A **46**, R1167 (1992); E. Tiesinga, B.J. Verhaar, and H.T.C. Stoof, *ibid.* **47**, 4114 (1993).
- [10] S. Inouye, M.R. Andrews, J. Stenger, H.-J. Miesner, D.M. Stamper-Kurn, and W. Ketterle, Nature **392**, 151 (1998).
- [11] B.J. Verhaar, K. Gibble, and S. Chu, Phys. Rev. A **48**, R3429 (1993).
- [12] B.M. Smirnov and M.I. Chibisov, Zh. Eksp. Teor. Fiz. **48**, 939 (1965) [Sov. Phys. JETP **21**, 624 (1965)].
- [13] M. Marinescu, H.R. Sadeghpour, and A. Dalgarno, Phys. Rev. A **49**, 982 (1994).
- [14] P. Kharchenko, J.F. Babb, A. Dalgarno, Phys. Rev. A **55**, 3566 (1997).
- [15] M. Marinescu, A. Dalgarno, and J.F. Babb, Phys. Rev. A **55**, 1530 (1997).
- [16] R.J. Le Roy, in *Semiclassical methods in molecular scattering and spectroscopy*, edited by M.S. Child (D. Reidel Publishing Company, London, 1979).
- [17] C.C. Tsai, R.S. Freeland, J.M. Vogels, H.M.J.M. Boesten, B.J. Verhaar, and D.J. Heinzen, Phys. Rev. Lett. **79**, 1245 (1997).

Summary

A remarkable aspect of the recently realized Bose-Einstein condensates in dilute gases of alkali atoms is the prominent role that atom-atom interactions play in them. They influence most of the important properties of these condensates, including their stability, size and shape, and collective excitations. The condensates are created by trapping atoms in a magnetic trap and cooling them to below the critical temperature by forced evaporation. Atomic interaction processes are also crucial in this process: a minimum rate of elastic collisions is required for efficient cooling and inelastic collisions should not occur too often. In addition, interactions between cold atoms will be an important factor in developments in the fields of atomic clocks, coherent matter waves and Fermi-degenerate gases. This thesis contains theoretical contributions to the investigation of cold-atom interaction processes and the determination of parameters that describe the interactions between cold rubidium, lithium and sodium atoms. Rather than describing complete interaction potentials with these parameters, we describe only the long-range parts using the standard parameters (dispersion coefficients and an analytical expression for the exchange energy) and summarize the information in the short-range parts in boundary conditions on the radial scattering wave functions in terms of accumulated WKB phases at a suitable internuclear separation [Sec. 2.4].

The scattering length characterizes two-body elastic collisions at very low temperatures and therefore also the atomic interactions in a dilute condensate. An interesting phenomenon in cold collision physics is the resonance behavior often shown by the scattering length as a function of the strength of an external magnetic field. These so-called Feshbach resonances make it possible to vary the strength of the interactions between the atoms in a condensate and even change them from effectively repulsive to attractive, which is predicted to cause a collapse of the condensate. An experiment investigating Feshbach resonances in a relatively dense sodium condensate showed that crossing a resonance while increasing the magnetic field at high ramp speed can also lead to a large loss of atoms from the trap. Using the nonconservation of energy due to the time dependence of the magnetic field, we describe a two-body decay mechanism [Sec. 3.2; Fig. 3.1] that can explain this observation [Eq. 3.4; Fig. 3.2]. An essential element in our picture is the concept of a global and a local resonance lifetime.

When the work for this thesis was started, the existence of Feshbach resonances in cold-atom scattering had been predicted but not yet observed. We show that photoassociation is a good probe for observing Feshbach resonances [Secs. 4.2 and 4.3]. In the photoassociation process a laser optically excites two colliding ground-state atoms into

a bound electronically-excited molecular state, which then decays back to free atoms with a translational energy large enough to escape from the trap; the resulting decrease in the number of trapped atoms is measured. A Feshbach resonance lengthens the time that the atoms spend in the internuclear distance range where the optical excitation occurs, so that the photoassociation signal increases [Figs. 4.2 and 5.1]. Our calculations show an enhancement by at least two orders of magnitude [Fig 4.1] for the broadest of the three resonances that had been predicted for ^{85}Rb and a suitable choice for the excited bound state. After this prediction, the photoassociation method was successfully applied by Heinzen and his group at the University of Texas, Austin, with whom we closely collaborated on this subject. Their observation of the ^{85}Rb resonance [Fig. 5.3], and the almost simultaneous observation of a Feshbach resonance in a sodium condensate by Ketterle's group at MIT, constitute the first observations of this phenomenon in cold collisions. The photoassociation spectra are analyzed [Sec. 5.4] leading to a precise prediction for the dependence of the scattering length on the magnetic field strength near the resonance [Fig. 5.5]. The ratio of the field width and the resonant field strength, which governs the degree of field control that is needed to stably change the sign of the scattering length, turns out to have a relatively favourable value for the ^{85}Rb resonance.

Because evaporative cooling does not work for spin-polarized fermions at very low temperatures, the creation of a Fermi-degenerate gas is more complicated than the creation of a Bose-Einstein condensate. We show, through analysis of photoassociation data and measured bound-state binding energies [Sec. 6.2], and via calculation of scattering properties [Table 6.1; Figs. 6.3 and 6.5], that there are two possible solutions in the case of ^6Li : sympathetic cooling (cooling the ^6Li atoms with evaporatively cooled bosonic ^7Li atoms) or using ^6Li atoms in different internal states.

The thesis is concluded with a simultaneous analysis [Secs. 7.3–7.5] of data from three different experiments on sodium: Na_2 bound-state energies, photoassociation data, and Feshbach resonance fields. We obtain a set of Na interaction parameters [Fig 7.2; Table 7.3] with a high precision that is in excellent agreement with all these experimental data; a discrepancy between the results of previous analyses of the bound-state energies and the photoassociation data is resolved. The interaction parameters are used to give accurate predictions for scattering lengths [Table 7.7] and resonance fields of several yet unobserved Feshbach resonances [Table 7.8] (one of which has been observed in the meantime at the right field strength). Preliminary results of our analysis have been of great help in locating and observing the Feshbach resonances in sodium by Ketterle's group. Moreover, our results have been used to confirm the reliability of *ab initio* calculations of van der Waals interactions.

Samenvatting

Een opmerkelijk aspect van de recent gerealiseerde Bose-Einsteincondensaten in ijle gassen van alkali-atomen is de belangrijke rol die interacties tussen de atomen daarin spelen. Zij beïnvloeden het merendeel van de relevante eigenschappen van deze condensaten, zoals hun stabiliteit, vorm en afmetingen, en collectieve excitaties. De condensaten worden gemaakt door atomen op te sluiten in een magnetische valkuil en ze af te koelen tot onder de kritische temperatuur door middel van geforceerd afdampen. Atomaire wisselwerkingsprocessen zijn ook van doorslaggevend belang in dit proces: voor efficiënt koelen is een minimale frequentie van elastische botsingen noodzakelijk en inelastische botsingen mogen niet te vaak voorkomen. Tevens zullen interacties tussen koude atomen een belangrijke factor zijn in ontwikkelingen op het gebied van atoomklokken, coherente materiegolven en Fermi-ontaarde gassen. Dit proefschrift bevat theoretische bijdragen aan het onderzoek naar deze wisselwerkingsprocessen en het vastleggen van parameters die de wisselwerking tussen koude rubidium-, lithium- en natriumatomen beschrijven. In plaats van de complete interactiepotentialen te beschrijven met deze parameters, beschrijven we alleen het lange-dracht deel met behulp van de standaardparameters (dispersiecoëfficiënten en een analytische uitdrukking voor de exchange-energie) en vatten we de informatie opgesloten in het korte-dracht deel samen in randvoorwaarden voor de radiële verstrooiingsgolffunctie in de vorm van geaccumuleerde WKB fasen bij een geschikte internucleaire afstand [§ 2.4].

De verstrooiingslengte karakteriseert elastische twee-deeltjesbotsingen bij zeer lage temperaturen en daarom ook de interacties in een ijl condensaat. Een interessant verschijnsel in de fysica van koude botsingen is het resonantiegedrag dat de verstrooiingslengte vaak vertoont als functie van de sterkte van een extern magnetisch veld. Deze zogenaamde Feshbachresonanties maken het mogelijk om de sterkte van de interacties tussen de atomen in een condensaat te variëren en zelfs om een effectief afstotende wisselwerking om te zetten in een aantrekkende, wat volgens voorspellingen leidt tot ineenstorting van het condensaat. Een experiment dat Feshbachresonanties onderzocht in een condensaat met een relatief hoge deeltjesdichtheid heeft aangetoond dat het passeren van een resonantie tijdens een snelle verhoging van de magnetische veldsterkte ook kan leiden tot een groot verlies van atomen uit de valkuil. Gebruik makend van het niet behouden zijn van de energie ten gevolge van de tijdafhankelijkheid van het magnetische veld, beschrijven we een twee-deeltjesvervalmechanisme [§ 3.2; Fig. 3.1] dat deze waarneming kan verklaren [Vgl. 3.4; Fig. 3.2]. Een essentieel onderdeel van ons beeld is het idee van een lokale en een globale levensduur van de resonantie.

Bij het begin van dit promotieonderzoek waren Feshbachresonanties in botsingen tussen koude atomen wel voorspeld maar nog niet waargenomen. We laten zien dat fotoassociatie een goed instrument is om deze resonanties waar te nemen [§ 4.2 en 4.3]. In dit proces exciteert een laser twee botsende atomen, die zich in de grondtoestand bevinden, naar een elektronisch aangeslagen gebonden toestand, die vervolgens weer vervalt naar vrije atomen met een translatie-energie groot genoeg om uit de valkuil te ontsnappen; de resulterende afname van het aantal atomen in de valkuil wordt gemeten. Een Feshbachresonantie verlengt de verblijftijd van de atomen in het gebied van internucleaire afstanden waar de excitatie plaatsvindt, zodat het fotoassociatiesignaal toeneemt [Fig. 4.2 en 5.1]. Onze berekeningen laten een versterking met tenminste twee grootte-orden zien [Fig. 4.1] voor de breedste van de drie resonanties die voor ^{85}Rb waren voorspeld en voor een geschikte keus voor de aangeslagen gebonden toestand. Na deze voorspelling is de methode succesvol toegepast door Heinzen en zijn groep aan de University of Texas in Austin, met wie we nauw hebben samengewerkt aan dit onderwerp. Hun waarneming van de resonantie bij ^{85}Rb [Fig. 5.3], en de vrijwel gelijktijdige waarneming van een Feshbachresonantie in een natriumcondensaat door de groep van Ketterle op MIT, vormen de eerste waarnemingen van dit verschijnsel in koude botsingen. De fotoassociatiespectra worden geanalyseerd [§ 5.4]. Dit levert een exacte voorspelling op voor de afhankelijkheid van de verstrooiingslengte van de magnetische veldsterkte in de buurt van de resonantie [Fig. 5.5]. De verhouding tussen de veldbreedte en de resonante veldsterkte, die de mate van controle over het veld bepaalt die nodig is om de verstrooiingslengte stabiel van teken te veranderen, blijkt relatief gunstig te zijn voor de resonantie bij ^{85}Rb .

Omdat afdampkoeling niet werkt voor spin-gepolariseerde fermionen bij zeer lage temperaturen, is het maken van een Fermi-gedegeneerd gas ingewikkelder dan het maken van een Bose-Einsteincondensaat. Via analyse van fotoassociatiedata en gemeten bindingsenergieën [§ 6.2], en het berekenen van verstrooiingseigenschappen [Tabel 6.1; Fig. 6.3 en 6.5], tonen we aan dat er in het geval van ^6Li twee oplossingen mogelijk zijn: sympathetic cooling (het koelen van de ^6Li atomen met door middel van afdampen gekoelde ^7Li atomen die zich gedragen als bosonen) of het gebruik van ^6Li atomen in verschillende interne toestanden.

Het proefschrift wordt afgesloten met een gecombineerde analyse [§ 7.3–7.5] van de meetresultaten van drie verschillende experimenten aan natrium: energieën van gebonden Na_2 toestanden, fotoassociatiedata, en veldsterkten waarbij Feshbachresonanties optreden. We verkrijgen een stel interactieparameters voor Na [Fig. 7.2; Tabel 7.3] met een grote precisie dat uitstekend in overeenstemming is met al deze experimentele gegevens; een discrepantie tussen resultaten van eerdere analyses van de gebonden-toestandsenergieën en de fotoassociatiedata wordt opgelost. De interactieparameters worden gebruikt voor nauwkeurige voorspellingen voor verstrooiingslengten

[Tabel 7.7] en resonantievelden van verschillende nog niet waargenomen Feshbachresonanties [Tabel 7.8] (waarvan er één inmiddels waargenomen is bij de juiste veldsterkte). Voorlopige resultaten van onze analyse zijn van grote waarde geweest bij het localiseren en waarnemen van de resonanties in natrium door Ketterle's groep. Bovendien is ons werk gebruikt om de betrouwbaarheid van *ab initio* berekeningen van Van-der-Waalsinteracties te bevestigen.

Dankwoord

Ik wil hier graag een aantal mensen bedanken die een belangrijke rol hebben gespeeld bij de totstandkoming van dit proefschrift. Allereerst natuurlijk Boudewijn Verhaar voor zijn stimulerende begeleiding en zijn grote rijkdom aan ideeën voor het aanpakken van fysische problemen waarvan ik veelvuldig gebruik heb mogen maken. Verder mijn collega's Johnny Vogels en Servaas Kokkelmans voor de prettige samenwerking. Johnny wil ik in het bijzonder bedanken voor het ter beschikking stellen van zijn programma voor het bepalen van interactieparameters uit gemeten gebonden-toestandsenergieën, waarmee de analyse in paragraaf 7.3 is uitgevoerd. Met Servaas, die gedurende het laatste halve jaar mijn kamergenoot was, heb ik veel plezier gehad.

Ook Hugo Boesten mag niet ongenoemd blijven. Door zijn werk aan de beschrijving van fotoassociatie-experimenten en zijn uitleg over dit onderwerp heb ik een vlotte start gehad bij mijn werk aan fotoassociatie als instrument voor het waarnemen van Feshbachresonanties.

I would like to thank Dan Heinzen, Philippe Courteille, and Riley Freeland for our cooperation and their contribution to chapters 4 and 5 of this thesis. Their photoassociation experiments have truly opened up new horizons.

En niet te vergeten alle mede-A.I.O.'s en andere leden van wat tegenwoordig het Werkverband Theoretische Natuurkunde heet. Zonder hen zou het een stuk minder gezellig zijn geweest. Tenslotte ben ik mijn ouders dankbaar voor hun steun en goede zorg tijdens de afgelopen jaren.

Curriculum Vitae

11 oktober 1970	geboren te Son en Breugel
1983–1989	Gymnasium B, Lorentz Lyceum te Eindhoven
1989–1996	studie Technische Natuurkunde, Technische Universiteit Eindhoven, doctoraal examen (cum laude) in april 1996
1996–1999	promotieonderzoek, groep Atoomfysica en Quantumelectronica, Faculteit Technische Natuurkunde, Technische Universiteit Eindhoven

STELLINGEN

behorende bij het proefschrift

Interaction Processes in Cold Gases of Alkali Atoms

van

Frank van Abeelen

Eindhoven, 16 december 1999

1

Bij een experiment aan een Bose-Einsteincondensaat van Na-atomen in een tijdafhankelijk magneetveld zagen Stenger et al. 80% van de condensaatatomen verdwijnen binnen de korte tijd van 1 μ s. Dit kan verklaard worden met een twee-atoomsvervalmechanisme.

- J. Stenger, S. Inouye, M.R. Andrews, H.-J. Miesner, D.M. Stamper-Kurn, and W. Ketterle, *Phys. Rev. Lett.* **82**, 2422 (1999).
- Dit proefschrift, hoofdstuk 3.

2

Met een kleine uitbreiding van de experimenten van Stenger et al. had een condensaat van moleculen, en daarmee een belangrijke stap op weg naar coherente chemie, waarschijnlijk reeds in 1998 een feit kunnen zijn.

- J. Stenger, S. Inouye, M.R. Andrews, H.-J. Miesner, D.M. Stamper-Kurn, and W. Ketterle, *Phys. Rev. Lett.* **82**, 2422 (1999).

3

De nauwkeurigheid van uit experimenten bepaalde interactieparameters voor alkali-atomen is de laatste jaren razendsnel toegenomen. De veelgebruikte vuistregel voor de relatie tussen de geaccumuleerde fasen van verschillende isotopen van één element, die stelt dat deze fasen zich verhouden als de wortels uit de massa van het isotoop, heeft zichzelf hierdoor overleefd.

- Dit proefschrift, hoofdstukken 1, 6 en 7.
- A. Messiah, *Quantum Mechanics* (North-Holland, Amsterdam, 1970), p. 234.

4

De nieuwe multiprocessor supercomputer UNITE heeft die eigenschappen in zich verenigd waardoor hij bij uitstek geschikt is voor rigoureuze quantummechanische berekeningen aan drie-deeltjesverstrooiing.

- <http://www.unite.nl>.
- J.M. Vogels, proefschrift Technische Universiteit Eindhoven (1999).

5

Het formalisme van Kievsky et al. voor drie-deeltjesverstrooiing vereist een efficiënt integratie-algoritme voor tweede-ordedifferentiaalvergelijkingen met eerste afgeleide. De gemodificeerde Numerovmethode, een beproefd algoritme voor tweede-ordedifferentiaalvergelijkingen zonder eerste afgeleide, kan na generalisatie aan deze eis voldoen.

- A. Kievsky, M. Viviani, and S. Rosati, *Phys. Rev. C* **56**, 2987 (1997).
- J. Raynal, in *Computing as a Language of Physics*, edited by A. Salam (IAEA, Wenen, 1972), p. 292.

6

Fotoassociatiespectroscopie in een variabel extern magneetveld is een verrijking van de experimentele technieken voor het bestuderen van koude botsingen.

- Dit proefschrift, hoofdstukken 4 en 5.

7

De formule van Gribakin en Flambaum voor de verstrooiingslengte is gebaseerd op de foutieve veronderstelling dat een atoombotsing voor alle internucleaire afstanden waar de potentiaal afwijkt van het Van der Waalsgedrag, semiklassiek beschreven kan worden.

- G.F. Gribakin and V.V. Flambaum, Phys. Rev. A **48**, 546 (1993).
- Ch. Boisseau, proefschrift Université Paul Sabatier de Toulouse (1999).

8

De zegswijze “stille wateren hebben diepe gronden” gaat ook op voor stabiele alkali-atomen: hoe dieper de singletpotentiaal, des te minder vibratieniveaus deze bevat.

- A.J. Moerdijk, *Notorious Table* (interne lijst met gegevens over alkali-atomen, groep Atoomfysica en Quantumelectronica, Technische Universiteit Eindhoven).

9

De beangstigend steile trappen in veel Nederlandse huizen getuigen van een doorgeschoten angst om ruimte te verspillen.

10

Dankzij satellietverbindingen en internet hoeft een grote oceaanzeilwedstrijd als de Whitbread Round The World Race wat betreft aantrekkelijkheid voor toeschouwers niet onder te doen voor het wereldkampioenschap voetbal.

- <http://www.whitbread.org>.

11

Een geslaagd dessert is door zijn presentatie en smaak in staat de verrukkingen van kunst en gastronomie in zich te verenigen.

12

“Eerst denken, dan doen” is de verkeerde filosofie in de omgang met Windows-programmatuur.